Metabolism and Motility: Characterizing Metabolic Changes that Lead to Metastasis

by

Lauren Danica Van Wassenhove

A dissertation submitted in partial fulfillment
of the requirements for the degree of
Doctor of Philosophy
(Cellular and Molecular Biology)
in the University of Michigan
2013

Doctoral Committee:

Professor Sofia D. Merajver, Chair
Christopher W. Beecher, NextGen Metabolomics
Professor Charles F. Burant
Professor Alexander J. Ninfa
Professor Kenneth J. Pienta

Dedication

I dedicate this work to my parents, who have always inspired me to always do the best I can do.

Acknowledgements

I would like to acknowledge my mentor, Sofia Merajver, for her role in developing both my technical and thinking skills into that of a scientist. She has inspired me to dedicate my life to cancer research and to strive to make a difference in patient's lives. My thesis committee members—especially Alex Ninfa, for teaching me how to purify my first protein (PII) and Chuck Burant for meeting with me early in the morning to discuss research and keep me excited about my work—for all of their support, guidance, and advice along the way. The Merajver Lab members, especially Devin Rosenthal, Michelle Wynn, Laura Nedjedlik, and Steve Allen have been essential in providing both advice and a willingness to discuss troubleshooting and experimental planning. ZhiFen Wu and LiWei Bao patiently trained me to do cell culture, western blots, and other techniques without which, I never would have been able to finish my thesis. I would like to thank Elizabeth Kennedy for her work on getting the mevalonate project underway. My parents, Brett and Kim McNeill have supported me completely in my endeavor to be a scientist, and encouraged me when I thought I would never finish my graduate work. I would like to thank my twin sister Brittany Achard for reading various versions of my thesis and supporting me in my decision to stay in school longer than anyone we know. My brother Colin McNeill has been instrumental in providing an outside scientific view, and for providing feedback when I would discuss what I was working on. I would like to thank my husband, Sandor, who helped to keep me sane when I was doing experiments in my sleep, listened to all my practice talks, and cooked dinner when I got home too late.

Table of Contents

List of Figures

List of Tables

List of Abbreviations

ASPA	aspartoacylase
AT	atorvastatin
ATP	adenosine-5'-triphosphate
CDCP1	CUB domain containing protein 1
cDNA	complementary DNA
CoA	coenzyme A
CXCL12	chemokine (C-X-C motif) ligand 12
CUB	complement C1r/C1s, Uegf, Bmp1
CXCR4	chemokine (C-X-C motif) receptor 4
DNA	deoxyribonucleic acid
DNTB	5,5-dithiobis-(2-nitrobenzoic acid)
E1	pyruvate dehydrogenase catalytic subunit
E2	dihydrolipoyl transacetylase
E3	dihydrolipoyl dehydrogenase
F1,6BPase	fructose-1,6-bisphophatase
FAD	flavin adenine dinucleotide
FBP	fructose-1,6-bisphosphate
FCCP	carbonyl cyanide-4-(trifluoromethoxy) phenylhydrazone
^{18}FDG	^{18}-fluoro-deoxyglucose
GAP	GTPase-activating proteins

GDI	guanosine nucleotide dissociation inhibitor
GDP	guanosine diphosphate
GEF	guanine nucleotide exchange factors
GGTI	geranylgeranyl transferase inhibitor
GPR	G-protein coupled receptor
GTP	guanosine-5'-triphosphate
GTPase	guanosine-5'-triphosphatase
HIF	hypoxia-inducible factor
HMG-CoA	3-hydroxy-3-methyl-glutaryl-CoA
HSD11B1/2	11β-hydroxysteroid dehydrogenase type 1/2
IBC	inflammatory breast cancer
IDH1/2	isocitrate dehydrogenase 1/2
MAPK	mitogen-activated protein kinase
MAT2A	methionine adenosyltransferase II, alpha
MMP	matrix metalloprotease
mRNA	messenger RNA
mTOR	mammalian target of rapamycin
MTT	3-(4,5-Dimethylthiazol-2-yl)-2,5-diphenyltetrazolium bromide
NAA	N-acetyl aspartate
NAD^+	nicotinamide adenine dinucleotide
$NADP^+$	nicotinamide adenine dinucleotide phosphate
NAT8L	N-acetyltransferase 8-like
PCR	polymerase chain reaction

PDH	pyruvate dehydrogenase
PDK1/2/3/4	pyruvate dehydrogenase kinase 1/2/3/4
PDP1/2	pyruvate dehydrogenase phosphatase1/2
PEP	phosphoenolpyruvate
PET	positron emission tomography
PFK	phosphofructokinase
PFKFB	6-phosophfructo-2-kinase/fructose-2, 3-bisphosphatases
PHDs	prolyl hydroxylases
PKL	pyruvate kinase L
PKM1/2	pyruvate kinase M1/2
PKR	pyruvate kinase R
RNA	ribonucleic acid
RTK	receptor tyrosine kinase
RT-PCR	reverse transcriptase PCR
SAM	S-adenosyl methionine
shRNA	short hairpin RNA
TAMs	tumor associated macrophages
TCA	tricarboxylic acid
TEM	transmission electron microscopy
TNF-α	tumor necrosis factor α
VEGF	vascular endothelial growth factor
ZA	zoledronic acid

Abstract

Cancer is an often devastating disease that affects populations throughout the world. The major cause of cancer-related death is metastasis, not the primary tumor. By understanding changes in cancer cells that allow them to locally invade and move into new tissues and organs, we may be able to identify new therapeutic targets for preventing metastasis. In this work, we approached studying aggressive breast cancer by examining how neoplastic cells use energy. We hypothesized that alterations in metabolism may define a switch that causes cancer cells to change their behavior from a highly proliferative state, like that of a primary tumor, to a more motile and invasive state, leading to the early steps of metastasis.

We found that inhibition of the mevalonate pathway, a metabolic pathway that makes cholesterol and isoprenoid precursors for the lipid bilayer as well as hormone precursors for signaling, leads to decreased motility and invasion in breast cancer cells. In addition, we identified an alternative mechanism for mevalonate inhibitor, zoledronic acid.

Studying the metabolic switch from a different perspective, we found that the rare and highly aggressive inflammatory breast cancer cell line SUM149 does not undergo oxidative phosphorylation. Rather, these cells use an alternative metabolic pathway to direct acetyl-CoA out of the tricarboxylic acid cycle, thereby preventing the production of oxidative phosphorylation intermediates. This pathway may enable these cells to

survive more readily in conditions of hypoxia, because oxidative phosphorylation, which consumes oxygen, would be unnecessary.

Finally, returning to our overall aim, we examined the behavioral switch between proliferation and motility directly by investigating an aggressive breast cancer cell line MDA-MB-231 in which we had knocked down mitogen activated protein kinase pathway member p38gamma. This results in highly proliferative, but less motile cells. We performed unbiased metabolomic screening and found that nucleotide synthesis, NADH metabolism, and C-21 steroid hormone biosynthesis are necessary for this change in behavior. From this work, we learned how individual metabolic pathways may regulate motility and invasion. Characterizing how these pathways interact to create the ideal environment to induce cancer cells to become metastatic will be the focus of discussion and future study.

Chapter I

Introduction

Metastasis of cancer cells is the cause of most cancer-related deaths[1]. Excluding basal and squamous skin carcinomas, breast cancer is the most common cancer in women, and the 2nd most deadly in terms of number of deaths per year[1]. Breast cancer normally follows a progression from the formation of a primary tumor, to secondary metastases principally to the bone, brain, liver or lung, if the primary tumor is not treated or eliminated before metastases form. In a primary tumor, cellular proliferation is very important for the tumor to gain its bulk mass. After a period of time, due to mechanisms not yet fully understood, tumor cells then regain or acquire the ability to move away from the primary tumor to a new area in the body. At this point, metabolic energy use is channeled mainly towards movement and invasion, instead of proliferation. Understanding the switch of energy use from proliferation to motility is crucial to understanding the molecular mechanisms of metastasis and a step toward the prevention of metastasis. This work focuses on the transition between proliferation and motility and thus on the metabolic changes that occur in cancer as well as on the motility processes involved in metastasis.

This chapter will cover the known alterations of metabolism in cancer cells and changes in motility that allow cancer cells to leave their initial location and invade the surrounding tissue and eventually metastasize.

Review of Cancer Cell Metabolism

Energy utilization is an important process in every living cell. Metabolic processes regulate cell growth, division, movement, and death. Alterations in metabolic pathways have been shown to both enable and cause cancer formation. One of the first experiments in this field was led by Otto Warburg in the 1920s. He showed that cancer cells use anaerobic metabolism even when sufficient oxygen was present[2]. This behavior was later named "The Warburg Effect". Warburg's pioneering work fell by the wayside with the discovery of new viral causes of cancer (such as Peyton Rous's discovery of tumor viruses in chickens) and genetic alterations called oncogenes[3]. The differences observed in the metabolism of cancer and non-cancer was not widely studied again until the late 1970s, when increased glucose uptake by cancer cells was discovered to be a useful diagnostic tool in the clinic [4, 5]. Since then, scientists have been working to discover why cancer cells use aberrant metabolism and how these changes might be manipulated to improve cancer therapy. Besides decreased oxidative metabolism and increased lactate production, a variety of specific metabolic changes are observed in cancer cells.

Cancer cells take up more substrates, or do so more rapidly, than normal cells

Increased nutrient and growth factor uptake by cancer cells is part of the process that allows them to grow faster than normal cells and also allows them to outcompete surrounding cells for nutrients and growth factors. Tumors express greater numbers of glucose transporters, known as GLUT proteins on the outside of their cells[6]. They also overexpress a variety of growth factor receptors[7]. The increased uptake and utilization of glucose in cancer cells is sufficiently different from normal cells that it can be used as

a diagnostic tool to identify areas of cancer in the body. In Positron Emission Tomography (PET) scans, a radiolabeled glucose analog 2-fluoro-2-deoxy-D-glucose (^{18}FDG) is given to the patient. ^{18}FDG can be taken up by the cells via the glucose transporters with the same efficiency of glucose, but because of the lack of the hydroxyl group at the 2-position, it is unable to become further metabolized by hexokinase, the first glycolysis enzyme. ^{18}FDG remains in the cell long enough to radioactively decay, producing an image. Areas where the ^{18}FDG accumulates are likely to be areas of high metabolic activity and are most likely (but not exclusively) cancerous. The uptake of glucose by clinical tumors can be up to an order of magnitude higher than in normal cells, allowing accurate and efficient diagnosis of the presence of metabolically active lesions by PET scanning.[8] Glucose uptake has been shown to correlate with tumor aggressiveness and prognosis in breast cancer, making PET diagnosis a very valuable tool in widespread use for predicting the outcome of breast tumors and response to therapy in some cases.[5, 9]

Glycolysis is often altered in cancer

Glycolysis is the main pathway used to break down glucose to pyruvate for entry into tricarboxylic acid (TCA) cycle and oxidative phosphorylation (Figure I.1, I.2). Pyruvate kinase is an important irreversible step in glycolysis that catalyzes the reaction that produces pyruvate from phosphoenolpyruvate (Figure I.2). The gene which encodes this enzyme is alternatively spliced in cells, resulting in tissue specific isoforms of pyruvate kinase. The L-isoform of pyruvate kinase (PKL) is expressed primarily in liver and kidney tissue, the R-isoform (PKR) is expressed in red blood cells, while the M-isoforms, PKM1 and PKM2 are expressed in muscle tissues. PKM2 is the embryonic

form and is important for development, whereas PKM1 is found predominantly in adult tissue [10]. Isoforms PKL, PKR, and PKM1 all can form a stable homotetramer; however, PKM2 can form both homotetramers and unstable homodimers. In cancer, embryonic PKM2 is often expressed instead of PKM1. PKM2 differs from PKM1 by 23 amino acids within a 56 amino acid stretch. This sequence difference alters the secondary and tertiary structure sufficiently that it prevents PKM2 from being stabilized in its normal tetramer form by the glycolysis metabolite fructose-1, 6-bisphosphate (FBP) [11]. As a result, PKM2 forms dimers instead of tetramers, and the dimeric complexes are much slower at catalyzing the reaction of phosphoenolpyruvate (PEP) to pyruvate. This, in turn, allows PEP to accumulate, allowing upstream metabolites to be available to be redirected through the pentose phosphate pathway to relieve this excess (Figure I.1). The pentose phosphate pathway is a major source of nucleotide synthesis, so increased flux through this pathway increases the rates at which nucleotides are made for replication. Additionally, PKM2 has been shown to promote serine synthesis [12]. Serine is known to activate PKM2 allosterically [13], increasing catalytic rate of PKM2 [12]. When low amounts of serine are present, PKM2 activity is low, and intermediates upstream in the glycolysis pathway accumulate. In response to low serine levels, the general control nonderepressible 2 kinase-activating transcription factor 4 (GCN2-ATF4) pathway is activated. This pathway then upregulates serine synthesis enzymes via the AT4 transcription factors. Glycolysis pathway intermediates can be used directly in serine synthesis, leading to an increase in serine levels in the cell. With more serine present, PKM2 can be activated such that more glycolysis proceeds forward and lactic acid is produced [12]. Additionally, serine is an important amino acid required for

protein, nucleotide and lipid synthesis, so increasing serine amounts in the cell will help the cell to proliferate more quickly[14].

Alterations in the regulation of the glycolysis enzyme phosphofructokinase (PFK) have also been identified in cancers. PFK is responsible for catalyzing the reaction of fructose-6-phosphate to fructose-1,6-bisphosphate (Figure I.2). This reaction is irreversible under physiological conditions and represents the first committed step in glycolysis, making it very important in the regulation and flux of glucose entering this pathway[15]. PFK is inhibited by adenosine-5'-triposphate (ATP), so that when high levels of ATP are present, little glucose enters glycolysis. However, PFK is activated by a metabolite not found in the glycolysis pathway, fructose -2, 6-bisphosphate. This activation is able to overcome inhibition by ATP. Fructose -2, 6-bisphosphate also potently inhibits the gluconeogenic enzyme known as fructose-1, 6-bisphosphatase (F1,6BPase), thereby preventing gluconeogenesis from occurring (Figure I.4). The level of fructose -2, 6-bisphosphate in the cell is maintained by a bifunctional enzyme family called 6-phosophfructo-2-kinase/fructose-2, 3-bisphosphatases (PFKFB), which phosphorylate fructose-6-phosphate to fructose-2, 6-bisphosphate and do the reverse dephosphorylation as well. PFKFB is encoded by a gene that is alternatively spliced resulting in four isoforms, termed PFKFB 1-4. Isoform PFKFB3 is highly overexpressed in cancer tissues and has reduced phosphatase activity compared to its kinase activity, which results in much higher amounts of intracellular fructose-2,6-bisphosphate in certain cancers [15]. This enables the cancer cells to turn glycolysis on via almost constitutive PFK activation even when ATP is at high levels within the cell. Next, I will describe the processes cancer cells use to make ATP.

Cancer cells use lactic acid fermentation preferentially to oxidative phosphorylation to produce energy (ATP)

Under aerobic conditions in normal cells, glucose is metabolized to pyruvate through glycolysis and pyruvate is changed to acetyl CoA, which enters the TCA cycle and undergoes oxidative phosphorylation (Figure I.1, I.2, I.3). This process yields a net ATP gain of 32-36 molecules of ATP per glucose molecule depending on the type of transporter used to bring the substrate into the mitochondria. Under anaerobic conditions, the cell metabolizes glucose to pyruvate through glycolysis, and pyruvate is changed to lactic acid via fermentation. This yields a net of 2 ATP molecules per glucose molecule. In cancer cells, however, lactic acid fermentation is performed preferentially to the TCA cycle and oxidative phosphorylation even when oxygen is present, yielding a much lower quantity of ATP per glucose molecule. Warburg postulated that cancer cells must have developed a defect in oxidative phosphorylation, leading to their need to undergo glycolysis to make their energy, a process he termed "aerobic glycolysis" as cancer cells opted for this pathway even when the cellular oxygen concentration was normal.[2] Later research showed that most cancer cells do not have a defect in oxidative phosphorylation; instead they use glycolysis preferentially over oxidative phosphorylation to convert glucose to ATP [16]. The fact that cancer cells use this less efficient way to produce energy might, at first glance, seem counterintuitive. However, some researchers have theorized that by increasing the rate of glycolysis, cancer cells can generate ATP more rapidly than normal cells, giving them a proliferative advantage[16]. In addition, another study showed that utilizing aerobic glycolysis may give cancer cells a survival advantage

by protecting them against damage from the reactive oxygen species produced during oxidative phosphorylation.[17]

Mutations of TCA cycle enzymes has been found in some cancers

Recent work in malignant brain gliomas has found mutations in TCA Cycle enzyme isocitrate dehydrogenase genes IDH1 and IDH2. These mutations decrease the ability of isocitrate dehydrogenase to catalyze the conversion of isocitrate to α-ketoglutarate (Figure I.3). In addition, this mutation allows isocitrate dehydrogenase to convert isocitrate to 2-hydroxyglutarate, which is toxic as it accumulates in the brain, thereby increasing morbidity of this disease [18, 19]. In addition, 2-hydroxyglutarate has been implicated in the regulation of histone and DNA-methylation, via its inhibition of dioxygenases [20]. This suggests that 2-hydroxyglutarate might affect cancer at the epigenetic level as well. Other work has shown mutations in fumarase, as well as succinate dehydrogenase[21]. These mutations lead to an accumulation of fumarate and succinate respectively within the mitochondria. Recent work show that these different TCA cycle mutations may lead to similar phenotypes. Fumarate and succinate inhibit a group of enzymes known as prolyl hydrogenases (PHDs), which are important for degrading hypoxia inducible factors (HIFs) [22]. HIF family proteins are very important for the cellular response to the stress of low oxygen conditions (hypoxia). In hypoxia, transcription factor HIF-1α activates to a wide array of genes that modify the cellular environment in response to lack of oxygen. For example, glycolysis enzymes are upregulated to increase lactic acid fermentation, and angiogenesis (the formation of new blood vessels) programs are activated in order to direct oxygen and nutrients to the cells. The activation of HIFs is vital to a cancer cells ability to survive hypoxia. In addition, it

may give them a selective advantage to have HIF activated in non-hypoxic situations in order to increase access to nutrients and oxygen via angiogenesis and increased glycolysis. Succinate and α-ketoglutarate may also be transported outside of the cytosol. Recent work has shown that they interact with a set of orphan receptors, GPR 91 and GPR 99, which are G-protein coupled receptors[23]. GPR91 has been shown to play a role in neuronal angiogenesis by stimulating vascular endothelial growth factor (VEGF) secretion in mice and is activated by succinate[24]. GPR99, being recently discovered, has no defined function yet, but has been found to be activated by α-ketoglutarate [23]. .These receptors react to extracellular succinate and α-ketoglutarate, so the cancer cells may secrete these metabolites into the bloodstream to signal to other cells. As a result, these metabolites may act in a way to induce changes in signaling. Further studies will need to be done to understand the impact of these metabolites in signaling.

TCA cycle intermediates are used for de novo lipid synthesis and nucleotide synthesis

The TCA cycle intermediates are required for a variety of other metabolic processes including lipid synthesis and nucleotide synthesis. A proliferating cell needs to double its cellular contents and DNA, making the production of lipids for cell membranes and nucleotides vital. Citrate can exit the cycle and is converted into acetyl CoA and malate via ATP citrate lyase. This acetyl CoA can then be incorporated into lipid synthesis. In cancer cells, the rate of lipid and nucleotide synthesis is increased, because of the increased proliferation rate of these cells. In particular, ATP citrate lyase as well as fatty acid synthase (FSN), responsible for the formation of palmitate from acetyl-CoA and malonyl-CoA, have much higher expression in cancer [25]. Nucleotide synthesis

may be higher in cancer due to increased flux of glycolysis intermediates into the pentose phosphate pathway via PKM2 inhibition as discussed in the previous sections.

Glutamine is used as an alternative fuel for the TCA cycle

Besides providing substrates needed to enter oxidative phosphorylation for ATP synthesis, TCA cycle intermediates are also required for fatty acid synthesis and nucleotide synthesis. Because cancer cells need to be able to double their contents in order to divide, they need to find another was to keep the TCA cycle running when most glucose is being made to generate lactate. Often, via a process called glutaminolysis, cancer cells metabolize glutamine to glutamate, which then can enter the TCA cycle as α-ketoglutarate. The use of α-ketoglutarate to replenish TCA cycle intermediates is called the anapleurotic or "filling up" reactions because this keeps the TCA cycle active when metabolites are exiting the cycle to be used for biosynthetic processes. Additionally, through the process of reductive carboxylation, α-ketoglutarate can be made into citrate which can be exported out of the mitochondria for use in fatty acid synthesis. By utilizing glutaminolysis to keep the TCA cycle active, the cell can generate the intermediates necessary for all of these processes.[26].

New evidence that cancer cells undergo gluconeogenesis

Gluconeogenesis is the process by which glucose is produced from other substances such as lactate, glycerol, and glucogenic amino acids [27]. This process is almost a reverse of glycolysis, with a substitution of a few enzymes which perform irreversible reactions in glycolysis (Figure I.4). When gluconeogenesis occurs in the context of strenuous exercise, a situation in which it is necessary to remove lactic acid from the muscles during movement and to return it to the muscles as glucose, this process

is called the Cori Cycle. It has been thought for many decades that only cells of liver, kidney, and intestinal origin performed gluconeogenesis [27, 28]. However, recent work in our lab has shown that cancer cells perform gluconeogenesis as well. This exciting new discovery may jumpstart therapies that may be very effective in tumors not derived from liver, kidney, or intestines, as the drugs would have no effect on the tissue surrounding the tumor.

Many metabolic changes as described above occur in cancer cells. In order to understand what role the changing metabolic environment may have on the ability of cancer cells to metastasize, a good understanding of motility in the cancer cell context is required. The following portion of this chapter reviews the cellular motility, especially in the context of cancer cell metabolism.

Review of Cancer Cell Motility

Discussion of Cell Movement

Cell motility is an important process required in normal embryonic development and wound healing. However, in adult, uninjured tissue, this process is abnormal and leads to invasion and metastasis of cancer [29]. In order for a cell to move, it must polarize, so that the movement machinery is localized in the direction of motion. To initiate movement, breast cells send out protrusions of either lamellipodia or filopodia, which are generated via actin polymerization. Next, new focal adhesions are formed, which attach the cell to the surrounding ECM (extracellular matrix) and signaling proteins via integrins. The cell then detaches older focal adhesions in the rear of the cell in order to move.

An important step for a cell to gain the ability to be motile is the formations of protrusions. These protrusions, either lamellipodia or filopodia, are tightly regulated by Rho proteins (Figure I.5)[30]. Rho family proteins are small GTPase proteins that are active when they are bound to GTP and inactive when bound to GDP [31]. Effector proteins called GAPs (GTPase activating proteins) and GEFs (Guanosine nucleotide exchange factors) aid in the exchange of GTP and GDP bound forms. GAPs help to catalyze the hydrolysis reaction of GTP to GDP, which inactivates the small GTPase protein. GEFs help the small GTPase to exchange its GDP for a GTP, thus activating it[31]. In addition GDIs (Guanine nucleotide dissociation inhibitors) bind to the GDP bound form of the small GTPase[32]. This prevents nucleotide exchange, thus holding the GTPase in an inactive state. In addition, GDIs prevent the localization of these proteins in the membrane by holding small GTPases in the cytoplasm [33]. When these proteins are unable to move to the membrane, they cannot direct cell motility by regulating protrusion formation.

The process by which a cancer cell begins to invade and metastasize into surrounding tissue is described by the Invasion-Metastasis Cascade [34]. This process includes local invasion, intravasation, survival of transport within the vasculature, stopping at distant sites, extravasation, survival to form micrometastases, and proliferation at new sites (colonization) [34].

Local Invasion

In normal mammary development, the milk duct is lined by epithelial cells. The middle of the duct is hollow, allowing space for breast milk to be secreted and stored. In breast cancer, tumors develop within the epithelial cells that line the milk duct [35]. As

these tumor cells proliferate, they begin to fill up the hollow area. Cells in the middle of the duct are furthest away from the vasculature and therefore have very limited access to nutrients and oxygen from the bloodstream. This starvation and low oxygen (hypoxic) environment induces cell death via necrosis in many of these cells[36]. Eventually, some cells acquire the ability to recruit new blood vessels (angiogenesis) by secreting vascular endothelial growth factor (VEGF), which induces growth of the vasculature[37]. By redirecting the blood supply to support their growth, cancer cells are able to get the nutrients they need to grow even faster. However, once the area can no longer sustain the size of the tumor, local invasion begins. In this process, cells develop the ability to move through the epithelial ductal layer and invade into the surrounding stromal tissues. To initiate movement, cancer cells secrete MMPs (matrix metalloproteases) which degrade the surrounding matrix, allowing the cells to move between other cells. To form normal tissue, cells express certain adhesion proteins on their cell membranes that allow the cells to adhere to their neighbors. These adhesion proteins, such as β-catenin and e-cadherin, are often not expressed by cancer cells. This allows cancer cells to dissociate from one another and invade the surrounding tissue as single cells. When these cell-adhesion markers are maintained in a cancer cell, the cells instead can use collective cell motility, and form fingerlike projections or clumps that push out into the surrounding stroma [38, 39].

Intravasation and survival within the vasculature

Intravasation is the process by which tumor cells enter the bloodstream and lymphatic system in order to metastasize. Within and around a tumor, blood vessels are often leaky due to their quick turnover in the process of angiogenesis, which may enable

cancer cells to enter the bloodstream [37]. Once inside the vasculature, tumor cells need to evade the immune system, and withstand the high forces that are generated within the blood vessels. One way that tumors do this is to form emboli, or clusters of cells [40]. These clusters can secrete factors that attract platelets within the blood to congregate around the emboli[41]. The platelets form a cloak that surrounds the emboli and prevents the natural killer cells, macrophages, and other immune cells from detecting the cancer cell and destroying it[42].

Stopping at distant sites, extravasation, survival, and proliferation

Once a cancer cell has survived the bloodstream or within the lymphatic system, it must find a new site to go to in the body. Often cells will lodge themselves in the capillary beds where the vessel walls are too small to support the cell cluster[34]. Once stopped, the cell must escape from the blood vessel wall. It is likely that some of the features that made it easy for the cell to intravasate such as leaky vessels and less immune cell guarding are not present far from the tumor. Some studies suggest that MMP secretion as well as the ability of the cell to compress in order to squeeze through gaps in the vessel wall are involved in extravasation [43]. Once the tumor cells have escaped the vasculature, they must survive and form micrometastases. Further, it must be able to reactivate its proliferative program in order to colonize the new area. The "seed and soil" hypothesis proposed in 1889 by Steven Paget, describes how the seed (metastasizing cancer cell) coming from cancer of a particular organ usually forms micrometastases only in particular soils (areas of the body)[44]. Different factors such the characteristics of the new area as well as available signaling molecules may make a particular area more suitable for colonization. For example, studies have shown that the bone has an ideal pH

and calcium content to encourage colonization by breast cancer cells. In addition, cytokines and growth factors present in the bone may help metastases grow. Recent studies tracking breast cancer cells from primary tumor to micrometastases show that CXCR4 is overexpressed in breast cells that successfully metastasize[45]. CXCR4 is a receptor for CXCL12, a chemotactic factor which is expressed in the stromal cells of the bone, brain, liver, and lung [46]. Additionally, infliximab, an FDA approved monoclonal antibody therapy approved for treating Crohn's disease is a tumor necrosis factor (TNF)-α antibody, and has been shown to reduce breast cancer metastasis to bone in a murine xenograft model. This effect was shown to be mediated by a reduction in CXCR4 expression [47]. The wide expression of CXCR4 in specific tissues is one possible explanation for why breast cancer cells form metastases primarily in the bone, brain, liver, and lung.

Causes of metastasis

In the literature, theories abound about what causes a tumor to metastasize, but the exact mechanism explaining both how and why a tumor cell leaves the primary tumor is not known. Some hypotheses include the development of cellular autonomy, response to chemoattractants, exhaustion of local resources, and hypoxia effects. López-Lázaro proposes a model in which the hypoxic environment of the tumor results in increased glycolysis leading to secretion of high amounts of lactic acid. This helps to aid the tumor in acidifying the area around neighboring cells[48]. Recent work has shown that lactic acid secretion is important for the invasive properties of malignant glioma [49]. Moreover, tumor cells have been found to produce more oxygen radicals and hydrogen peroxide, which can also be released to do damage on surrounding cells [50, 51]. Finally,

increased hydrogen peroxide and accumulation of glycolytic intermediates due to upregulation of glycolysis can activate HIF-1 signaling. HIF-1 can activate a variety of genes, among which are matrix-metalloprotease-2 and vimentin, which are important in the metastatic process [52]. HIF-1 also inhibits the cell-adhesion cadherin proteins, which would allow cells to detach and move freely [53].

The mevalonate pathway: crossroads of metabolism and motility

The mevalonate pathway, also known as the cholesterol synthesis or isoprenoid biosynthesis pathway, is necessary for the production of a wide variety of metabolites including cholesterol and hormone precursors[54]. In addition, this pathway produces prenyl groups, which are required for the membrane localization of small GTPase proteins. The prenyl groups, farnesyl pyrophosphate and geranylgeranyl pyrophosphate are covalently added to specific targeting sequences on proteins, such as the CaaX box on RhoC, where C is a cysteine residue, a is an aliphatic amino acid, and X is a specific terminal amino acid which varies among the different enzymes[55]. The prenyl groups on small GTPases allow them to embed themselves into the cell membrane, which enable them to direct cell motility [56]. In this way, the mevalonate pathway lies on the intersection of cell motility and metabolism.

Statin drugs, such as atorvastatin (Lipitor) have been used for many years to treat hypercholesterolemia. Statins target HMG (3-hydroxy-3-methylglutaryl)-CoA reductase, the first enzyme in the mevalonate pathway[55]. This pathway is also targeted by bisphosphonate drugs, which are used primarily to increase bone mass in osteoporosis patients[55]. In addition, both GGTIs (geranylgeranyl transferase inhibitors) and FTIs (farnesyl transferase inhibitors) target this pathway. New evidence suggests that

targeting the mevalonate pathway may be an effective way to treat cancer. Nitrogen-containing bisphosphonate drug zoledronic acid is currently used in the clinic to decrease incidence of skeletal related events and bone loss in breast cancer patients [57-59]. Additionally, the mevalonate pathway may play a role in breast cancer incidence. Some studies suggest that colorectal cancer risk is reduced in patients on long-term statin therapy[60]. Also, retrospective studies of women taking zoledronic acid have reduced breast cancer risk[61].

MAPK p38 gamma introduction

Recent work has shown that RhoC expression level is regulated by p38γ, an important member of the MAPK (mitogen-activated protein kinase) signaling cascade [62]. The MAPK cascade is an important regulator of cell proliferation, migration and motility [63]. The p38 protein has four splice-isoforms, α, β, γ, and δ. Isoforms α and β are homologous as are isoforms γ and δ, however it appears that all isoforms have a unique function. In the literature, primarily isoforms α and β are studied, and known p38 chemical inhibitors are only active against a conserved ATP binding site present in α and β isoforms that γ and δ isoforms lack[64]. Knockdown of p38γ abrogated cell motility and increased the proliferative rate in these cells.[62]

The MAPK pathway is frequently dysregulated in cancer[65]. To initiate signaling of the MAPK pathway, ligands such as growth factors bind to membrane bound tyrosine kinase receptors (RTKs) which dimerize and transphosphorylate their cytoplasmic tails. These phosphorylated tails then recruit other proteins to dock and form signaling complexes. In cancer, the RTKs are often altered by mutations making them constitutively active, where they do not require ligand or dimerization to be activated, or

RTK genes are amplified, resulting in a greater overall signal due to increased dimerization partners available[63]. In addition, cancer cells may increase both autocrine and paracrine signaling, which leads to increase MAPK activation[63].

The MAPK pathway and the AKT/PI3K pathway interact to regulate cell growth and proliferation with the mammalian target of rapamycin (mTOR) [66]. In addition, these pathways work together to modulate HIF-1α, which is critical for regulating the response to hypoxia[15]. Because mTOR plays such a significant role in regulating cell metabolism, fully understanding the interactions and cross-talk between the MAPK and AKT/PI3K pathways and mTOR will be vital to teasing out the regulation of metabolism in cancer cells.

The remaining chapters of this work discuss the mevalonate pathway and its potential as a therapeutic target, TCA cycle metabolism and an alternative metabolic pathway found in a breast cancer cell line, and studies examining the altered metabolism found in p38γ knockdown cells. A brief synopsis of each chapter follows.

Chapter II: Zoledronic acid treatment prevents phosphorylation of CUB-domain containing protein 1 and leads to decreased motility and invasion in breast cancer

In this chapter, the effect of three different inhibitors of the mevalonate pathway – atorvastatin, zoledronic acid, and GGTI-298–is examined on metastatic properties of breast cancer cells. In addition, an alternative mechanism independent of mevalonate pathway inhibition is proposed for zoledronic acid. In this mechanism, zoledronic prevents the activation of CUB-domain containing protein 1 (CDCP1), which is an

important regulator of invasion and metastasis. CDCP1 must be both cleaved and phosphorylated on its tyrosine residue to recruit its downstream signaling partners. Zoledronic acid prevents phosphorylation of CDCP1, thus preventing signaling downstream of CDCP1.

Chapter III: Alternative pathway for acetyl CoA metabolism prevents inflammatory breast cancer cell line SUM149 from undergoing oxidative phosphorylation

In this chapter, the metabolic properties of inflammatory breast cancer cells are examined using the cell line model SUM 149. An alternative pathway is uncovered in which acetyl-CoA is used for the synthesis of N-acetyl aspartate instead of citrate synthesis. The redirection of acetyl-CoA prevents accumulation of other substrates in the TCA cycle required for oxidative phosphorylation. As a result, SUM149 cells do not undergo oxidative phosphorylation.

Chapter IV: Unbiased metabolomic screening reveals key metabolic pathways responsible for energy switch from proliferation to motility in breast cancer cells

In this chapter, unbiased metabolomic screening is used to uncover a possible behavioral switch in cancer cells that results in a change of energy use from a proliferative program to a motility program. In this paper, MDA-MB-231 cells are used as a model with p38γ MAPK stably knocked down with shRNA. Several metabolic pathways are discovered to be differentially regulated by p38 γ knockdown.

Perturbations of these pathways show which is the most important in the metabolic switch between proliferation and motility.

Discussion and Future Work

Dissecting the metabolic alterations that lead to metastasis will provide a new prospective for understanding the process by which cells gain the ability to metastasize. Understanding metabolic alterations that occur in cancer progression can lead to the identifications of targets for chemotherapy, as well as new treatments to prevent breast cancer metastasis. Because cancer often relies on certain pathways and is unable to redirect its metabolism as easily as a normal cell, metabolic therapies may be much more effective in cancer cells and have little to no effect on normal cells.

Figures

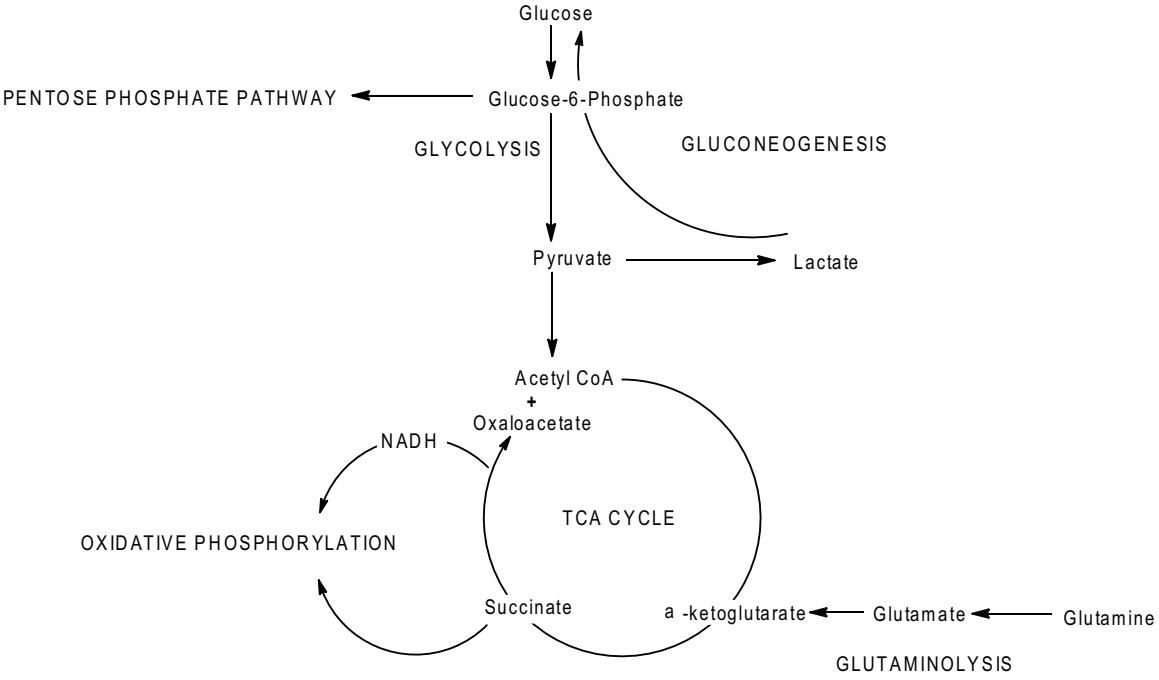

Figure I.1: Overview of Glucose Metabolism
Glucose is broken down into pyruvate via glycolysis and either made into lactate or acetyl-CoA for entry into the TCA cycle where substrates for a variety of biological processes are generated including succinate and NADH for oxidative phosphorylation.

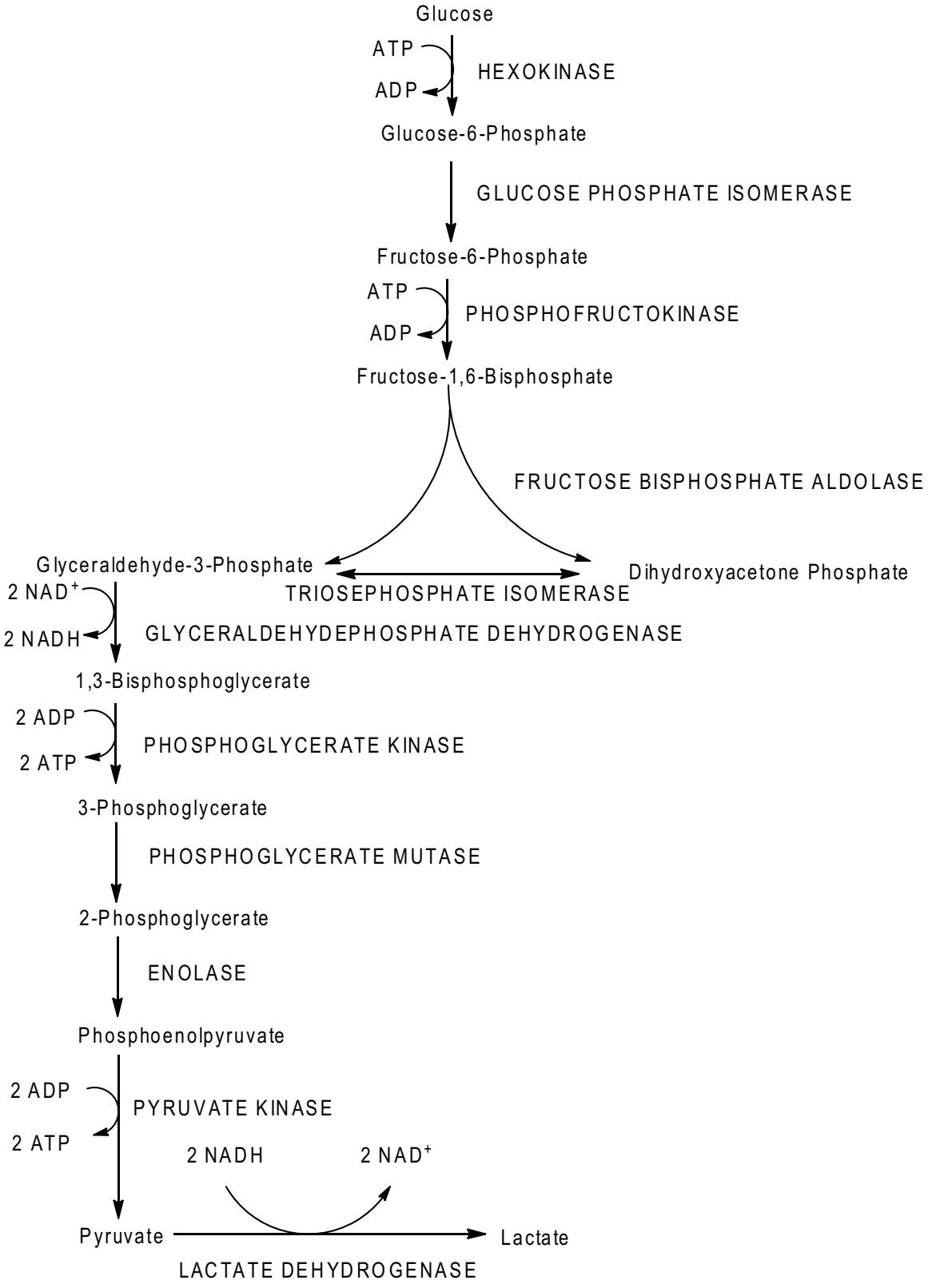

Figure I.2: Glycolysis

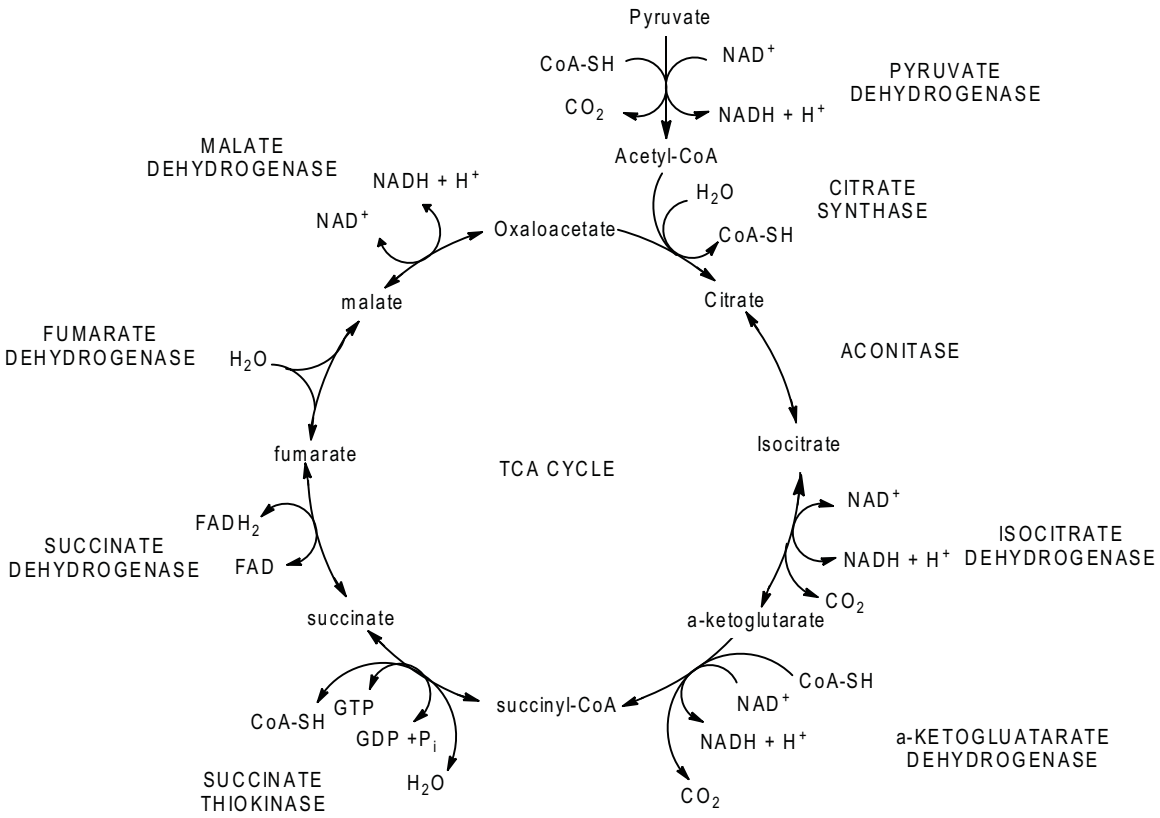

Figure I.3: The TCA Cycle

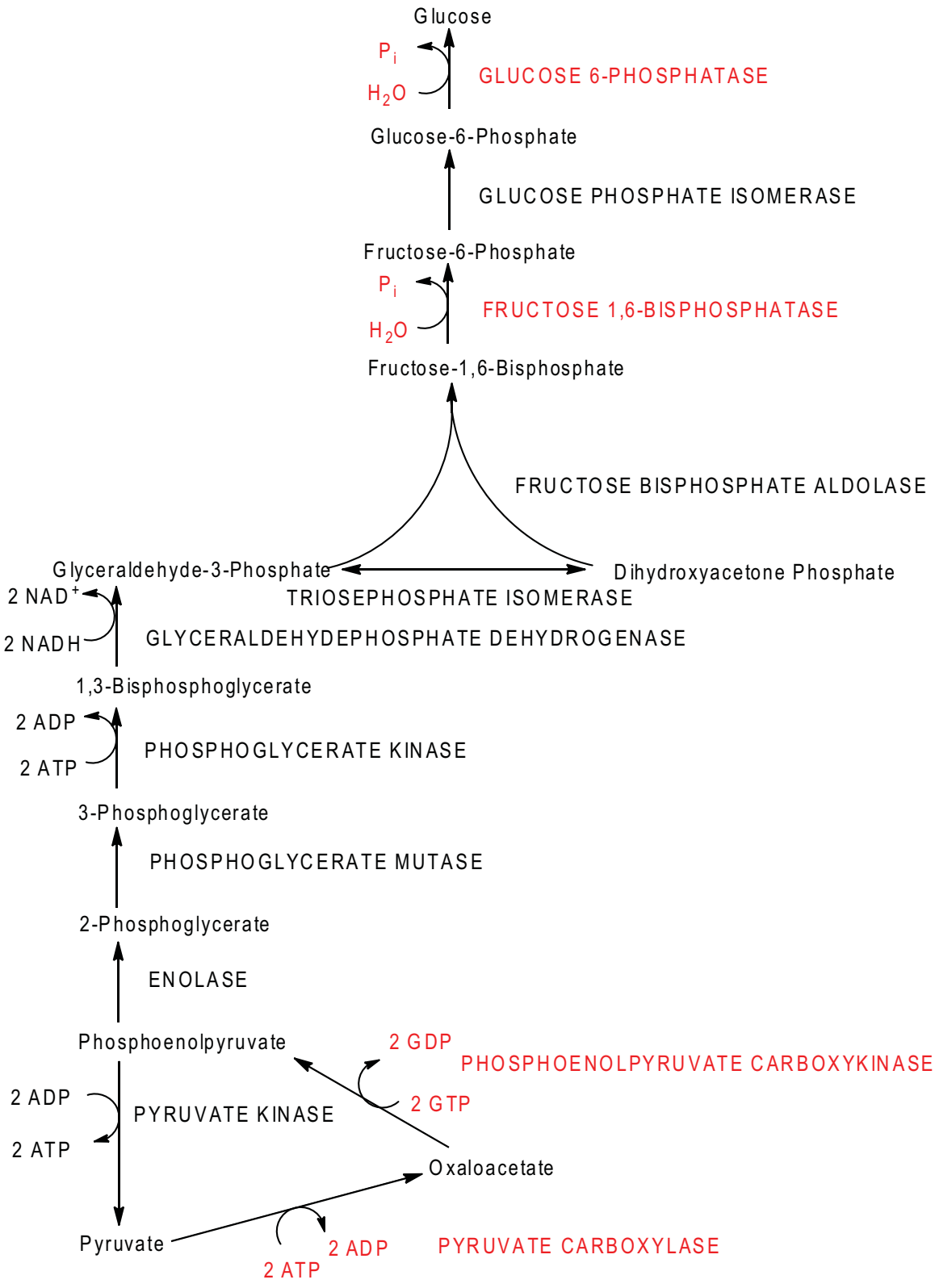

Figure I.4: Gluconeogenesis
Enzymes different from those used in glycolysis are shown in red with their reaction products and requirements.

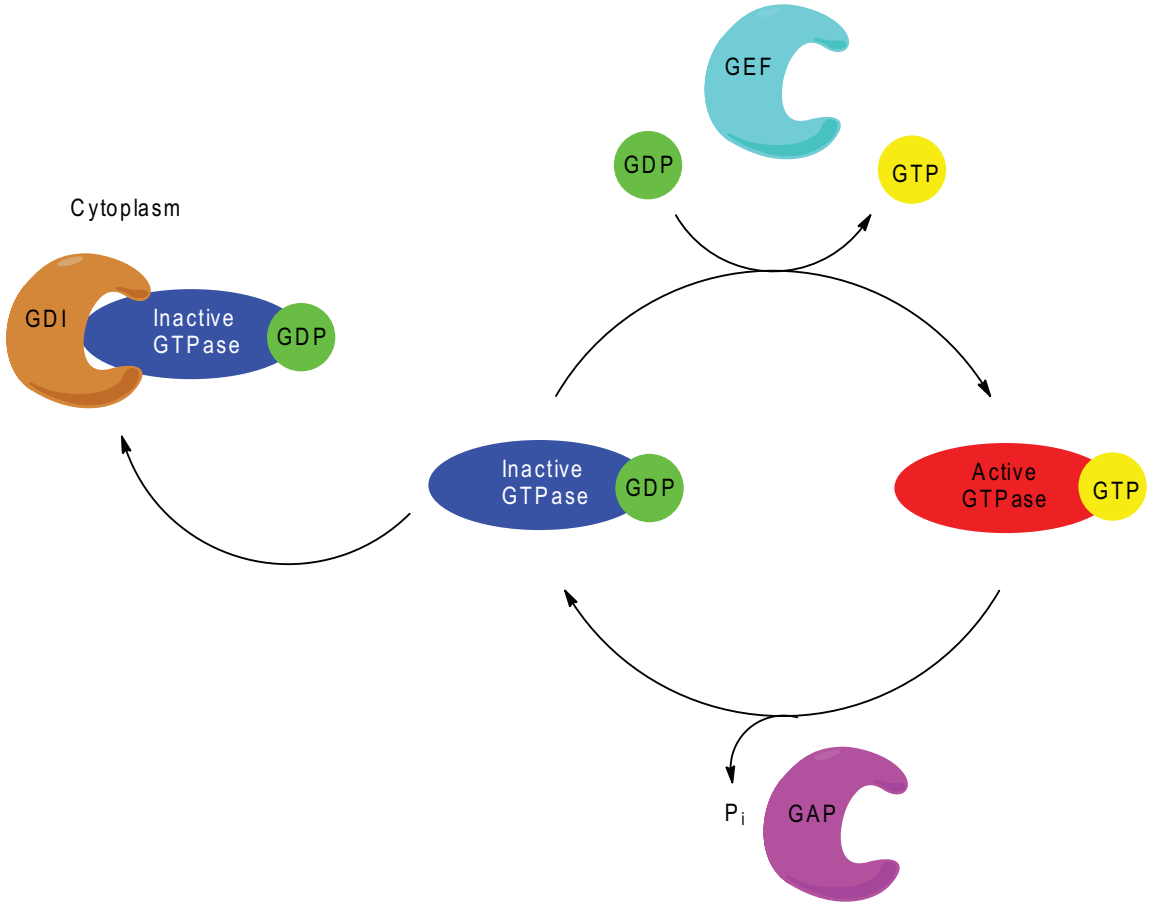

Figure I.5: The small GTPase cycle

Chapter II

Zoledronic acid treatment prevents phosphorylation of CUB-domain containing protein 1 and leads to decreased motility and invasion in breast cancer

Abstract

Zoledronic acid (ZA) has been shown to retard the spread of breast cancer to bone and viscera and is used in the clinic to ameliorate the effects of bone metastases and for the treatment of osteoporosis. As ZA is a known inhibitor of the mevalonate pathway enzyme farnesyl pyrophosphate synthase, the mechanism behind ZA's effect on metastasis was studied in comparison with two other mevalonate pathway inhibitors: atorvastatin (AT), a known HMG-CoA inhibitor, and GGTI-298, a geranylgeranyl transferase inhibitor. Treatment with AT and GGTI-298, but not ZA, decreases the membrane localization of motility regulators RhoC, RhoA, Rac and Cdc42, which is a robust surrogate for their activation. Despite the fact that ZA did not induce an effect on small GTPases localization, ZA decreased cell motility and invasion in these cells, suggesting an alternate mechanism of action for ZA. For the first time, a novel effect of ZA on the modulation of CUB-domain containing protein 1 (CDCP1) activity, an important regulator of cancer cell invasion and motility, is identified. ZA altered both the expression and activation of CDCP1 via phosphorylation.

Introduction

The acquisition of metastatic capabilities by cells often accompanies the development of mesenchymal characteristics, such as a reduction in cell-cell adhesion, an increase in protease secretion, and an elongated morphologic phenotype[67-70]. This multimodal transformation is termed the epithelial-to-mesenchymal transition (EMT) and is one of the first steps in the metastatic cascade [67, 69]. An important component of metastasis is cellular motility, which is regulated in many normal mesenchymal-like cells by small GTPase proteins, including Rac, Cdc42, RhoA and RhoC; all of which are prenylated and thus their function is intertwined with the mevalonate pathway, as they play major roles in aberrant motion and focal adhesion dynamics in various cancers[71, 72]. These proteins control the polymerization and depolymerization of actin filaments including lamellipodia, filopodia, and stress fibers in the protrusion-retraction cycle of cell motility [31, 73, 74]. Lamellipodia, controlled by active Rac, are flat, wide protrusive filaments. Filopodia, controlled by active Cdc42, are small extensions. Lastly, stress fibers, controlled by RhoA and RhoC, pull the rear of the cell forward [70, 73, 74]. The fact that these GTPase proteins are up-regulated in aggressively metastatic breast cancers has generated interest in studying inhibitors of their activation or function as potential anti-cancer drugs that specifically inhibit metastases.[31, 75]

Inflammatory breast cancer (IBC) is used in this study because of the prominent role that Rho GTPases play in this metastatic and lethal form of breast cancer[76]. One powerful molecular hallmark of IBC is overexpression of the small GTPase RhoC, which is present in over 90% of IBC tumor samples and causes an IBC-like phenotype when expressed at high levels in non-cancerous cells [72, 77-79]. While primary IBC tumors

have the potential to metastasize quickly, they do not undergo complete classical EMT and instead retain cell-cell adhesion markers such as E-cadherin and β-catenin, and invade through surrounding tissue in cell groups or sprouts, termed emboli [68, 80].

The relative abundance and activation of Rho GTPase proteins in breast cancers in general, and RhoC in IBCs in particular, motivated the exploration of the signaling pathways responsible for their activation as potential therapeutic targets. The mevalonate pathway synthesizes prenyl groups, namely both farnesyl and geranylgeranyl groups, and attaches these groups to many proteins including the small GTPase proteins Rac, Cdc42, RhoA and RhoC. Attachment of prenyl groups targets these proteins to the lipid membrane for activation.[75, 81-83] Prenylation is considered key to the function of GTPases in motility and invasion.

In order to address the role of the mevalonate pathway in modulating metastases, inhibitors of three different enzymes in the pathway were compared: (1) the HMG-CoA (3-hydroxy-3-methylglutaryl CoA reductase) inhibitor atorvastatin (AT), (2) geranylgeranyl transferase inhibitor GGTI-298, and (3) the farnesyl pyrophosphate synthase inhibitor[84, 85] zoledronic acid (ZA) (Figure II.1A). Each of these drugs either shows anti-cancer activity in pre-clinical testing (GGTI-298) or is already in widespread use for neoplastic or non-neoplastic conditions (AT and ZA).

Statins, including AT, are approved to treat hypercholesterolemia, and have recently been shown to hinder tumor cell adhesion, migration, proliferation, and invasion in some cancer cell lines [86-90]. Geranylgeranyl transferase inhibitors (GGTIs) are known to inhibit in vitro invasion, proliferation and cancer cell migration, and induce RhoA translocation from the cytoplasm to the membrane in breast and colorectal cancer

cells [56, 90, 91]. Nitrogen-containing bisphosphonates, the most potent of which is zoledronic acid, are effective at treating osteoporosis and skeletal-related disease [57, 59, 92]. Nitrogen-containing bisphosphonates also inhibit cancer cell invasion and migration, induce apoptosis and cell cycle arrest, and prevent prenylation of RhoA [93, 94]; however detailed work uncovering the exact mechanism for its anti-cancer potential has not been fully elucidated.

In this chapter, the effects of three mevalonate pathway inhibitors (Figure II.1A) — ZA, AT, and GGTI-298 — on the metastatic properties of an aggressive, triple-negative breast cancer cell line (MDA-MB-231) and an IBC derived cell line (SUM149) are studied. The results reveal that GGTI-298 and AT inhibit every major in vitro cellular property believed to be characteristic of metastatically-enabled cells (MDA-MB-231 and SUM149), but not in non-transformed epithelial cells (MCF10A cells), implicating the mevalonate pathway as a crucial pathway for metastasis that is differentially active in these cancer cells. Despite the fact that ZA also inhibits in vitro live cell motility and invasion, it does not affect prenylation of RhoC, RhoA, Cdc42 or Rac, suggesting that it acts via a divergent mechanism. An alternative mechanism of action for ZA on cell motility and invasion is reported. In this mechanism, the activation of CDCP1, an important regulator of motility and metastasis that is often dysregulated in cancer, [95] is inhibited by ZA.

Results

Mevalonate pathway inhibitors atorvastatin and GGTI-298 significantly alter the morphology of breast cancer cells.

The effect of the three mevalonate pathway inhibitors on cell morphology was examined with immunofluorescence (Figure II.1B). Both AT and GGTI-298 altered the round cell shape to a more elongated or fusiform shape. This change was quantified (Figure II.1C) by measuring the aspect ratio, as described in the methods. ZA did not affect the cell shape of any of the cell lines, while AT had a significant effect on the shape of all three cell lines. GGTI only affected the shape of the two breast cancer cell lines. The changes in cell shape suggest that the mevalonate pathway inhibitors may also alter the ability of these cells to move [96]. This finding led us to examine motility in these cells.

Mevalonate pathway inhibitors decrease both individual and collective cell motility

In cancer progression, cancer cells often use either individual or collective cell movement to invade into their surrounding environment. To determine the effect of mevalonate pathway inhibition on cell motility, both individual and collective motility were examined. Single cell motility was studied with a bead motility assay and live cell microscopy (Figure II.2A, II.2B, II.7). These experiments showed that the mevalonate pathway inhibition decreased the motility of the cancer cell lines, but not the normal breast cell line MCF-10A. In addition, ZA had no effect on the individual cell motility of SUM149 inflammatory breast cancer cells.

To examine collective cell motility, quantitative wound-healing assays were performed (Figure II.2C, D). The mevalonate pathway inhibitors GGTI-298 and AT

were also effective in decreasing collective cell motility. Interestingly, ZA had no effect on the collective cell motility of MDA-MB-231 cells, but affected collective cell motility in SUM149 cells, which is a very important characteristic in IBC, because it is reported that IBC uses primarily collective cell motility to invade[68]. These results suggest that ZA may affect motility through a different mechanism than GGTI-298 and AT in these cell lines.

Mevalonate pathway inhibitors alter cell-cell adhesion in aggressive breast cancers

Collective cell migration depends on both the actin cytoskeleton and cell-cell adhesion. Due to the striking differences in collective cancer cell migration observed upon drug treatment, the expression and localization of cell-cell adhesion markers E-cadherin and β-catenin were analyzed (Figure II.3). E-cadherin expression was unchanged in SUM149 cells upon treatment with all 3 drugs, but its localization was more dispersed throughout the cytoplasm instead of mainly existing in the plasma membrane (Figure II.3A). The expression of β-catenin in SUM149 cells decreased upon drug treatment (Figure II.3B, C). As reported in the literature, MDA-MB-231 does not express E-cadherin with or without drug treatment (Figure II.3C). A weak β-catenin signal in MDA-MB-231 cells was observed, which increased upon treatment with AT and GGTI-298 (Figure II.3C), but not ZA.

Inhibition of the mevalonate pathway reduces the invasion of breast cancer cells

Another important component of the metastatic process is the invasion of tumor cells into the surrounding tissue. Invasion was measured and quantified using a Boyden chamber assay (Figure II.4A, B). The mevalonate pathway inhibitors effectively reduced the invasion of cells through the membrane, except for ZA in SUM149 cells. MCF-10A

cells were not used in this experiment because they, like other non-tumorigenic cells, do not possess the ability to invade.

Mevalonate pathway inhibitors alter the cellular localization of small GTPases.

Because treatment of cancer cells with mevalonate inhibitors led to a reduction of motility and invasion, it was hypothesized that this was caused by an inability of the small GTPase motility proteins to properly localize within cells. This change in localization could be due to a reduced addition of prenyl groups to these proteins via the effects of GGTI-298 or a reduced production of these groups due to AT or ZA action (Figure II.1A). To test the hypothesis, the expression levels of small GTPase proteins in both membrane and cytoplasmic cell fractions were measured (Figure II.5). Both AT and GGTI-298 prevented the localization of GTPases RhoC, RhoA, Rac, and Cdc42 to the membrane of cancer cells. This is shown by the reduction of these proteins in the membrane fraction and accumulation in the cytoplasm. ZA was unable to prevent membrane localization, however, suggesting that ZA may act through a different mechanism from that of either AT or GGTI-298. It has been suggested that at low concentrations ZA and other bisphosphonate drugs may act independently of inhibition of farnesyl phosphate synthase [85].

ZA modulates protein expression and prevents phosphorylation of CDCP1

To identify alternative targets for the mechanism of action of ZA on the motility and invasion of cancer cells, a gene expression microarray screen was performed on untreated cells and cells treated for 72 hours with ZA (Figure II.8). Three cell lines were used in the screen: SUM149, MDA-MB-231, and MCF10A. When gene expression in the cells treated with ZA was compared to gene expression in the untreated cells, six

genes were identified that had a fold change greater than 2 and were common to all 3 cell lines. An additional 36 genes with a fold change greater than 2 were common to both cancer cell lines (Figure II.8A). Of these 42 genes, 18 were selected for further validation by quantitative RT-PCR because they were either upregulated in both of the cancer cell lines or downregulated in both of the cancer cells lines compared to MCF-10A (Figure II.8B, II.6A, II.9). The other 18 were oppositely regulated in MDA-MB-231 and SUM 149. Of these 18 genes chosen for quantitative RT-PCR validation, seven were found to have significantly different levels of mRNA expression after ZA treatment. Of these seven genes, CUB-domain containing protein 1 (CDCP1) was selected for further analysis because of its prominence in the cancer literature.

CDCP1 is a 135 kDa protein that is cleaved in vitro to a 70 kDa protein and once phosphorylated plays an important role in mediating the activation of the PI3K/AKT and MAPK/ERK pathways, resulting in increased cell survival, motility, and adhesion [97, 98]. At the protein level, increased expression of both cleaved and uncleaved forms of CDCP1 was observed in the membrane fraction of cell lysates in the cancer cells studied (Figure II.6B). To measure CDCP1 activation by phosphorylation on tyrosine residues, we conducted an immunoprecipitation experiment with anti-phospho-tyrosine and anti-CDCP1 (Figure II.6C). The data show that ZA treatment prevents phosphorylation of CDCP1 in the cancer cell lines. Taken together, these data suggest an alternate mechanism by which ZA can alter breast cancer cell behavior by modulating CDCP1 activation.

Discussion

While mevalonate pathway inhibitors have been studied in terms of in vivo primary tumor growth and prevention, as well as in vitro proliferation and apoptosis, their effects on metastatic properties have not been comparatively delineated or studied in depth. In this study, cell lines with varying degrees of metastatic behavior were compared: MDA-MB-231, an aggressive breast cancer line and SUM149, an IBC derived line. These lines were used as models of aggressive breast cancers. The effects of AT, GGTI-298 and ZA were not previously studied in IBC, despite the anti-metastatic potential of these drugs and its widespread use in patients at high risk for metastases or those with bone metastases. This study demonstrates that treatment with mevalonate pathway inhibitors induce a less aggressive phenotype in SUM149 cells across a broad range of in vitro assays. Moreover, this study suggests that these drugs may act through unique mechanisms due to the different inhibitory properties observed in distinct assays.

While some tumors (e.g. MDA-MB-231) metastasize in vivo primarily via single cells detaching from the primary tumor and targeting to lymphatic or blood vessels, a few tumor types (e.g. SUM149) undergo only partial EMT, and metastasize via groups or clusters of cells[68]. The single-cell migration results in this study are in agreement with previous work in which decreased migration of MDA-MB-231 cells upon treatment with fluvastatin or GGTI was observed [83]. The finding that all three drugs block collective cell migration for SUM149 cells and single-cell migration in MDA-MB-231 cells suggests that all of the drugs, including ZA, have therapeutic potential to prevent metastasis in both types of breast cancer in vivo.

Based on these results, the expression of two key cell-cell adhesion markers E-cadherin and β-catenin, which are known to be involved in EMT, were analyzed. In MDA-MB-231 cells, β-catenin expression increases upon treatment with AT and GGTI-298. Because MDA-MB-231 cells undergo a classical EMT, this increase in cell-cell adhesion likely indicates a relative loss of mesenchymal-like characteristics and it is presumed to result in a greater propensity for single cells to escape the primary tumor mass. This may explain the loss of collective cell migration observed in MDA-MB-231 cells when treated with AT and GGTI-298, but not when treated by ZA, which itself does not change expression of β-catenin.

The changes observed in single cell migration with drug treatment match those seen in invasion. This finding supports the notion that the force generated by actin protrusion and retraction in the membrane corresponds to the ability of cells to invade through the extracellular matrix [70]. Additionally, invasion may also be affected by mevalonate pathway inhibitors because of the role of Rac and Cdc42 in inducing the expression of secretion proteases, such as MMPs, which serve to break down the extracellular matrix [67].

Invasion is the most studied biological property with respect to the effect of mevalonate pathway inhibitors. Invasion is thought to be one of the *in vitro* properties of cells that most closely aligns with *in vivo* metastatic potential, because of its use of a 3D matrix that closely simulates the extracellular matrix [99]. Many groups report that AT, cerivastatin, simvastatin and lovastatin treatments prevent invasion of MDA-MB-231 cells, melanoma cells, H-Ras MCF10A cells, and COLO 320DM colon cancer cells respectively, through a Matrigel transwell chamber [81, 89, 90]. In addition, Kusama et

al. report that use of GGTI-298 also inhibits the invasion of COLO 320DM colon cancer cells [90]. Our results are in agreement with the literature and indicate that statins may have promising anti-metastatic potential *in vivo*.

Several studies have reported translocation of RhoA and RhoC from the membrane to the cytoplasm upon treatment with statins and GGTI-298 in melanoma, colon and breast cancer cells [81, 83, 86, 90]. The data presented here strongly support these results in additional cell lines and has led to the recognition that Rac and Cdc42 undergo the same translocation upon treatment with these inhibitors. ZA, despite having been ascribed a similar mechanism of action in the literature, is much less effective than statins or GGTIs at preventing Rho GTPase membrane localization.

The decrease in Rac activation can explain the significant loss of lamellipodia in AT and GGTI-298 treated MDA-MB-231 and SUM149 cells. The long, thin projections remaining after drug treatment could be simply elongated filopodia (controlled by active Cdc42), or stress fibers (controlled by RhoA and RhoC). The inability of ZA to prevent activation of the small GTPase proteins is a plausible explanation for its minimal effects on cytoskeletal architecture, which is a surprising result of our study.

The inability of ZA to prevent small GTPase localization to the membrane in aggressive breast cancer cells led to an investigation of the possibility that ZA may be targeting an alternate pathway. Utilizing gene expression microarrays, several plausible alternate targets were identified and validated by quantitative RT-PCR. It was found that ZA alters mRNA and protein expression levels of CDCP1 in aggressive breast cancer cells. In addition, it was found that ZA prevents the phosphorylation of CDCP1, which is required for this protein's activation. The possibility that inhibition of activation of

CDCP1 is a major effector of the action of ZA in aggressive breast cancers is depicted by a mechanistic model, shown in Figure II.6D.

CDCP1 expression has been implicated in several cancers as a potential anti-tumor target. CDCP1 protein is activated by both a cleavage event and phosphorylation. CDCP1 cleavage has been shown to activate the pro-survival, anti-apoptotic AKT pathway [100], while phosphorylation of CDCP1 by src-family kinases (SFKs) leads to the recruitment of PKC-δ, and increased cell motility and resistance to anoikis [100]. Because ZA treatment increased both the cleaved and uncleaved forms of CDCP1 and CDCP1 cleavage has been shown to activate the pro-survival, anti-apoptotic AKT pathway, we postulate that ZA's inhibition of CDCP1 activation via phosphorylation leads to increased CDCP1 expression at the mRNA and protein level in an attempt to overcome this inhibition.

Along with identifying CDCP1 as a potential target of the anti-tumor action of ZA, the gene expression microarray analysis also identified 23 genes that are regulated in opposite directions by ZA in the MDA-MB-231 and SUM149 cell lines. This may help to explain the differential ability of ZA to modulate the metastatic potential of MDA-MB-231 and SUM149 cells. We propose that these genes may be worthy of further investigations in this regard.

Recently, retrospective studies have shown that women taking ZA to prevent osteoporosis have reduced incidence of breast cancer [59, 61]. The mechanism explaining how ZA might act to prevent breast cancer occurrence is currently unknown. The new model we propose for the mechanism of action of ZA may also help to explain this drug's role as a breast cancer prevention agent. In the future, it will be informative to

test mice that are genetically modified to develop breast cancer with ZA to evaluate for delays of onset or reduction in breast cancer risk.

Based on these data, we conclude that the mevalonate pathway remains an attractive candidate pathway for drugs targeting metastasis. Statins and bisphosphonates are routinely used for treatment of other diseases with minimal toxicity. First-generation GGTIs, however, have shown unacceptable toxicities in mice and human patients. Lobell et al. report that GGTIs may cause edema and decreased blood pressure at doses high enough to prevent Ki-Ras prenylation [101]. However, Sun et al. report no negative side effects for GGTI treatment at lower doses [102]. In our studies, MCF-10A, used as a normal-like control cell line, shows little evidence of direct toxicity upon treatment with GGTI, with the exception of lower single cell velocity with GGTI-298. However, in vivo toxicity testing at corresponding doses in mice has not been conducted. Therefore, both AT and ZA appear to be excellent drugs for future detailed murine studies to delineate their anti-metastatic properties in vivo for further clinical development as anti-metastatic agents.

Methods

Cell culture and drug treatment

MCF10A cells were cultured in 1:1 Ham's F-12 and Dulbecco's modified Eagle's medium (DMEM) with 2 mM L-glutamine supplemented with 5% horse serum, extracellular growth factor, cholera toxin, insulin, hydrocortisone, gentamycin, fungizone, and penicillin/streptomycin at 37ºC under 5% CO_2. MDA-MB-231 cells were cultured in RPMI 1640 supplemented with 10% fetal bovine serum, gentamycin, fungizone and penicillin/streptomycin at 37ºC under 5% CO_2. SUM149 cells were

cultured in Ham's F-12 with L-glutamine supplemented with 5% fetal bovine serum, insulin, hydrocortisone, gentamycin, fungizone and penicillin/streptomycin under 10% CO_2.

For drug treatment, all cells were grown to 30-50% confluence, serum starved for 16-20 hours, then treated with 10μM AT (dissolved in methanol) or 10μM GGTI-298 (dissolved in DMSO) for 48 hours total, or with 10μM ZA(dissolved in PBS) for 72 hours total in serum-containing medium. Medium containing ZA was replaced after 48 hours. Drug concentration and treatment times were determined based on what has been previously reported in literature [83, 102-105] and results from cell proliferation assays (MTT assays, data not shown). The concentrations used were effective at inhibiting growth of MDA-MB-231 and SUM149, but not MCF10A cells.

Phospho-CDCP1 Immunoprecipitation/Western blotting

Protein was extracted from 70% confluent cells with radioimmunoprecipitation assay buffer with Complete Mini protease inhibitor cocktail (Roche) added. Total protein extracts were incubated with primary antibody (anti-CDCP1 or anti-phospho-tyrosine) overnight at 4°C. The following morning protein–antibody complexes were captured by incubation with protein A/G beads (eBioscience). Immunoprecipitates were run on an SDS-PAGE gel, transferred to a polyvinylidene fluoride (PVDF) membrane, and probed with the appropriate reciprocal antibody (anti-CDCP1 or anti-phospho-tyrosine). All immunoprecipitation and Western blot data represent at least 3 independent experiments.

Protein extraction and Western blot

Cells were washed with cold phosphate-buffered saline (PBS) and lysed in a radioimmunoprecipitation assay buffer plus protein inhibitor cocktail. Cells were sheared

with a 23 gauge syringe and protein was collected after centrifugation. 30-60μg of protein was electrophoresed onto a SDS-PAGE gel (12.5%). The protein was transferred to a PVDF membrane using a semidry apparatus (BioRad). The membrane was blocked using 5% milk in TBST and incubated in 5% bovine serum albumin (BSA) in TBST with Cell Signaling antibodies anti-RhoC (1:1000 dilution), anti-Rac (1:2500), anti-Cdc42 (1:500) or Santa Cruz antibodies anti-RhoA (1:500), anti-E-cadherin (1:500), and anti-β-catenin (1:500) or BD antibody anti-β1 integrin (1:500). The membrane was incubated in 5% milk in TBST with Santa Cruz antibody anti-actin (1:1000) or in 3% milk in PBS with Upstate antibody anti-RhoGDI (1:1000). Membranes were incubated with anti-rabbit, anti-rat or anti-mouse secondary antibodies conjugated to horseradish peroxidase (HRP) at concentrations of 1:5000 in 5% milk in TBST. Protein bands were detected by autoradiography. All Western blot data represent at least 3 independent experiments.

Subcellular fractionation

Subcellular fractionation into membrane (M) and cytosol (C) fractions was performed as described previously [106]. Briefly, cells were washed, treated with lysis buffer and scraped from cell plates. Lysates were homogenized using a Teflon pestle and a Dounce Homogenizer. Homogenized cells were centrifuged to pellet nuclei, and then the supernatant was spun to pellet the membrane. Cytosol remained in the supernatant. A Bradford assay was conducted to measure total protein of each fraction.

Immunofluorescent staining

Cells were plated in 4-well collagen I-coated glass slides prior to drug treatment. After drug treatment, cells were fixed with 4% paraformaldehyde in PBS and permeabilized in 0.5% TritonX-100 at 4°C. Cells were blocked with 10% goat serum in

PBS and incubated with primary antibodies (the same antibodies and concentrations as for Western blots) and anti-rat or anti-mouse fluorescently tagged secondary antibodies (at 1:1000 dilutions) in goat serum. Cells stained only with Rhodamine/AF568-Phalloidin (actin) were fixed, permeabilized and incubated with a 1:50 dilution for 20 minutes. Coverslip was attached using Prolong Gold with DAPI.

Aspect Ratio Measurement

The aspect ratio (longest length divided by perpendicular width) of cells was measured using Image J software. Between 50 and 120 cells were measured for each condition.

3D cell culture

Cells were cultured on top of BD Collagen Matrigel in 8-well glass slides in normal medium supplemented with 5% Matrigel according to the protocol developed by Lee et al. 2007[107]. MCF10A cells were plated at a density of 500 cells per well, and were grown for a total of 7-8 days (3-4 days prior to drug treatment). MDA-MB-231 cells were plated at a density of 1500 cells per well for a total of 6-7 days (2-3 days prior to drug treatment). SUM149 cells were plated at a density of 1500 cells per well for a total of 8-9 days (4-5 days prior to drug treatment). Cell medium was replaced every two days.

Bead motility assay

The Cell Motility Assay (Thermo Scientific Cellomics) was used to measure single cell motility. Blue fluorescent beads were washed using 1X wash buffer (Dulbecco's PBS) at pH 7.2. Beads were plated into a collagen-coated 96-well plate and incubated at 37°C for 1 hour. The beads in the wells were washed 5 times with 1X Wash buffer. Pre-treated MCF10A, MDA-MB-231 and SUM149 cells were plated in the bead-

coated wells at a density of 400-600 cells/well and incubated for 16-24 hours (MCF10A and MDA-MB-231) or 40-48 hours (SUM149). Longer incubation times for SUM149 cells were required because they migrate slower than MDA-MB-231 cells in vitro, despite their motile and aggressive behavior in vivo. Images were taken of the center of each well (20X) using a Leica DMIRB microscope. 2 separate experiments with 5 replicates each were performed.

Live cell imaging

Cells were plated in 2 or 8 well Collagen I-coated glass-bottomed slides. Cells were treated in the slides and imaged 24 hours prior to the end of the treatment. Cells were imaged on an Olympus Deltavision-RT microscope once every 3 minutes for 12-18 hours total. For each experiment, 10 videos were taken per sample. At least 2 experiments were done per cell line per drug treatment to verify that cell behavior was the same, but only one experiment (75 cells) was analyzed for cellular velocity. Cellular velocity was analyzed using the ImageJ MTrackJ plugin.

Invasion assay

1-5×105 SUM149 or MDA-MB-231 cells were plated in BD BioCoat Matrigel Invasion Chambers in serum-free medium and chemoattractant (growth medium with serum) was added to the well beneath. Cells were incubated in the chambers for 24 hours (MDA-MB-231) or 48 hours (SUM149). Cells attached to the bottom of the inserts were fixed and stained with 1% crystal violet in methanol. Stained inserts were imaged using a Leica MXFL III stereo microscope. The stain was dissolved in 10% acetic acid and absorbance measured at 590nm. Before being plated into the invasion wells, cells were pre-treated such that the total treatment time (including the time the cells spent in the

invasion wells) was 48 hours for AT and GGTI-298 and 72 hours for ZA. A control assay was performed to verify that passaging the cells post-treatment did not affect their ability to adhere again to tissue culture plates upon continued treatment (data not shown).

Scratch assay

Cells were plated into 6-well plates at the following densities: 0.6×105 MCF10A cells per well, 1.5×105 MDA-MB-231 cells per well, and 2.5×105 SUM149 cells per well. Confluent plates were scratched with a sterile pipette tip 3 days after cells were plated for all three cell lines. Images were taken immediately after the scratch and the plate was marked in order to locate the same spot again either 24 hours later (for MCF10A and MDA-MB-231 cells) or 48 hours later (for SUM149 cells). Though in this experiment the SUM149 cells were incubated for a longer period of total time with the drug, their cell plates were also scratched one day earlier and the result was identical. Wound closure was quantified using ImageJ software.

Microarray Methods

RNA was isolated from MCF10A, MD-MBA-231, and SUM-149 cell lines grown with or without ZA treatment using Trizol according to the instructions. RNA was cleaned using the RNAeasy MinElute Cleanup Kit (Qiagen) according to instructions, and submitted to the University of Michigan Microarray Core. One experiment was done in duplicate. Expression values for each gene were calculated using the robust multi-array average method [108] . Only probesets with a 2 fold or higher change (when ZA treated cells were compared to untreated cells) were selected for comparison across the three cells lines, provided that one of the two samples had an expression value of at least 2^6.

Quantitative RT-PCR methods

RNA was isolated from cell lines grown with or without ZA treatment using Trizol. The Promega Reverse Transcription System was used according to package instructions to make cDNA from isolated RNA. SYBR Green Mastermix was used according to directions for Quantitative PCR. Three experiments were done in triplicate.

Figures

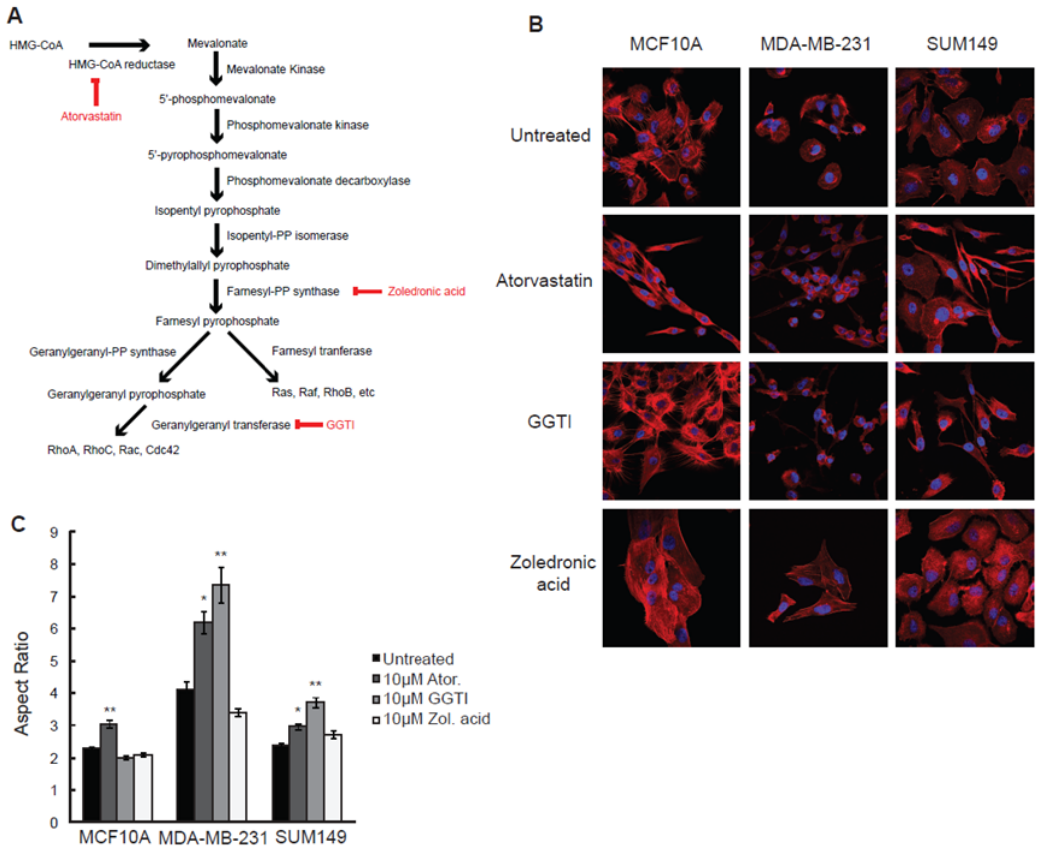

Figure II.1: Mevalonate pathway inhibitors alter the actin cytoskeleton and cellular shape of aggressive breast cancers in vitro
MCF10A, MDA-MB-231, and SUM149 cells were treated with inhibitors and stained immunocytochemically. (A) Diagram of mevalonate pathway illustrating the point of inhibition for each inhibitor used in this study. (B) Representative Phalloidin immunofluorescent stain for MCF10A, MDA-MB-231, and SUM149 cells treated with indicated inhibitor. Blue=DAPI, Red=Actin. (C) The aspect ratio (longest length divided by perpendicular width) of treated and untreated cells was measured. 50-120 cells were analyzed per sample.

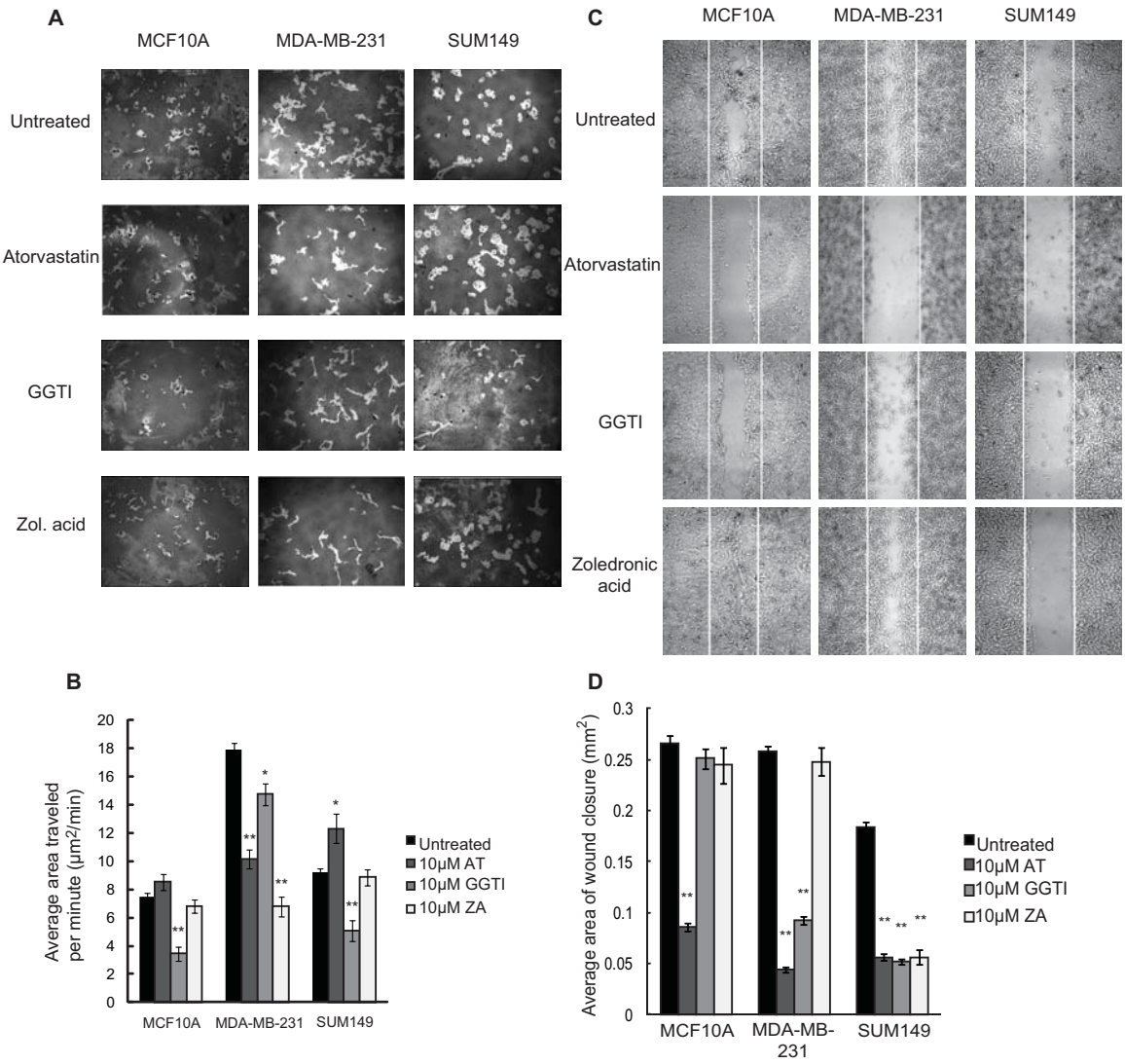

Figure II.2: Mevalonate pathway inhibitors reduce both single-cell motility and collective cell motility in aggressive breast cancers

(A) Treated and untreated MCF10A, MDA-MB-231, and SUM149 cells were plated in bead-coated wells and incubated according to the methods. Images were taken of the center of each well (20X). Representative images of 2 experiments, 5 replicates each. (B) Cell tracks were analyzed using ImageJ, and converted to μm2/min. At least 10 images were analyzed per sample. * indicates $p<0.05$ and ** indicates $p<0.0005$. Error bars, ±SD. (C) Wound healing assays according to the methods. The white lines represent original scratch mark prior to wound closure. A representative image of 2-3 separate experiments with 4 replicates each is displayed. (D) The area of wound closure was quantified using ImageJ for at least 8 images per sample. ** indicates $p<5\times10\text{-}6$. Error bars, ±SD.

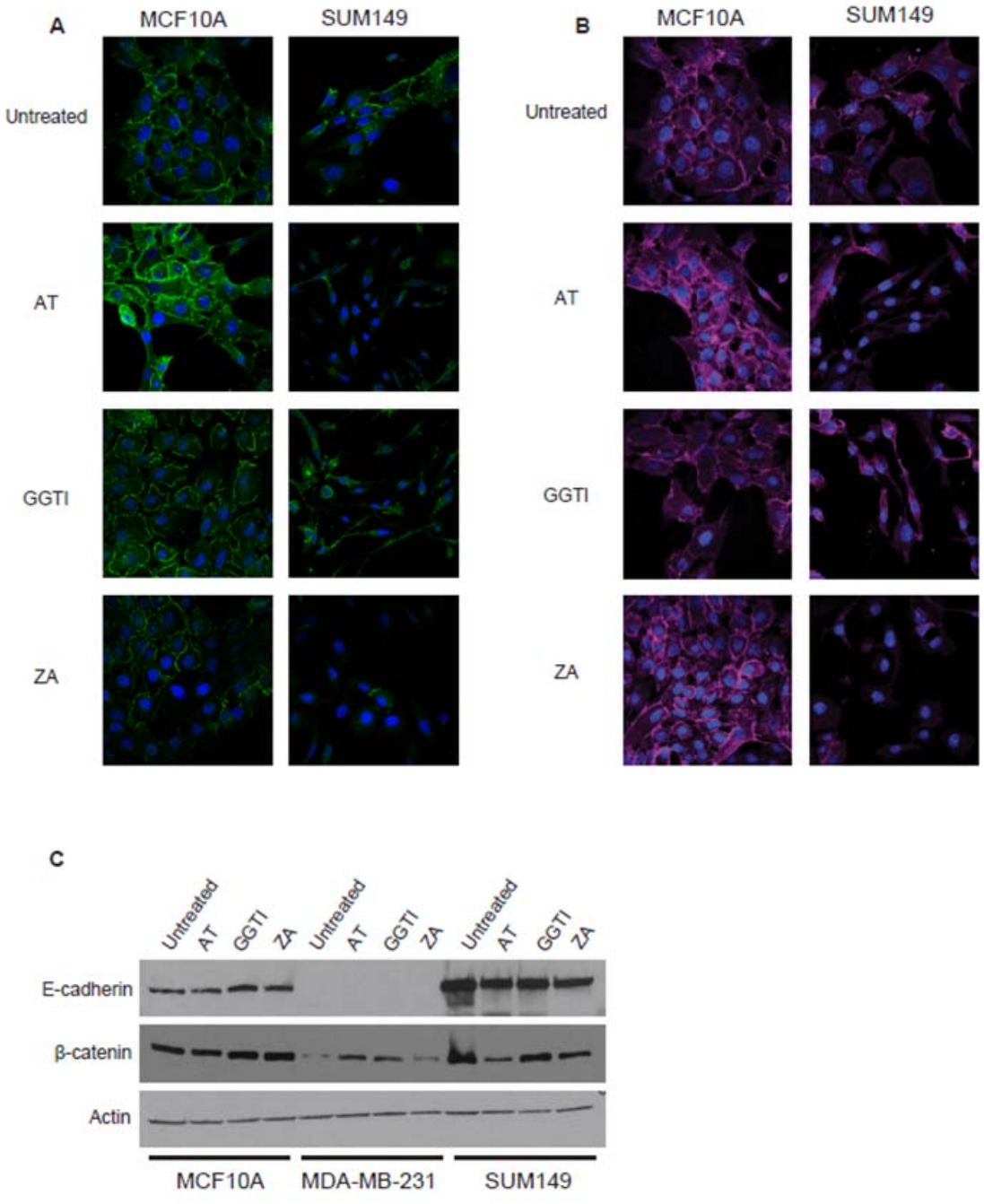

Figure II.3: Mevalonate pathway inhibitors alter cell-cell adhesion in aggressive breast cancers
MCF10A, MDA-MB-231, and SUM149 cells were treated with inhibitors and stained immunocytochemically as described in methods. Representative E-cadherin (A) and β-catenin (B) immunofluorescent stains for MCF10A and SUM149 cells untreated or treated separately with atorvastatin, GGTI-298, or zoledronic acid are shown. Blue=DAPI, Green=E-cadherin, Magenta=β-catenin. (C) Representative Western blot for total protein (n=3), indicating levels of E-cadherin, β-catenin, and Actin (+ loading control).

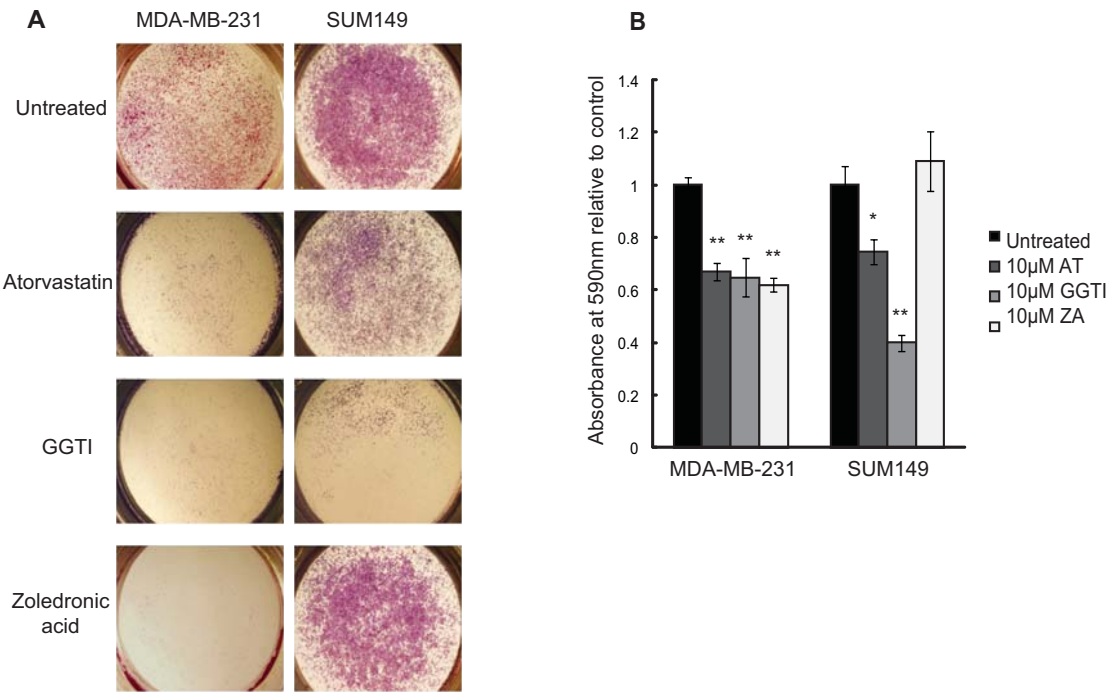

Figure II.4: Mevalonate pathway inhibitors inhibit invasion of aggressive breast cancers in vitro
(A) Transwell invasion assays were performed according to the methods. Representative images of crystal violet stained inserts at 2.5X. Two identical experiments were performed in triplicate. (B) Invasion assays were quantified by dissolving the crystal violet in acetic acid and measuring the absorbance at 590nm. Quantification includes all six inserts per sample. Treated samples were normalized to the control for the respective cell line. * indicates $p<0.05$, ** indicates $p<0.005$. Error bars, ±SD.

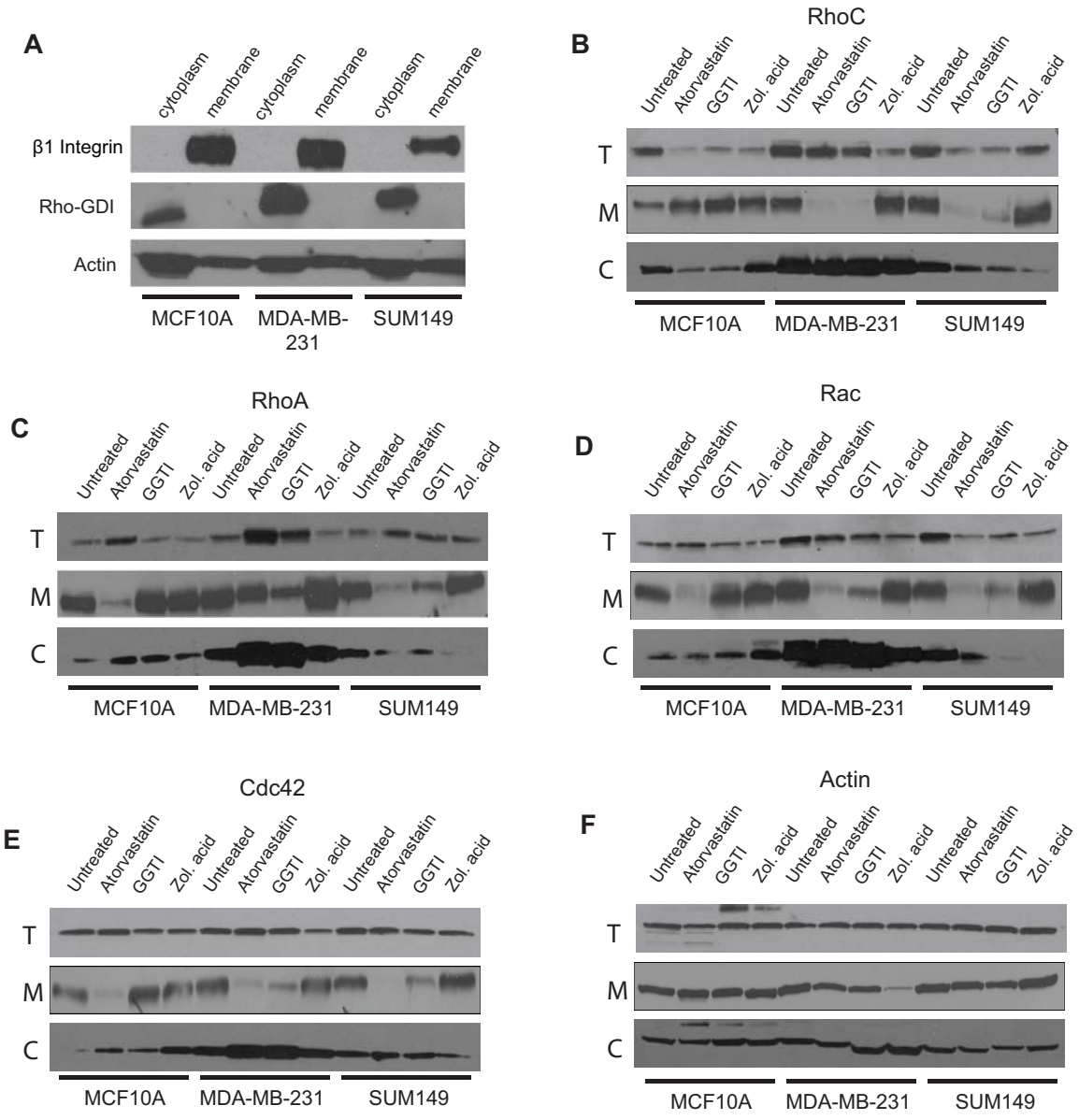

Figure II.5: AT and GGTI-298, but not ZA, induce RhoC, RhoA, Rac and Cdc42 translocation to the cytoplasm in MDA-MB-231 and SUM149 cells

MCF10A, MDA-MB-231, and SUM149 drug treatment, protein extraction and differential centrifugation were performed according to the methods. (A) Displays a positive control showing the purity of the cytosolic and membrane fractions. β1 integrin is the control membrane-bound protein and Rho-GDI is the control cytosolic protein. Representative western blots for total protein (T) (n=3), membrane-bound (M) fraction (n=2) and cytosolic (C) fraction (n=2), indicating levels of RhoC (B), RhoA (C), Rac (all isoforms, D), Cdc42, and (E) Actin (+ loading control, F) are shown.

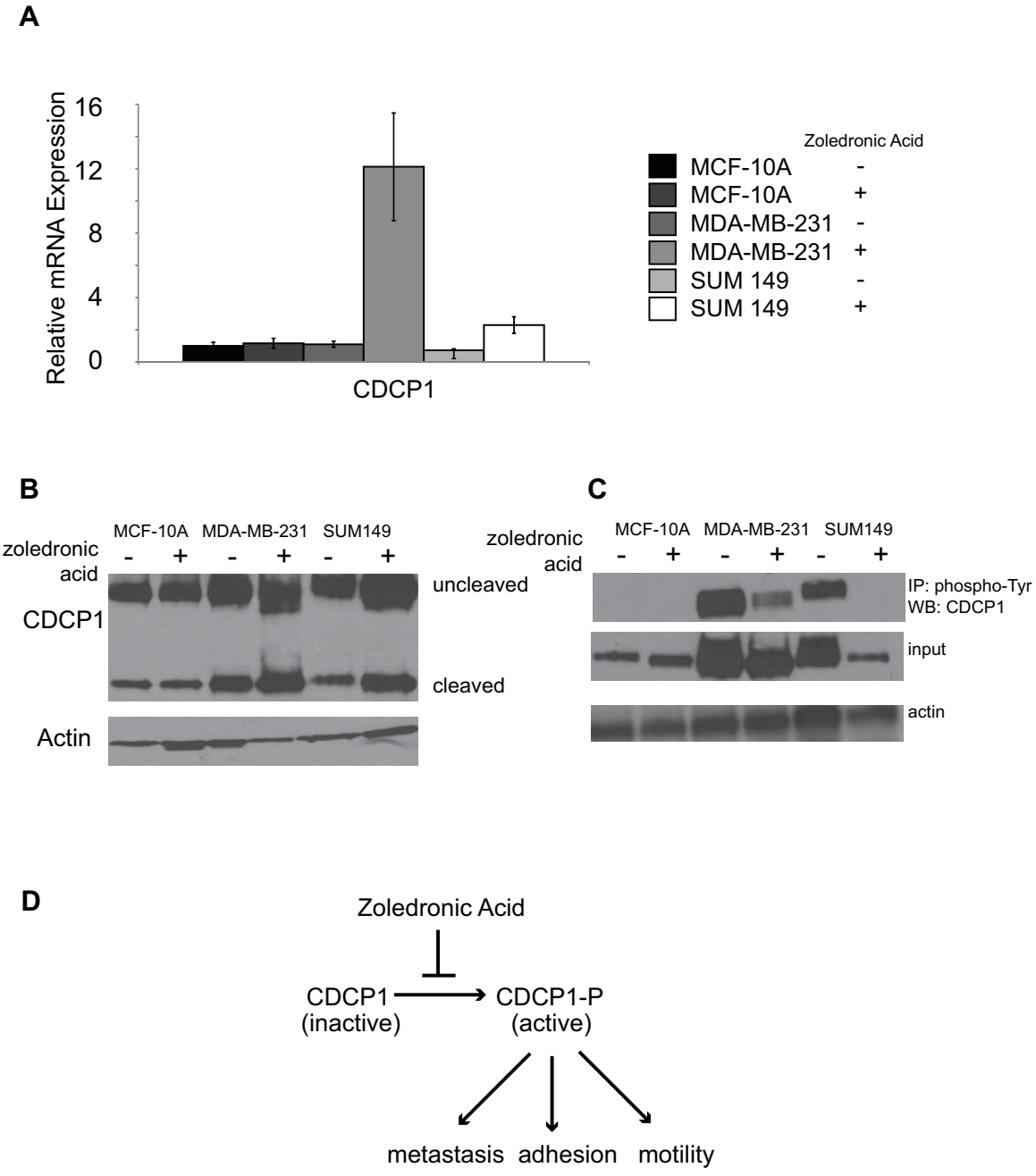

Figure II.6: Treatment of cell lines with ZA increases expression of CDCP1, and prevents phosphorylation

(A) Quantitative RT-PCR validation showing changes in mRNA expression of CDCP1 with ZA treatment in cancer cell lines. (B) Western blot of membrane-bound CDCP1. (C) Western blot of CDCP1 after IP of phospho-tyrosine. (D) Proposed model of action of ZA on CDCP1.

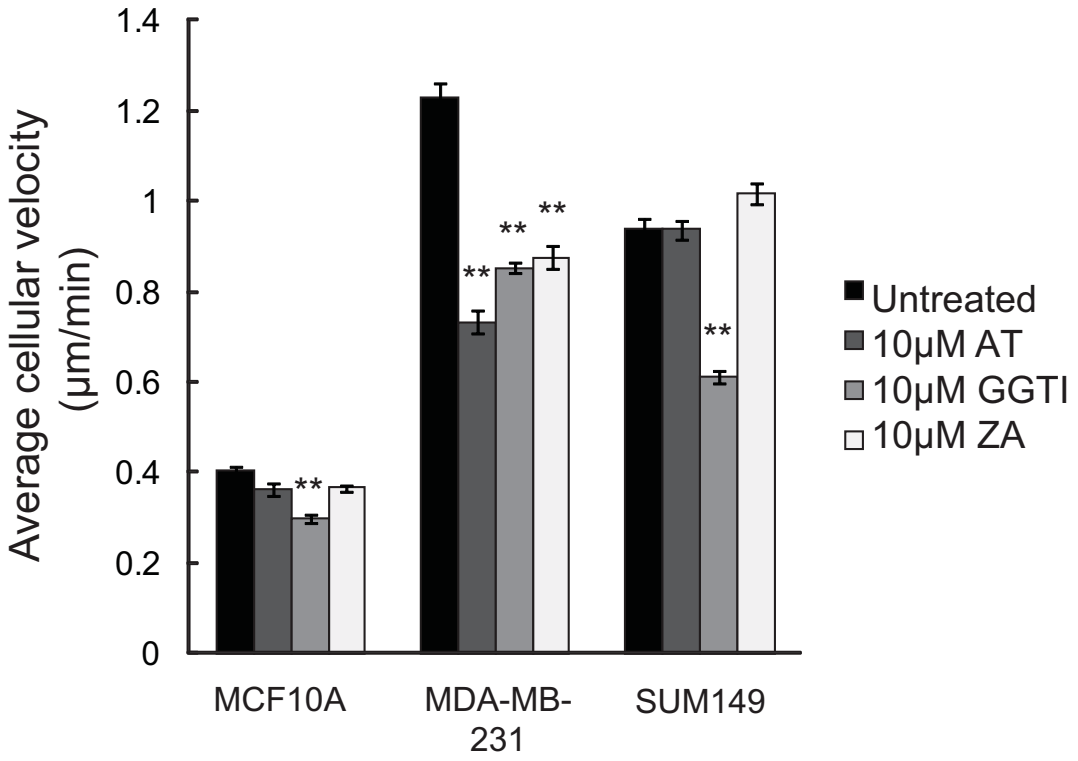

Figure II.7: Real-time imaging of cell movement
MCF10A, MDA-MB-231, and SUM149 cells were imaged according to the methods. Cellular velocity was measured using ImageJ plugin MTrackJ. 75 cells were analyzed per sample. ** indicates $p<5\times10\text{-}5$ Error bars, ± s.e.m.

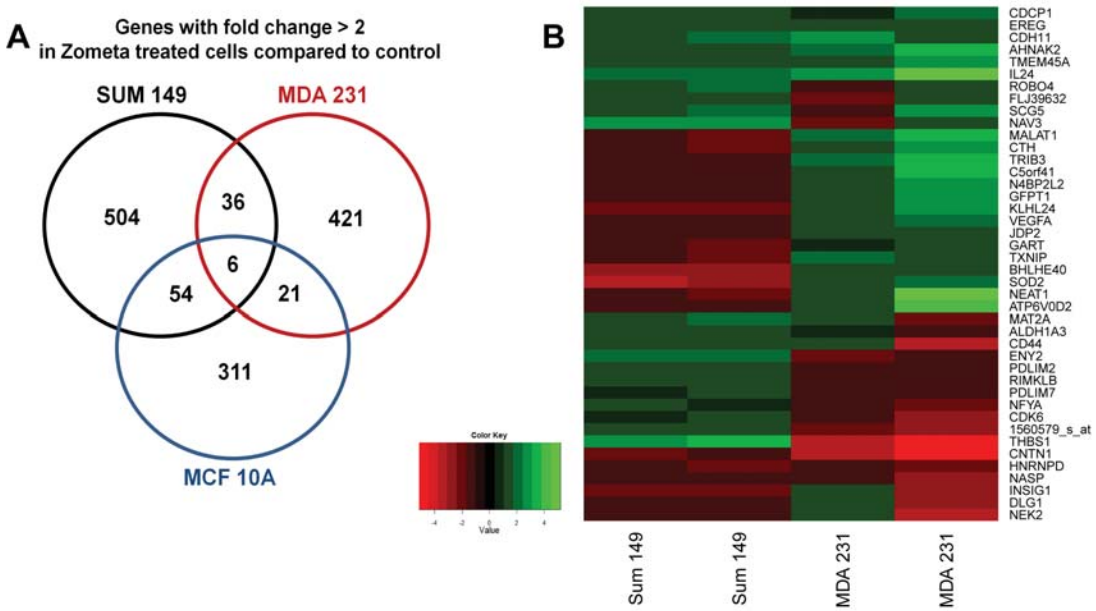

Figure II.8: Microarray to look for alternative gene targets of zoledronic acid in aggressive breast cancer cells
(A) Venn Diagram of gene counts differentially expressed greater than two-fold with zoledronic acid treatment. (B) Heatmap of 6 genes that were differentially expressed in all cell lines tested after zoledronic acid treatment as well as 36 genes that were differentially expressed in MDA-MB-231 and SUM149 (but not MCF10A) cells.

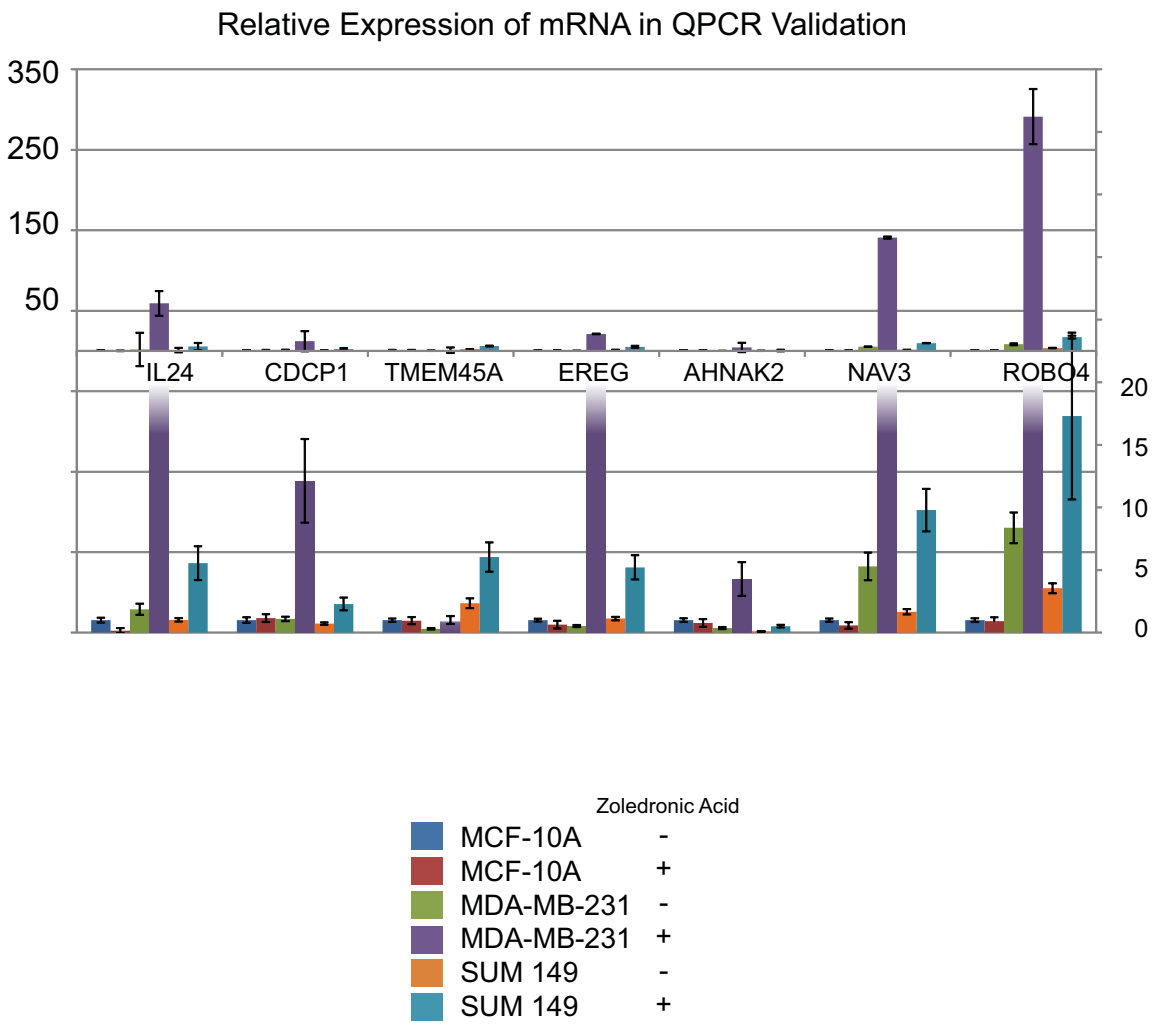

Figure II.9: Validation of hits from microarray data using Quantitative RT-PCR
Quantitative RT-PCR was used to validate selected microarray data. Only mRNA that showed significant expression level changes with ZA treatment are shown. Top panel shows complete data, bottom panel shows truncated data to show detail. This experiment was done three independent times in triplicate.

This chapter represents a "manuscript in submission" currently in review at *Molecular Cancer* under the title "Zoledronic acid treatment prevents phosphorylation of CUB-domain containing protein 1 and leads to decreased motility and invasion in breast cancer" by Lauren D. Van Wassenhove, Elizabeth J. Kennedy, ZhiFen Wu, LiWei Bao, Michelle L. Wynn, Sepideh Ashrafzadeh, Ling-Chen Chien, Eric A. Bracken, and Sofia D. Merajver.

Chapter III

Alternative pathway for acetyl CoA metabolism prevents inflammatory breast cancer cell line SUM149 from undergoing oxidative phosphorylation

Abstract

In the last 20 years, great advances have been made in the field of cancer metabolism. For example, alterations leading to changes in glycolysis due to differences in isoform expression of pyruvate kinase and regulation changes in phosphofructokinase have been identified [10, 11, 15]. Additionally, mutations in tricarboxylic acid (TCA) enzymes including isocitrate dehydrogenase have been discovered [18, 19]. However, the metabolic changes that occur in the rare and very aggressive inflammatory breast cancer (IBC) have not been previously studied. To characterize metabolic homeostasis that occurs in IBC, our lab used the cell line SUM149, derived from an IBC tumor, as well an aggressive triple negative breast cancer cell line, MDA-MB-231; normal-like breast epithelial cell line MCF-10A was used as a control. We performed bioenergetic profiling and mass-spectrometry-based metabolomics to assess metabolic differences between these cell lines. We demonstrate that SUM149 cells lack the ability to undergo oxidative phosphorylation. Additionally, these cells produce high levels of the metabolite N-acetyl-aspartate (NAA), a compound previously uncharacterized in IBC cells. Correspondingly, SUM 149 cells show near 20-fold upregulation of N-acetyl-aspartate transferase 8-l9ke (NAT8L) mRNA. This metabolic pathway may divert

pyruvate-derived acetyl CoA from the TCA cycle to formation of NAA, potentially contributing to the observed defect in oxidative metabolism.

Introduction

Inflammatory breast cancer is the most deadly form of breast cancer. It is very aggressive and consists mainly of large clusters that behave as tumor emboli, plugging lymphatic vessels in the skin overlying the breast and metastasizing sometimes even before the primary lesion is detected [109]. Because of the lack of targeted therapy for this disease, studies of the metabolic phenotype of this type of cancer were pursued in order to uncover special metabolic vulnerabilities that may be exploitable for therapeutic purposes. It has been shown that metabolic alterations that occur in cells play an important role in the development and aggressiveness of cancer [110, 111]; however the metabolic characteristics of inflammatory breast cancer have never been elucidated in detail.

By probing various metabolic pathways via bioenergetic profiling, mitochondrial enzyme activity assays and mass-spectrometry based metabolomics, we report here that SUM149 cells lack the ability to undergo oxidative phosphorylation due to an unknown defect which prevents the formation of TCA cycle intermediates for use in oxidative phosphorylation. Specifically, SUM149 cells do not direct acetyl-CoA made from pyruvate via glycolysis into the TCA cycle, but instead use it to acetylate aspartate generated from glutamine entering the TCA cycle via glutaminolysis. N-acetyl aspartate, a metabolite of unknown function outside the central nervous system, builds up to very high levels in the cell. As a result, very low amounts of early TCA cycle intermediates, like citrate and isocitrate, are available in the mitochondrial pool. The role that N-acetyl

aspartate plays in these cells, outside of serving as a *de facto* sink for acetyl-CoA, is yet to be uncovered.

Results

Inflammatory breast cancer cells do not use oxidative phosphorylation

In order to determine the basal respiration and respiratory capacity of each of the cell lines of interest, a bioenergetic profile assay and an extracellular acidification rate assay were performed on live cells (Figure III.1A-C). While MDA-MB-231 cells display a reduced oxidative capacity compared to the MCF-10A cells as predicted by the Warburg effect, SUM149 cells do not consume oxygen under the assay conditions, nor do they respond to any of the mitochondrial inhibitors. SUM149 cells produce an abundance of lactate, as indicated by the increased extracellular acidification rate (ECAR).

In order to determine whether SUM149 cells can be forced to undergo oxidative phosphorylation under different metabolic conditions, the same experiment was performed under low-glucose conditions of 2.5 mM. Even under conditions of low glucose, oxygen consumption rates did not change significantly (45 ± 11 pMoles/min under 2.5 mM glucose to 40 ± 9 pMoles/min with 11 mM glucose). Additionally, no response was observed when mitochondrial inhibitors were used (Figure III.5). As expected, in MCF-10A cells, low glucose increased consumption of oxygen and reliance of the cells upon oxidative phosphorylation for energy production. Once more glucose was added to return the concentration to 11mM glucose normally used in this assay, lactic acid production increased to a maximum of 72 ± 12 mpH/ min, which is twice that of the lactic acid production rate under low glucose conditions (32 ± 5), thus accounting for the additional glucose present.

In another attempt to force SUM149 cells to undergo oxidative phosphorylation, galactose was given as a substrate in lieu of glucose. Metabolism of galactose to pyruvate by glycolysis results in no net production of ATP, which means it can only serve as an energy-generating substrate through TCA cycle metabolism and oxidative phosphorylation. When SUM149 cells are given galactose, they respond weakly to mitochondrial inhibitors (Figure III.1C). These experiments suggest that the SUM149 cells may lack sufficient mitochondria, that their mitochondria might be damaged, dysfunctional, or inefficient, or that some signaling defect is preventing SUM149 cells from using their mitochondria. In order to delineate any potential mitochondrial defects, we undertook the next series of experiments.

SUM149 cells have sufficient numbers of mitochondria

Several different approaches were used to determine whether SUM149 cells have sufficient mitochondria. First, the protein expression of the mitochondrial marker Cox 4 was measured. Cox 4, a subunit of complex IV within the mitochondria, was decreased at the protein level in SUM149 cells (Figure III.6A). Next, the number of mitochondria per cell were examined using transmission electron microscopy (TEM), shown in Figure II.6B-D. This experiment illustrated that SUM149 have morphologically normal appearing mitochondria. Finally, quantitative-PCR was used to measure the ratio of mitochondrial DNA to nuclear DNA in each cell (Figure III.6E). This experiment found no significant difference between quantities of mitochondria per cell in each of the cell lines.

SUM149 cells have reduced protein expression of and less efficient mitochondrial enzymes

Once it was determined that SUM149 cells had sufficient mitochondria, their mitochondrial efficiency was investigated. To this end, the protein expression and activity of several key mitochondrial enzymes were measured. Citrate synthase, which catalyzes the conversion of acetyl CoA and oxaloacetate to citrate, had much lower expression in SUM149 and MDA-MB-231 cells (Figure III.2A). Citrate synthase activity was also reduced in both cancer cell lines to 20-30 % of the activity of that in MCF-10A cells (Figure III.2B). The mRNA of citrate synthase for all three cell lines was sequenced to look for mutations that would lower expression or activity. No mutations were found in any of the cell lines (not shown). The conversion of pyruvate to acetyl CoA for entry into the TCA cycle is catalyzed by a multisubunit complex called the pyruvate dehydrogenase (PDH) complex. This complex is made up of 3 catalytic subunits (E1, E2, and E3) and the E3 binding protein (E3bp). The activity of this complex is regulated by 2 phosphatases (PDP1 and PDP2) which activate the complex, as well as 4 kinases (PDK1-4) which inhibit the complex. The protein expression of the PDH complex was measured using an antibody that detects both the E2 subunit and E3 binding protein (E3bp). This experiment showed that E3bp was decreased in both MDA-MB-231 and SUM149 cells. Since the E3bp is important for holding the E2 and E3 catalytic subunits together in the complex, a lesser amount of E3bp may result in a lower overall stability of the complex[112]. In an activity assay, we found that the endogenous activity level of pyruvate dehydrogenase in SUM149 is about one-third the activity of MCF-10A cells and

suggests that this enzyme is mostly in its phosphorylated or "off" state, possibly due to regulation by the pyruvate dehydrogenase lipoamide kinases PDK1-4 (Figure III.2E).

Pyruvate is not being used as a fuel for the TCA cycle in inflammatory breast cancer cells.

Because SUM149 cells appear not to undergo oxidative phosphorylation, it was considered informative to investigate whether or not pyruvate is able to enter the mitochondria and be used as a TCA cycle substrate. A stable isotope labeling study using 2, 3-$^{13}C_2$ pyruvate was performed to track pyruvate metabolism in the cell (Figure III.3). This experiment showed an abundance of labeled pyruvate being converted into lactate in the SUM149 cells (III.3A). Although pyruvate was also metabolized to acetyl CoA, as is evident by the $^{13}C_2$ labeling in the acetyl-CoA pool after 15 minutes (III.3B), no label was detected in citrate or isocitrate in SUM149 cells (III.3C). The fact that ^{13}C labeling is detected in malate, a metabolite further downstream in the TCA cycle, suggests that glutamine is likely fulfilling an anapleurotic role, entering the TCA cycle as α-ketoglutarate (III.3D). The low levels of TCA cycle intermediates in SUM149 cells, and the lack of labeled pyruvate entering the pathway to make citrate and isocitrate suggested that acetyl-CoA may be shunted to a different pathway in these cells.

SUM149 cells undergo gluconeogenesis

To further describe how SUM149 cells utilize energy from we conducted experiments to investigate whether they are capable of undergoing gluconeogenesis. Experiments tracking 2, 3-$^{13}C_2$ pyruvate metabolism showed a portion of labeled 2-phosphoglycerate and 3-phosphoglycerate as well as fructose-1, 6-bisphosphate in all three cell lines examined (Figure III.3E, F). The presence of ^{13}C label in these glycolysis

intermediates suggests that the cells undergo gluconeogenesis. SUM149 cells perform the highest fraction of gluconeogenesis compared to the other cell lines investigated, with about 50% of 3-phosphoglycerate and fructose-1, 6-bisphosphate being made from pyruvate after 15 minutes incubation with label.

Acetyl-CoA is used to acetylate N-acetyl-aspartate in SUM149 cells

To further investigate alternative pathways that may be active in SUM149 cells, we conducted an unbiased metabolomic screen using MCF-10A, MDA-MB-231, and SUM149 cells (Figure III.4). Principle component analysis identified N-acetyl aspartate as the metabolite responsible for the greatest degree of separation between cell lines. We observed a very large pool of N-acetyl aspartate in both cancer cell lines compared to a very small pool in MCF-10A cells (Figure III.4A). N-acetyl aspartate is a metabolite that is important for brain function, but has no known function outside the nervous system [113, 114]. We conducted absolute quantification of the levels of N-acetyl aspartate with mass spectrometry (III.4B). This quantification showed a great abundance of N-acetyl aspartate in SUM149 cells, roughly 11.5 times the level of this metabolite in MCF-10A cells. The source of substrates for the synthesis of N-acetyl aspartate, as well as the enzymes responsible for its synthesis and degradation, are depicted in Figure 4C. The gene N-acetyl-aspartate transferase 8-like (NAT8L) encodes an acetyltransferase enzyme that acetylates aspartate. This gene is highly overexpressed in SUM149 cells at the mRNA level (Figure III.4D). In addition, the aspartoacylase (ASPA) gene encodes the hydrolase enzyme that breaks down N-acetyl-aspartate to acetic acid and aspartate. At both the mRNA level and protein level, SUM149 cells do not express this enzyme (Figure III.4D, E). Additionally, we observe ASPA protein expression only in MDA-

MB-231 cells, suggesting that while MDA-MB-231 cells are able to accumulate N-acetyl aspartate, they can also degrade it via ASPA (Figure III.4E).

Discussion

In this work, we found that SUM149 cells do not undergo oxidative phosphorylation. In the literature, reduced oxidative phosphorylation as well as a preference for glycolysis in cancer cells has long been understood (the Warburg Effect); however, such a severe phenotype which is entirely unresponsive to all mitochondrial inhibitors has not been described. When we examined the mitochondria of SUM149 cells, we found that they were morphologically similar to MCF-10A and MDA-MB-231 cells, and were present in similar numbers, suggesting that a lack of mitochondria or the presence of visually defective mitochondria does not explain their defect in oxidative phosphorylation. When we examined the expression and activity of mitochondrial enzymes including citrate synthase and pyruvate dehydrogenase, we observed reduced protein expression and activity in both breast cancer cell lines. This alone was not sufficient to explain the strong oxidative phosphorylation defect in SUM149 cells. Stable isotope flux studies using ^{13}C-labeled pyruvate revealed that SUM149 cells have very low levels of TCA cycle intermediates and that the labeled pyruvate is not being used to synthesize citrate or isocitrate. Because labeled acetyl-CoA was detected, we theorized that acetyl-CoA was being used for some other purpose. To identify other pathways that might be altered in SUM149 cells, unbiased metabolomic screening was performed on all three cell lines. This experiment pointed to the accumulation of N-acetyl aspartate in SUM149 cells. This substrate has no known function outside of the central nervous system. We subsequently demonstrated that NAT8L, the enzyme that catalyzes the

acetylation of aspartate using acetyl-CoA as a substrate was highly overexpressed at the mRNA level in these cells. Additionally, ASPA, the enzyme that deacetylates aspartate was silenced at the mRNA level and not expressed at the protein level. Further work to determine whether NAT8L overexpression and the production of N-acetyl acetate are able to completely account for the defect in oxidative phosphorylation must be pursued. We hypothesize that knockdown of NAT8L expression or overexpression of ASPA protein may be able to rescue some portion of the defect in SUM149 cells. Additionally, overexpression of NAT8L in MCF-10A cells may reduce their oxidative capacity.

The outcome of these experiments will raise important questions regarding the role of N-acetyl aspartate in these cells and in cancer cell biology in general. Further study will need to be done to fully understand the impact that this metabolite may have on signaling or other cellular processes. Additional *in vitro* studies are needed to determine if overexpression of NAT8L and production of N-acetyl aspartate is a cell line specific effect, or if it can be generalized to other aggressive breast cancers.

An additional intriguing finding from this work is that both normal breast and breast cancer cells undergo gluconeogenesis. This result is novel, as most work suggests that only liver and kidney cells perform gluconeogenesis[27]. The SUM149 cell line undergoes gluconeogenesis at a much greater rate than the other cell lines, as evidenced by the fact that approximately 50 percent of its 2-phosphoglycerate and 3-phosphoglycerate as well as fructose-1, 6-bisphosphate metabolites come from gluconeogenesis. This suggests that another way of treating this aggressive breast cancer may be to target gluconeogenesis enzymes. This might have the advantage of causing

fewer side effects, as most cells outside of the liver and kidney do not undergo gluconeogenesis.

Glutamine's role as a TCA cycle substrate has been studied extensively in cancer [26, 115], and the results obtained from isotope tracer experiments match what is shown in the literature. Downstream TCA cycle intermediates like malate (Figure III.3D) showed a higher percentage of labeling in SUM149 cells, suggesting that they rely more on flux through glutamine than other cell lines do. This may be due to the need for increasing aspartate production for N-acetyl aspartate via glutamate dehydrogenase, which catalyzes the reaction of oxaloacetate and glutamate to produce α-ketoglutarate for TCA cycle entry and aspartate. Further work should characterize the reliance of SUM149 cells on glutaminolysis for TCA cycle derived metabolites and substrates for lipid and nucleotide synthesis.

Methods

Cell Culture

MCF-10A cells were cultured in 1:1 Ham's F-12 and Dulbecco's modified Eagle's medium (DMEM) with 2 mM L-glutamine supplemented with 5% horse serum, extracellular growth factor, cholera toxin, insulin, hydrocortisone, gentamycin, fungizone, and penicillin/streptomycin at 37ºC under 5% CO_2. MDA-MB-231 cells were cultured in RPMI 1640 supplemented with 10% fetal bovine serum, gentamycin, fungizone and penicillin/streptomycin at 37ºC under 5% CO_2. SUM149 cells were cultured in Ham's F-12 with L-glutamine supplemented with 5% fetal bovine serum, insulin, hydrocortisone, gentamycin, fungizone and penicillin/streptomycin under 10% CO_2.

Bioenergetic Profiles (BEP) and Extracellular Acidification Rate (ECAR) Measurements

Cells were trypsinized and seeded with 100 µL fresh growth media into 24 well plates. After 1 hour of incubation, an additional 150 µL of media was added. After overnight incubation, media was replaced with XF Assay Medium Modified DMEM (Seahorse Biosciences) supplemented with 11 mM glucose and 10 mM pyruvate. Cells were incubated in a 37°C non-CO_2 incubator for 1 hour before being used for experiments. Oligomycin, FCCP, and rotenone were used to achieve final concentrations of 1uM, 300 nM, and 100 nM respectively in the cell. Galactose, when present, was at 11 mM final concentration. Low glucose experiments were performed using 2.5 mM glucose, and were later spiked with 87.5 mM glucose to bring the concentration back to the 11mM standard amount. All experiments were performed using a Seahorse XF-24 Extracellular Flux Analyzer according to standard protocols developed by the manufacturer (Seahorse Biosciences).

Protein Extraction and Western Blot

Cells were washed with cold phosphate-buffered saline (PBS) and lysed in radioimmunoprecipitation assay (RIPA) buffer plus Complete protein inhibitor cocktail (Roche). Cells were sheared with a 23 gauge syringe and protein was collected after centrifugation to remove cellular debris. 30-60µg of protein was electrophoresed onto a SDS-PAGE gel. The protein was transferred to a nitrocellulose membrane using a semidry apparatus (BioRad). The membrane was blocked using 5% milk in TBST and incubated in either 5% milk in TBST or 5% bovine serum albumin (BSA) in TBST. Membranes were incubated with the appropriate secondary antibodies conjugated to

horseradish peroxidase (HRP) at concentrations of 1:5000 in 5% milk in TBST. Protein bands were detected by electrochemiluminescence.

Transmission electron microscopy sample preparation and analysis

Cells were plated in 10 cm dishes. Cells were rinsed in serum free media, and fixed for 1 hour in 2.5% glutaraldehyde in 0.1M Sorensen's buffer, pH 7.4. Cells were left at 4°C overnight in Sorensen's buffer. Cells were rinsed to remove glutaraldehyde and postfixed in 1% osmium tetroxide in Sorensen's buffer. Cells were then rinsed in water, and scraped off the plates. Cells were pelleted and En Bloc stained for 15 minutes. Pellets were rinsed with water and then dehydrated in increasing ethanol solutions. Epon was then infiltrated into the pellet with increasing resin concentrations. Pellets were then polymerized at 60°C for 24 hours. Pellets were cut using a microtome and images taken at 25,000X magnification using a CM100 Phillips TEM scope. Images were stitched together using Adobe Photoshop.

Mitochondrial Isolation

Mitochondria were isolated as reported previously by Frezza et al [116]. Briefly, cells were grown to confluence in 10 cm culture plates. Cells were washed with PBS and scraped off plates. Cells were resuspended in Cell Isolation Buffer (IB_c) and homogenized with a Teflon pestle. Samples were then spun to remove nuclei, and then spun again to isolate the mitochondria. A Bradford assay was completed on the mitochondrial isolates to determine concentration of total protein.

Citrate Synthase Assay

Isolated mitochondria were thawed and frozen in 3 cycles to disrupt mitochondrial membranes. A Bradford assay was completed to correct for protein

content. Reaction mixture containing 100mM Tris-HCl, 100 μM DTNB, .4% TX-100 final concentration was added to each well in a 96 well plate. Mitochondrial isolates were added at concentrations of 1-15 μg/well. Acetyl CoA was added at a final concentration of 50 μM. The plate was incubated at 37°C for 5 minutes to allow all endogenous oxaloacetate to be exhausted. 100 μM final concentration of oxaloacetate was added, and the plate was read at 412 nm for 15 minutes reading every 12 seconds.

Sequencing of Citrate Synthase mRNA

RNA was isolated from cell lines using Trizol according to package instructions. The Promega Reverse Transcription System was used according to package instructions to make cDNA from isolated RNA. PCR amplification of citrate synthase mRNA was conducted using the following primers:

Forward: CTGCCGCAGCTCTCTCCCTT

Reverse: AGGCTTCCTCACTTTCTGGTAGTCA

The PCR product was run on an agarose gel. The band was excised and purified using the Qiagen QIAquick Gel extraction kit. The purified PCR product was then submitted to the University of Michigan DNA Sequencing Core for direct Sanger sequencing.

Pyruvate Dehydrogenase Activity Assay

Pyruvate dehydrogenase (PDH) activity was measured using a modified version of the method by Schwab et al [117]. Briefly, cells the cells were trypsinized, pelleted and rinsed, and then suspended in isolation buffer (250 mM sucrose, 1mM EGTA, 10 mM HEPES, 5 mg/mL BSA, pH 7.5. Half of cells were incubated with 5 mM final concentration of dichloroacetic acid (DCA) to fully activate the PDH complex for 15 minutes at 37°C. The other half were incubated without DCA. Cells were homogenized

with a Teflon pestle. Cells were then spun at 13,000 rpm in a microcentrifuge and frozen. The next day cells were freeze-thawed three times and resuspended in buffer (.1% Triton X-100, 1 mM CaCl2, 5 mM MgCl2, 50 mM KCl, 250 mM Sucrose, 20 mM Tris-HCl pH 7.5). The cells were sonicated for 20s on 50% duty cycle at 20% amplitude. Cells were then spun at 15,000 x g for 5 min, and the supernatant was used to measure protein content by a Bradford Assay. 100 µL aliquots were made for each sample containing 4.25 mg/mL protein. 18 µL of each sample was added to 5 wells in a 96 well plate. Bovine Heart Mitochondrial Lysate (abcam) was used as a positive control after solubilization with 1% Lauryl Maltoside final concentration and spinning at 15,000 x g. 182 µL reaction mixture (5mM L-carnitine, 2.5 mM NAD, .2mM TPP, .1mM CoA, 5 mM pyruvate, .1% Triton X-100, 1 mM MgCl2, 1 mg/mL BSA, .6 mM INT, 6.5 µmol PMS in .05M potassium phosphate buffer pH 7.5) was added to each well in a 96 well plate. 1.7 µL of .6M fluoropyruvate was added to 2 of the 5 wells to determine the amount of nonspecific activity. The plate was read using kinetic assay settings at 500 nm with reads every 30 seconds for 1-3 hours depending on time to reach saturation.

Quantitative RT-PCR methods

RNA was isolated from cell lines using Trizol according to package instructions. The Promega Reverse Transcription System was used according to package instructions to make cDNA from isolated RNA. SYBR Green Mastermix was used according to directions for Quantitative PCR. Three experiments were done in triplicate.

Preparation of Extracts for Targeted Metabolomics and ^{13}C mass isotopomer analysis

Cell extracts were prepared and analyzed according to a modified protocol from Lorenz et al, [118]. Cells were grown to 80% confluence on 6 cm collagen-coated tissue

culture plates. Cells were then changed to unbuffered media, either XF Assay Medium Modified DMEM (Seahorse Biosciences) or Dulbecco's modified Eagle's medium base (D5030) supplemented with 11mM glucose, 10 mM sodium pyruvate, 2.5 mM glutamine and 0.015g/L phenol red. Cells were incubated at 37°C for 1 hour in a non-CO_2 incubator. Cells were then changed to the same media containing 2,3-$^{13}C_2$-pyruvate and incubated for 0 or 15 minutes. Cells were then rinsed by rapid addition and removal of 3 mL of distilled water, after which metabolism was immediately quenched by pouring liquid nitrogen into the plate. Plates were stored at -80°C until extraction. Cells were extracted by adding 500 µL of ice-cold 8:1:1 methanol:water:chloroform to the frozen cell surface and scraping with a cell scraper. The extract and residual cell debris were transferred to polypropylene microcentrifuge tubes and centrifuged for 5 min at 15,000 x g at 4°C. The supernatant was transferred to autosampler vials and analyzed by LC-MS.

Preparation of Extracts for Unbiased Metabolomic Screening

7 x 10cm plates for each cell line were grown for 2-3 days to 80% confluence in growth media. The plates were changed to fresh growth media one hour before quenching with liquid nitrogen. Three plates from each cell line were reserved for protein normalization. After the one hour incubation, the remaining four plates were rinsed with 4 mL deionized water and quenched with liquid nitrogen as above, then stored at -80°C. Cell plate extraction was performed as described previously, except that the extraction solvent contained 18 µg/mL of a ^{13}C amino acid mix (Sigma, part 426199) to serve as an internal standard and the volume used was increased to 1mL per plate to accommodate the larger plate size. Following centrifugation, 500 µL of supernatant was

dried under nitrogen and reconstituted in 250 µL of water containing tert-butyloxycarbonyl-protected amino acids to serve as injection standards.

LC-MS Methods and Data Analysis

For targeted metabolomics and ^{13}C mass isotopomer analysis, samples were analyzed on an Agilent 1200 LC / 6520 qTOF MS system. To obtain good retention of the polar, predominantly anionic metabolites of glycolysis and the TCA cycle, chromatographic separation was performed by mixed mode hydrophilic interaction – anion exchange using a Luna NH2 3µ column, 150 mm x 1 mm ID (Phenomenex, Torrance, CA). Mobile phase A was acetonitrile and mobile phase B was 5 mM ammonium acetate in water, adjusted to pH 9.9 using ammonium hydroxide. The gradient was a 15 minute linear ramp from 20 to 100%B, followed by a 5 minute hold at 100%B and a 17-minute requilibration period at 20%B. The column temperature was 25°C and the flow rate was 0.07 mL/min, which was ramped to 0.09 mL/min between 20 to 32 minutes. The injection volume was 10 µL. Electrospray ionization was carried out in negative ion mode using a source gas temperature of 350° C, a drying gas temperature of 10 L/min, a nebulizer pressure of 20 psig, and a capillary voltage of 3500 V. Data were collected in TOF full-scan mode over m/z 50-1200 at an acquisition rate of 1 spectra/s with reference mass correction enabled. Data were analyzed using Masshunter Quantitative Analysis software. Metabolites and their ^{13}C isotopes were identified by retention time and m/z values determined from authentic standards. Quantification was performed by peak area after manual inspection of integration accuracy.

For unbiased metabolomics, samples were analyzed on an Agilent 1200 LC / 6530 qTOF MS system using a Waters Acquity HSS T3 reversed-phase column, 50 mm x 2.1 mm ID. For positive ion mode runs, mobile phase A was water with 0.1% (v/v) formic acid and mobile phase B was methanol with 0.1% formic acid. For negative ion mode runs, the formic acid was replaced with 0.1% (m/v) ammonium bicarbonate. The gradient was as follows: 0-0.5 min 1% B, 0.5-2 min 1-99% B, 2-6 min 99% B, 6-6.1-9 min 1% B. The flow rate was 0.35 mL/min and the column temperature was 40° C. The injection volumes for positive and negative mode were 5 and 8 µL, respectively. ESI-MS conditions were the same as for targeted analysis except that the Agilent Jetstream source was used, the nebulizer pressure was 30 psig, and the sheath gas temperature and flow rate were 350° C and 11 L/min. Data analysis was performed using a two-step approach using Agilent Masshunter Qualitative Analysis Software. First, known compounds were identified by searching the LC-MS data against an in-house metabolite library of approximately 600 previously-analyzed authentic standards using the find by formula algorithm. Then, the molecular feature extractor algorithm was used to detect additional unknown features, the features were aligned between samples by mass and retention time, and finally these features were selected and quantitated using find by formula. Principle component analysis was applied to the data to rank features in order of their contribution to differences in the metabolome between cell types.

Protein Normalization of Mass Spectrometry Data

Three additional plates were grown up in each experiment per cell line. Cells were rinsed twice with cold PBS, and then treated with RIPA buffer with complete protease inhibitor cocktail (Roche) added at suggested concentration for 25 minutes with

gentle agitation at 4°C. Protein was scraped off the plate and sheared with a 23-gauge syringe 3-4 times. Protein was collected in microcentrifuge tubes and spun for 15 minutes at 13,000 rpm at 4°C to pellet cellular debris. A Bradford assay was performed to quantify the amount of protein in each sample. This data was averaged and used to normalize the mass spectrometry data to account for differences in the growth rate of cells.

Figures

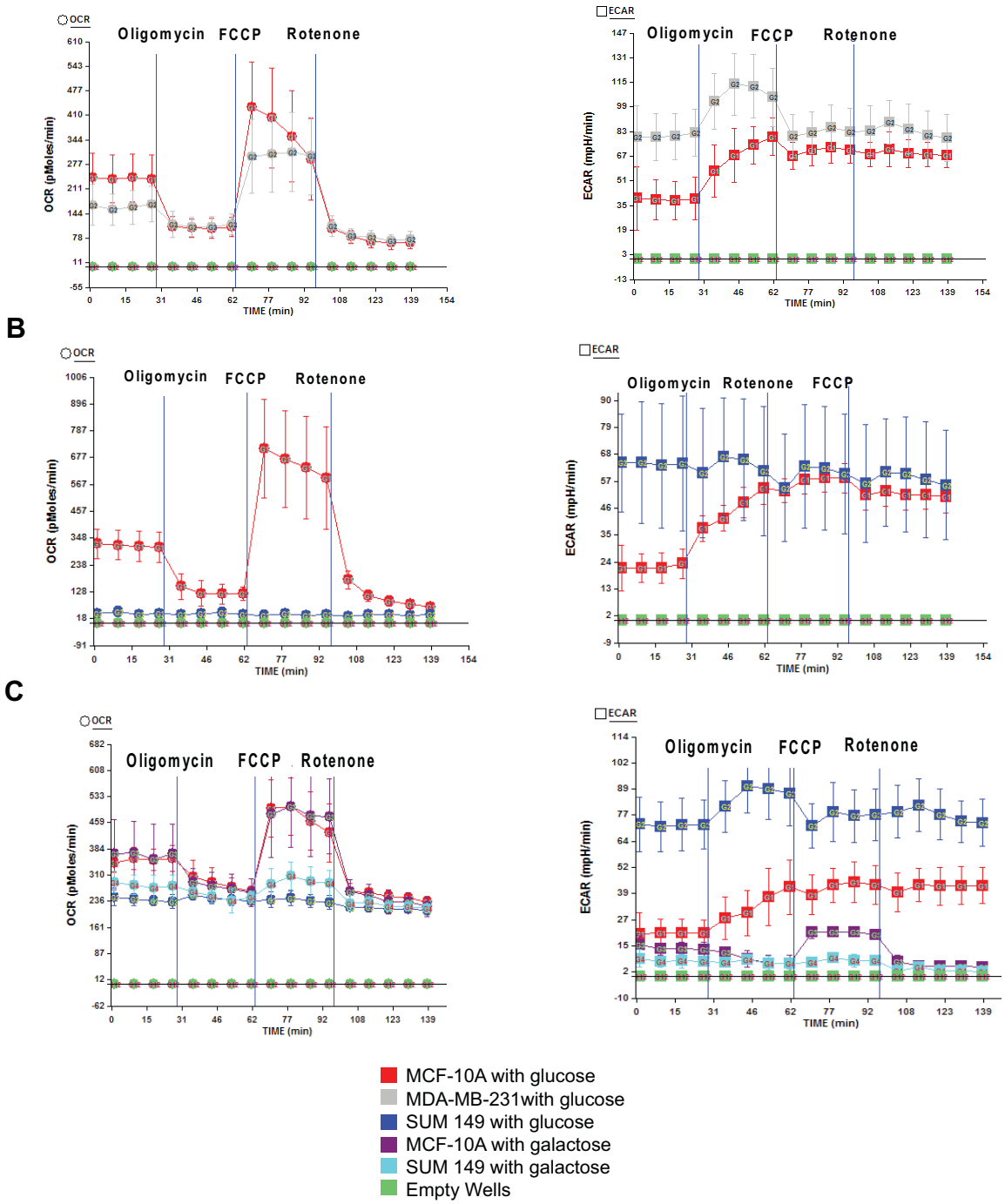

Figure III.1: SUM149 cells do not use oxidative phosphorylation
Bioenergetic profiles measuring oxidative consumption rate (OCR) on left and extracellular acidification rate (ECAR) on right of normal and breast cancer cell lines. A. MDA-MB-231 compared to MCF-10A B. SUM149 compared to MCF-10A C. SUM149 and MCF-10A using galactose as an alternative substrate

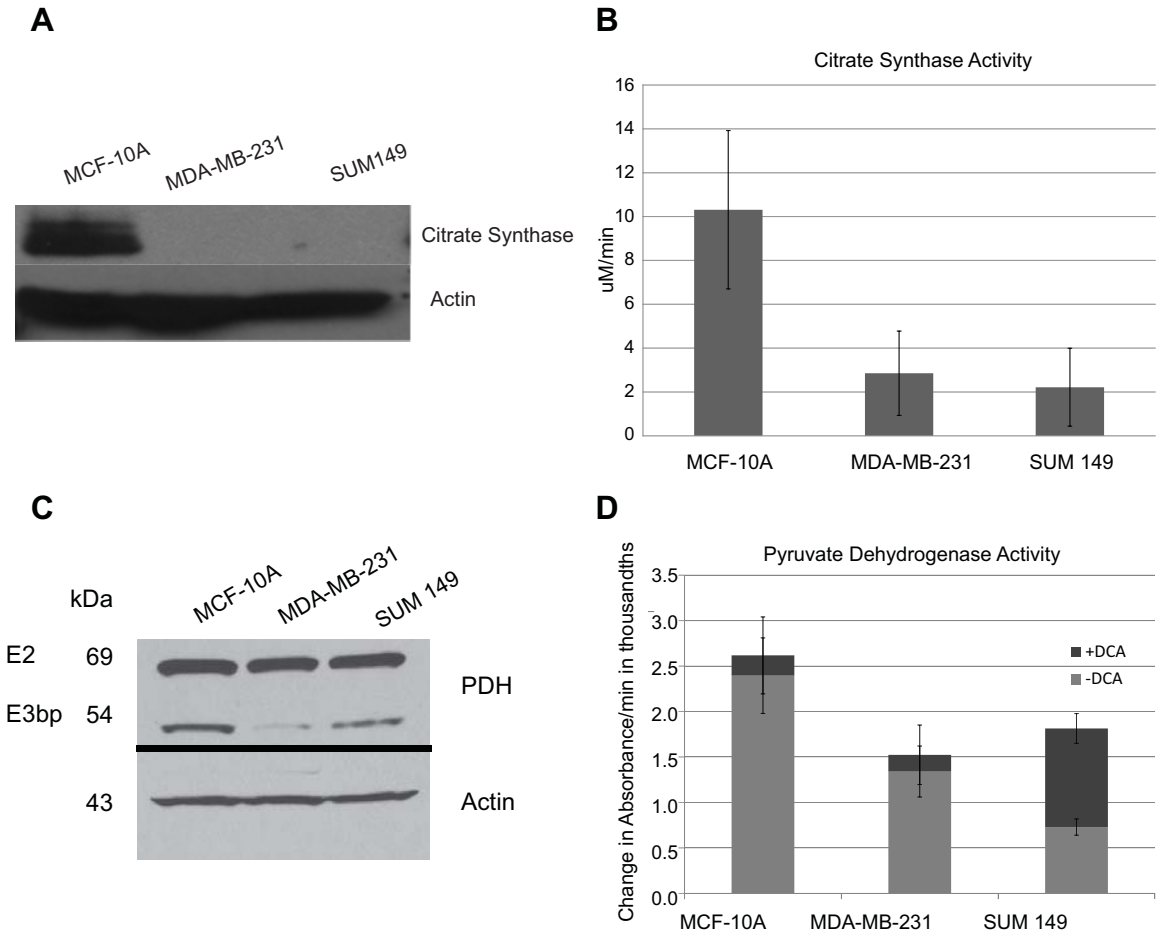

Figure III.2: SUM149 cells have less efficient mitochondrial enzymes
Protein expression and enzyme activity of selected mitochondrial enzymes A. Citrate synthase protein expression B. Citrate synthase activity C. Pyruvate dehydrogenase protein expression level D. Quantification of Pyruvate dehydrogenase protein expression level E. Pyruvate dehydrogenase activity

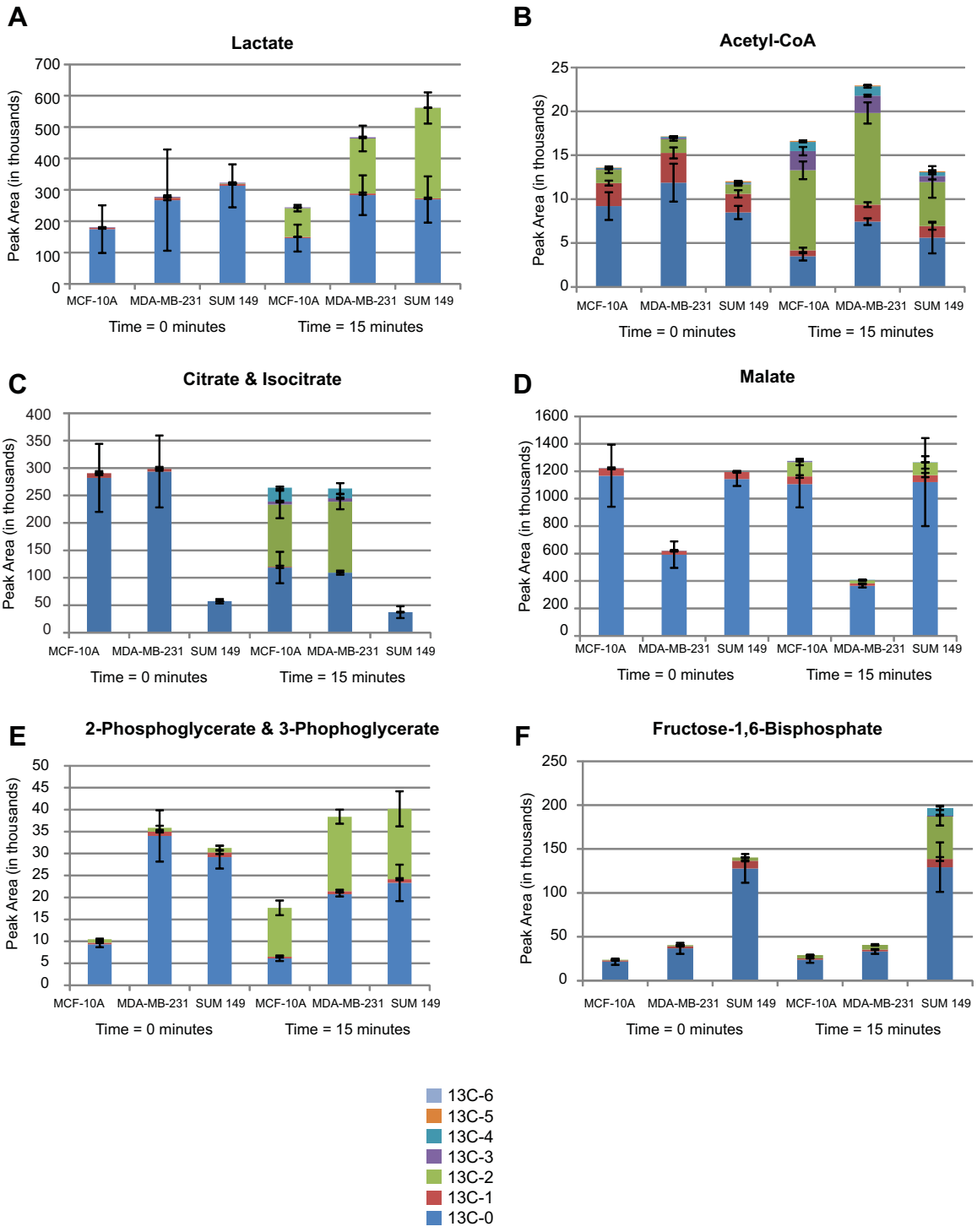

Figure III.3: SUM149 cells do not use acetyl-CoA to make citrate and perform gluconeogenesis
Stable isotope tracer experiments with 2, 3-$^{13}C_2$-pyruvate measuring peak intensity area under the curve of the following metabolites A. Lactate B. Citrate/Isocitrate C. Acetyl-CoA D. Malate E. 2-Phosphogluycerate/3-Phosphoglycerate F. Fructose-1,6-Bisphosphate

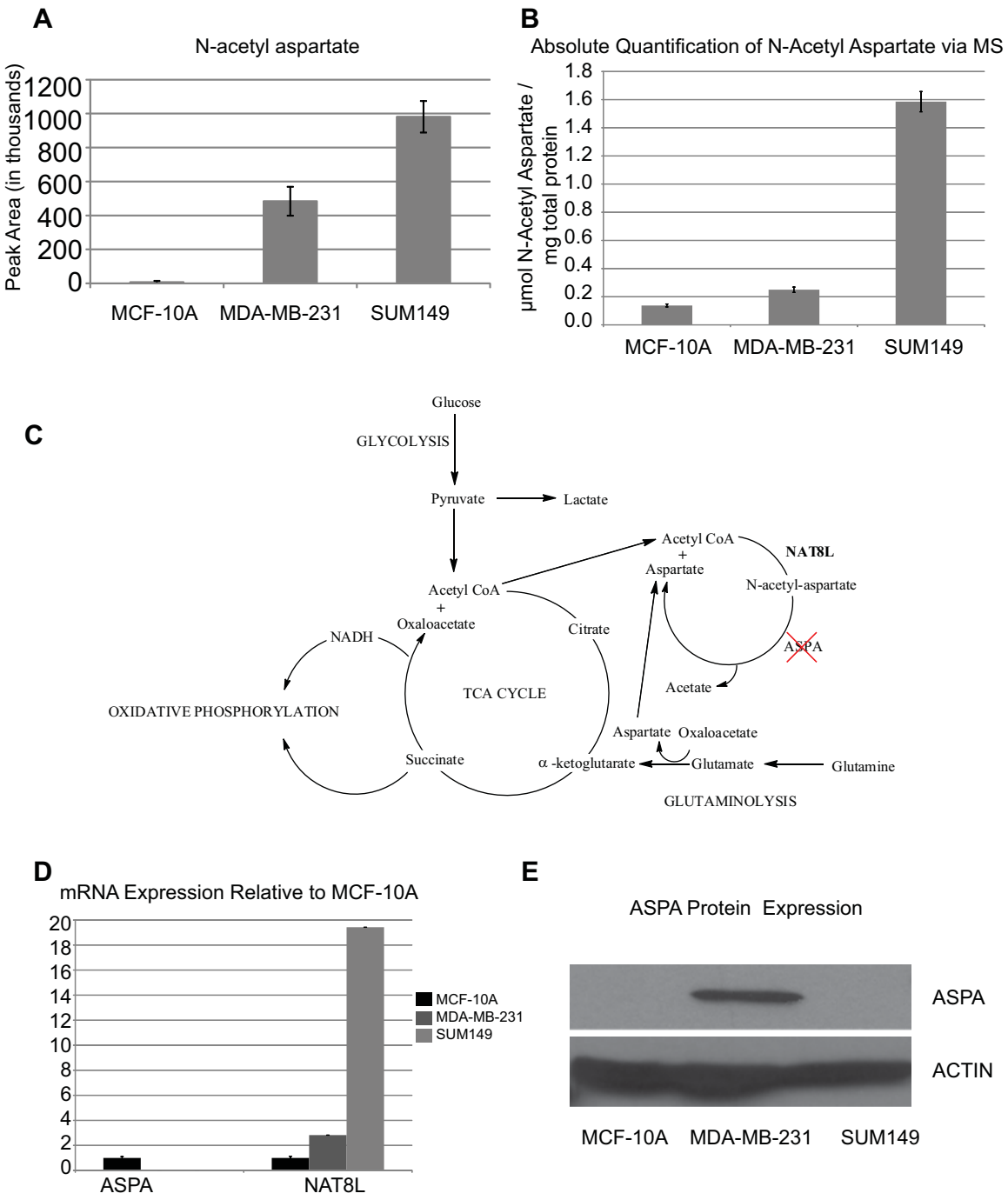

Figure III.4: N-Acetyl Aspartate Pool Identified in Unbiased Metabolomic Screen
Identification and validation of N-acetyl aspartate pool in SUM149 cells. A. Peak Area of N-Acetyl-Aspartate Pool B. Quantification of N-Acetyl-Aspartate in stable isotope experiments C. Model showing substrate source for acetylation of aspartate D. QPCR of NAT8L, ASPA E. Western Blot of ASPA

A

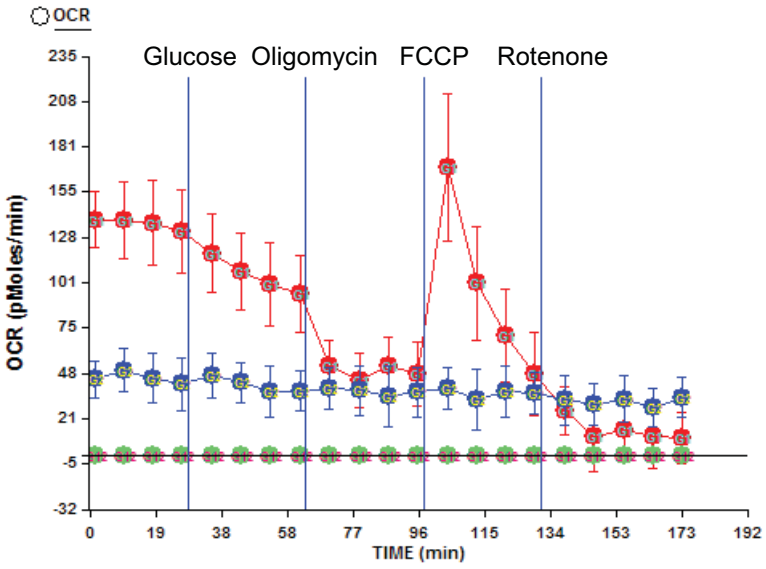

B

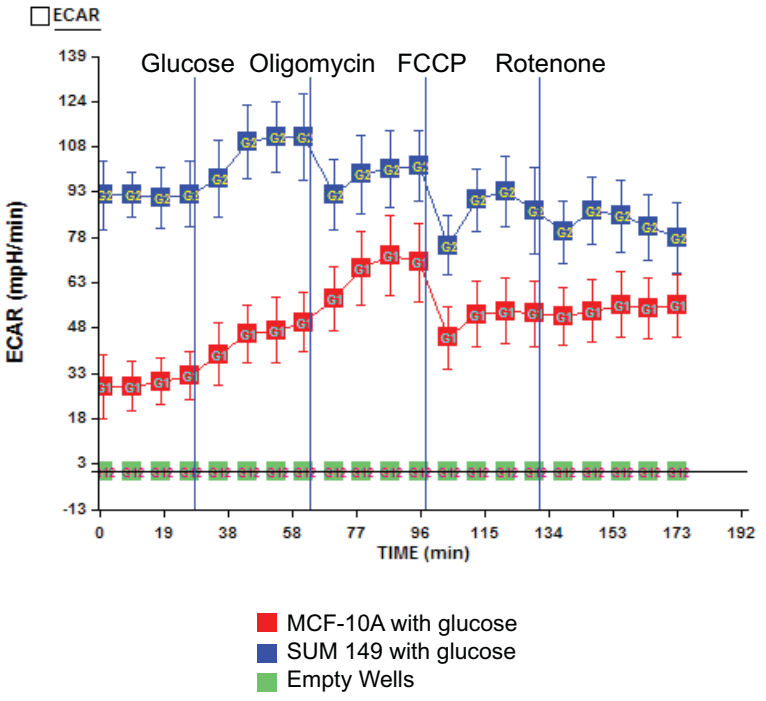

Figure III.5: Low Glucose does not induce SUM149 cells to undergo oxidative phosphorylation
BEP (A) and ECAR (B) of SUM149 cells grown in low (2.5 mM), and then spiked with glucose to reach 11mM final concentration.

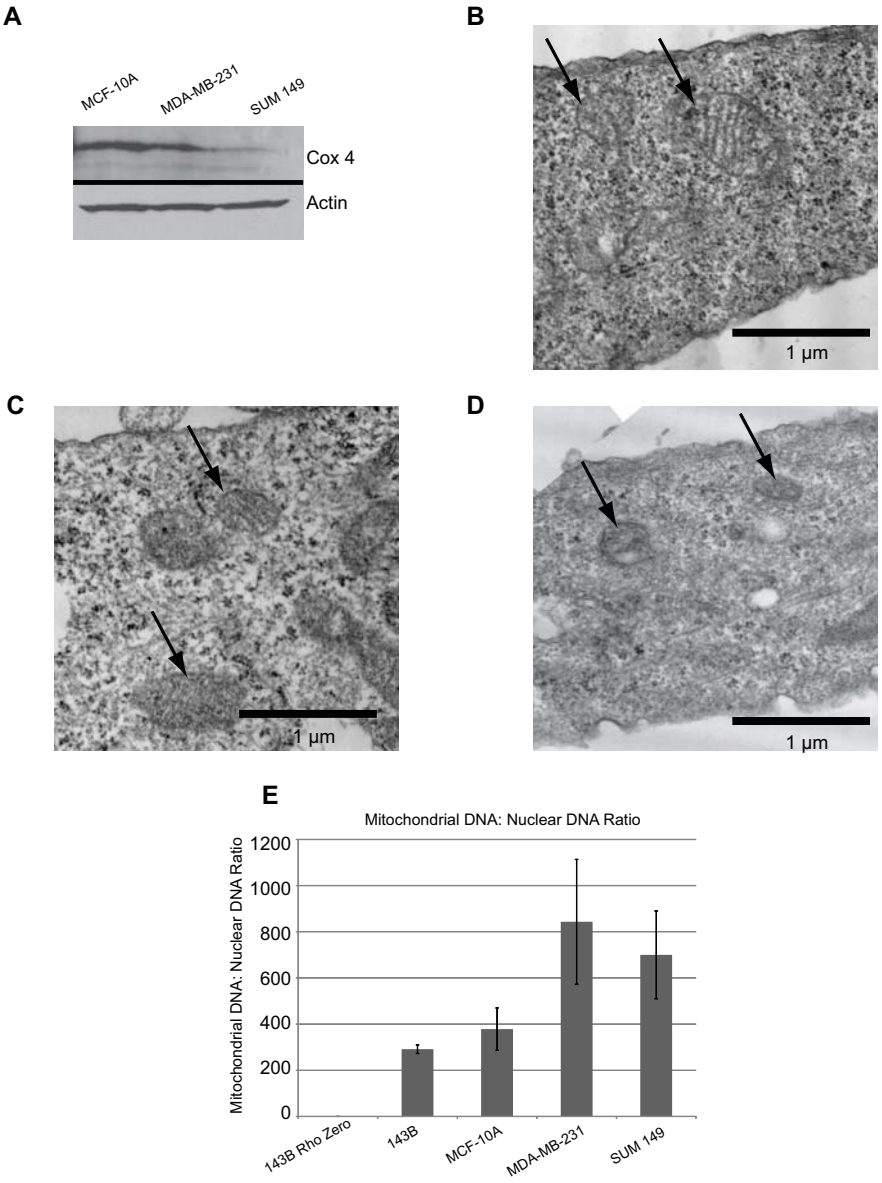

Figure III.6:SUM149 cells have sufficient mitochondria
Quantification of mitochondria per cell A. Cox 4 protein expression; TEM images of B. MCF-10A cell C. MDA-MB-231 cells D. SUM149 Cells E. Mitochondria DNA: Nuclear DNA ratio.

This chapter represents a "manuscript in progress" and will be submitted for publication under the title "Alternative pathway for acetyl CoA metabolism prevents inflammatory breast cancer cell line SUM149 from undergoing oxidative phosphorylation"

by Lauren D. Van Wassenhove, Charles Evans, Sydney Bridges, Sepideh Ashrafzadeh, ZhiFen Wu, LiWei Bao, Charles F. Burant, and Sofia D. Merajver.

Chapter IV

Unbiased metabolomic screening reveals key metabolic pathways responsible for energy switch from proliferation to motility in breast cancer cells

Abstract

Understanding the switch that cancer cells undergo from a proliferation predominant phenotype to a motility predominant phenotype required for metastasis is an important step towards preventing metastasis. These studies require a model in which the switch from proliferation to motion is modulated in a genetically well-controlled system. In previous work in our laboratory, such a model was developed by modulating the expression of p38γ. In this paper, we use the breast cancer cell line MDA-MB-231 stably transfected with a vector encoding shRNA against mitogen-activated protein kinase (MAPK) p38γ or with a vector encoding a shRNA scrambled control. As is demonstrated in the literature, this single molecular change results in increased proliferation and decreased motility in this cell line, reverting this aggressive breast cancer to a less malignant phenotype. This body of work uses novel, unbiased metabolomic screening techniques to uncover differences in metabolic pathway regulation that ultimately leads to modulation of the energy utilization phenotypic switch.

Introduction

The MAPK pathway is a key regulator of cellular proliferation, apoptosis, and genetic regulation. The p38 arm of this pathway has been implicated in metabolic

diseases and cancer [119]. The p38 protein has 4 different isoforms in humans, α, β, γ, and δ. Isoforms α, β are the most homologous to each other by sequence compared to the other isoforms. Likewise, γ and δ are most homologous to each other by sequence. Studies have shown that each isoform has unique regulatory properties and do not appear to have redundant function [62]. Most of the studies in the literature focus on the α and β isoforms, and commonly used inhibitors of p38 are pyridinyl imidazole inhibitors, which are specific to the ATPase binding pocket of α and β, and have little effect on the other isoforms [64]. Our lab has shown in previous work that MAPK p38γ is an important regulator of cellular motility, especially through its interaction with small GTPase RhoC [62]. In order to identify the effect that knocking down p38γ in MDA-MB-231 cells has on metabolism, we conducted an unbiased metabolic screen to measure the relative concentrations of metabolites in the p38γ knockdown cells compared to that of the scrambled shRNA control cell line. This work is the first time that a single molecular change in an identical genetic background has been examined using unbiased metabolomic screening.

Results

Knockdown of p38γ causes changes in the relative amounts of a variety of different metabolites.

This screen detected 304 known metabolites. The compounds detected are depicted by red hexagons (Figure IV.1). The metabolites detected are members of a variety of different pathways, showing good representation of the entire metabolome. The relative size of the red hexagons shows whether the compound was found to be increased or decreased after p38γ knockdown. Because this experiment is not a time

course, it is important to be aware that a decrease in a particular compound could indicate one of two mechanisms: either that the cell is not making as much of this metabolite (due to overall pathway down regulation, or a decrease in synthesizing enzyme, etc.) or the cell is using more of this particular compound such that the pool size in the cell is low (due to overall pathway upregulation, or increase in a catabolizing enzyme, etc.). Likewise if a metabolite is increased, it could indicate that the cell is making more of the particular compound or that it is not being used up by the cell, so a larger pool is allowed to accumulate. In order to tease out which of the possible scenarios are occurring, further experiments including changes over time as well as functional assays will have to be done. The unbiased metabolic screen found changes in a few specific pathways highlighted below.

Knockdown of p38γ causes increases in metabolites in the nucleotide synthesis pathway.

This screen identified metabolites belonging to the nucleotide synthesis pathways that are significantly increased in p38γ knockdown cells. Metabolites in both purine and pyrimidine synthesis are increased in p38γ knockdown cells, (Figure IV.2A, 2B). Because it is important for the rapidly proliferating cell to generate the nucleotides needed for DNA synthesis to copy its genome the daughter cell, it is likely that the increase we see in these metabolites is due to upregulation of nucleotide synthesis in p38γ knockdown cells.

Knockdown of p38γ causes increases in metabolites in the NADH synthesis pathway

Knockdown of p38γ causes an increase in metabolites involved in the NADH synthesis pathway (Figure IV.3A). NADH is an electron carrier and is required to provide energy in reduction-oxidation (redox) reactions. Many metabolic pathways require

NADH (or NAD+) to provide (or take up) electrons including glycolysis and oxidative phosphorylation. Because of the increased needs of the replicating cells, NADH synthesis may be increased to provide the needed reducing power.

Knockdown of p38γ causes a decrease in metabolites in the C-21 steroid hormone biosynthesis pathway.

Knockdown of p38γ decreased the relative abundance of C-21 steroid hormone biosynthesis pathway (Figure IV.3B). The C-21 steroid hormone pathway is important not only for the synthesis of a variety of signals required for growth and proliferation, but also is involved with the production of precursors for lipid molecules within the plasma membrane [120]. These may be involved in the direction of energy into motility, as changes in the cell cytoskeleton and membrane provide the force that allows the cell to move. Because of the known importance of steroid hormones in certain types of cancer [121-125], we chose to focus on the C-21 steroid hormone pathway for further study.

Inhibition of the C-21 steroid hormone pathway with cortisone leads to decreased proliferation

Because p38γ knockdown was shown in previous work to lead to a reversion of the very aggressive MDA-MB-231 breast cancer cell line to a less aggressive phenotype, we hypothesized that the decreased amount of metabolites seen in the C-21 pathway was due to downregulation of the pathway, not increased usage of the pathway. To see if regulation of this pathway is important for the switch from a proliferative to motile state, we perturbed this pathway with cortisone. We hypothesized that the addition of cortisone would cause an increase in the C-21 steroid hormone biosynthesis pathway and lead to decreased proliferation. We found that concentrations of 4 uM cortisone were able to

effectively decrease cell proliferation in p38γ knockdown cells to that of the untreated scrambled control cells (Figure IV.4A). Concentrations above 10 uM were lethal to the cells (not shown).

Discussion

In this study, we examined the aggressive breast cancer cell line MDA-MB-231 and the effects of a single molecular change, the knockdown of MAPK signaling pathway member p38γ on metabolic pathways. Knockdown of p38γ induced a behavioral change in the cells from a highly motile state to a highly proliferative state. We hypothesized that p38γ knockdown affected the regulation of metabolic pathways so as to induce a metabolic switch redirecting the energy from motility use to proliferation use. Knockdown of p38γ was found to induce significant changes in the following pathways: nucleotide synthesis, NADH synthesis, and C-21 hormone synthesis.

Nucleotide synthesis is very important in the rapidly dividing cell, because of the need to replicate the cellular genome before cell division [126]. The highly proliferative p38γ knockdown cells displayed increased synthesis of nucleotides. NADH synthesis was also found to be increased in p38γ knockdown cells, suggesting an increased need for cellular reducing power.

We also found that the steroid hormone biosynthesis pathway was decreased in p38γ knockdown cells, suggesting a decreased need for these metabolites in the rapidly dividing cell. Upon the addition of cortisone to the cells, we found that they had decreased proliferation. Additional experiments will need to be performed to see if treatment with cortisone will also increase proliferation, which would indicate a reversion back to the parent/scrambled control state. If so, inhibition of the C-21 steroid

biosynthesis pathway may prevent metastasis, or revert aggressive breast cancers to a less aggressive phenotype. Estrogen, a steroid hormone important in normal breast growth and maturation, binds to estrogen receptor (ER). This causes ERs to dimerize and activate a signaling pathways that results in the activation or suppression of a variety of genes via transcription factors. In addition, estrogen has been shown to induce cross talk affecting both the Her2/Neu pathway as well as the MAPK pathway [121, 123, 127]. Dysregulation of steroid hormones can lead to inflammation and cancer, often leading to hormonal cancers including breast, ovarian and prostate cancers. Additionally, recent work has shown that the MAPK pathway inhibits the activity of hydroxysteroid (11-β) dehydrogenase 2, an enzyme which is encoded by the gene HSD11B2, and converts cortisol to cortisone. Cortisol plays a crucial role in the activation of both glucocorticoid and mineralocorticoid receptors. These receptors regulate a wide range of activities including immune suppression and sodium and potassium ion homeostasis. Cortisol, once hydroxylated via HSD11B2 enzyme, becomes cortisone, a much less potent activator of these receptors. The activity of ER crosstalk with the MAPK pathway, as well as the inhibitory activity of MAPK on HSD11B2 has suggested a model in which knockdown of p38γ prevents crosstalk of these pathways and prevents inhibition of HSD11B2 (Figure IV.5). This results in less of the active cortisol being present in the cell, as observed in Figure IV.3B. Due to this, the cells lose the ability to move, and begin to proliferate rapidly. However, when additional cortisone is added, and due to the activity of HSD11B1, which catalyzes the opposite reaction, more active cortisol is available. This then may rescue the motility and invasion of these cells.

This study shows that the p38 pathway widely affects a variety of metabolic pathways. The elucidation of the signaling between p38 and metabolic signaling pathways like mTOR and PI3K/AKT is just beginning to be studied in the literature. Understanding the crosstalk of these pathways may result in further understanding of how cancer cells dysregulate their proliferation rate and motility.

This study identified three other pathways that were significantly altered with p38γ knockdown. Studying the purine, pyrimidine, and NADH pathways may help to understand further what metabolic changes occur when a cell switches from a highly proliferative to a highly motile state.

Methods

Cell Culture

Stably transfected MDA-MB-231 cells were cultured in RPMI 1640 media supplemented with 10% FBS, 5% Pen-Strep, and 5% fungizone with antibiotic selection with 1 μg/mL puramycin under 5% CO_2 at 37°C. Media was changed every 3-4 days, and cells were passed upon reaching confluence.

MTT assay

Cells were plated in replicates of six in six 96 well plates, 1000 cells per well. Cells were allowed to adhere to the plates, and then were serum starved overnight (12-18hours) to synchronize. Serum free media was replaced with growth media with 0, 4 or 4.5 uM cortisone. Timepoints were taken at 0, 1,2,3,4,5,6,7 days after treatment with cortisone. For each timepoint, 50 μL of MTT (3-(4,5-Dimethylthiazol-2-yl)-2,5-diphenyltetrazolium bromide) was added to each well. After 1 hour incubation at 37°C,

media and MTT solution was removed from each well. 100 µL DMSO was then added and the plate was shaken for 5 min. Absorbance was read at 595 nm.

Bead Motility Assay

Cells were serum starved overnight and then treated for 24 hours with 0, 4, or 4.5 uM cortisone and then plated on a field of fluorescent beads and incubated overnight. Cell tracks were quantified using ImageJ.

Treatment of cells with cortisone

Cells were treated with 0, 4, 4.5 uM cortisone for 24 hours. Concentrations greater or equal to 10 uM were found to kill the cells. Measurement of proliferation and motility assays were conducted as before.

Preparation of Extracts for Unbiased Metabolomic Screening

Cell extracts were prepared and analyzed according to a modified protocol from Lorenz et al, (Lorenz, 2011). 13 x 10cm plates for each cell line were grown for 2-3 days to 80% confluence on collagen coated plates in standard growth media. The plates were changed to fresh growth media one hour before quenching with liquid nitrogen. Three plates from each cell line were reserved for protein normalization. After the one hour the remaining ten plates were then rinsed by rapid addition and removal of 4 mL of distilled water, after which metabolism was immediately quenched by pouring liquid nitrogen into the plate. Plates were stored at -80°C until extraction. Cells were extracted by adding 1 mL of ice-cold 8:1:1 methanol:water:chloroform containing 18 µg/mL of a ^{13}C amino acid mix (Sigma, part 426199) to serve as an internal standard to the frozen cell surface and scraping with a cell scraper. The extract and residual cell debris were transferred to polypropylene microcentrifuge tubes and centrifuged for 5 min at 15,000 x g at 4°C. The

supernatant was transferred to autosampler vials and analyzed by LC-MS. Following centrifugation, 500 µL of supernatant was dried under nitrogen and reconstituted in 250 µL of water containing tert-butyloxycarbonyl-protected amino acids to serve as injection standards.

LC-MS Methods and Data Analysis

For targeted metabolomics, samples were analyzed on an Agilent 1200 LC / 6520 qTOF MS system. To obtain good retention of the polar, predominantly anionic metabolites of glycolysis and the TCA cycle, chromatographic separation was performed by mixed mode hydrophilic interaction – anion exchange using a Luna NH2 3µ column, 150 mm x 1 mm ID (Phenomenex, Torrance, CA). Mobile phase A was acetonitrile and mobile phase B was 5 mM ammonium acetate in water, adjusted to pH 9.9 using ammonium hydroxide. The gradient was a 15 minute linear ramp from 20 to 100%B, followed by a 5 minute hold at 100%B and a 17-minute requilibration period at 20%B. The column temperature was 25°C and the flow rate was 0.07 mL/min, which was ramped to 0.09 mL/min between 20 to 32 minutes. The injection volume was 10 µL. Electrospray ionization was carried out in negative ion mode using a source gas temperature of 350° C, a drying gas temperature of 10 L/min, a nebulizer pressure of 20 psig, and a capillary voltage of 3500 V. Data were collected in TOF full-scan mode over m/z 50-1200 at an acquisition rate of 1 spectra/s with reference mass correction enabled. Data were analyzed using Masshunter Quantitative Analysis software. Metabolites and their ^{13}C isotopes were identified by retention time and m/z values determined from authentic standards. Quantification was performed by peak area after manual inspection of integration accuracy.

For unbiased metabolomics, samples were analyzed on an Agilent 1200 LC / 6530 qTOF MS system using a Waters Acquity HSS T3 reversed-phase column, 50 mm x 2.1 mm ID. For positive ion mode runs, mobile phase A was water with 0.1% (v/v) formic acid and mobile phase B was methanol with 0.1% formic acid. For negative ion mode runs, the formic acid was replaced with 0.1% (m/v) ammonium bicarbonate. The gradient was as follows: 0-0.5 min 1% B, 0.5-2 min 1-99% B, 2-6 min 99% B, 6-6.1-9 min 1% B. The flow rate was 0.35 mL/min and the column temperature was 40° C. The injection volumes for positive and negative mode were 5 and 8 µL, respectively. ESI-MS conditions were the same as for targeted analysis except that the Agilent Jetstream source was used, the nebulizer pressure was 30 psig, and the sheath gas temperature and flow rate were 350° C and 11 L/min. Data analysis was performed using a two-step approach using Agilent Masshunter Qualitative Analysis Software. First, known compounds were identified by searching the LC-MS data against an in-house metabolite library of approximately 600 previously-analyzed authentic standards using the find by formula algorithm. Then, the molecular feature extractor algorithm was used to detect additional unknown features, the features were aligned between samples by mass and retention time, and finally these features were selected and quantitated using find by formula. Principle component analysis was applied to the data to rank features in order of their contribution to differences in the metabolome between cell types.

Protein Normalization of Mass Spectrometry Data

Three additional plates were grown up in each experiment per cell line. Cells were rinsed twice with cold PBS, and then treated with RIPA buffer with complete

protease inhibitor cocktail (Roche) added at suggested concentration for 25 minutes with gentle agitation at 4°C. Protein was scraped off the plate and sheared with a 23-gauge syringe 3-4 times. Protein was collected in microcentrifuge tubes and spun for 15 minutes at 13,000 rpm at 4°C to pellet cellular debris. A Bradford assay was performed to quantify the amount of protein in each sample. This data was averaged and used to normalize the mass spectrometry data to account for differences in the growth rate of cells.

Validation of Unbiased Screening

Directed metabolomic studies were performed as described above to validate pathways in which changes were observed in the unbiased screening experiment.

Data Analysis

Metscape, a plugin for Cytoscape was used to analyze data visually from the unbiased experiment.

Figures

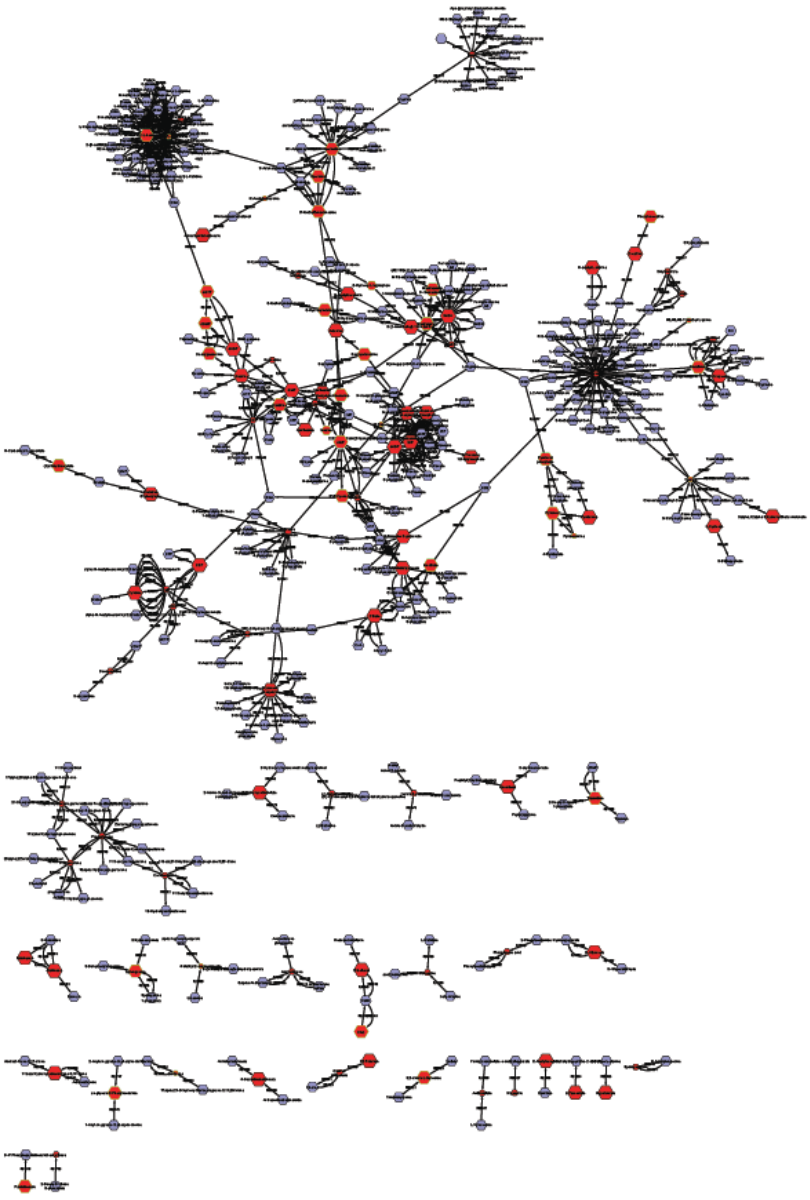

Figure IV.1: Unbiased metabolic screening yields information about pathway changes upon p38γ knockdown

Metabolic map of data. Red hexagons represent compounds that were detected; blue hexagons represent compounds filled in by Metscape data program. Relative size of hexagons indicate whether compounds was found in increased or decreased abundance in p38γ knockdown cells compared to scrambled control. Compounds outlined in green were found to be statistically significant.

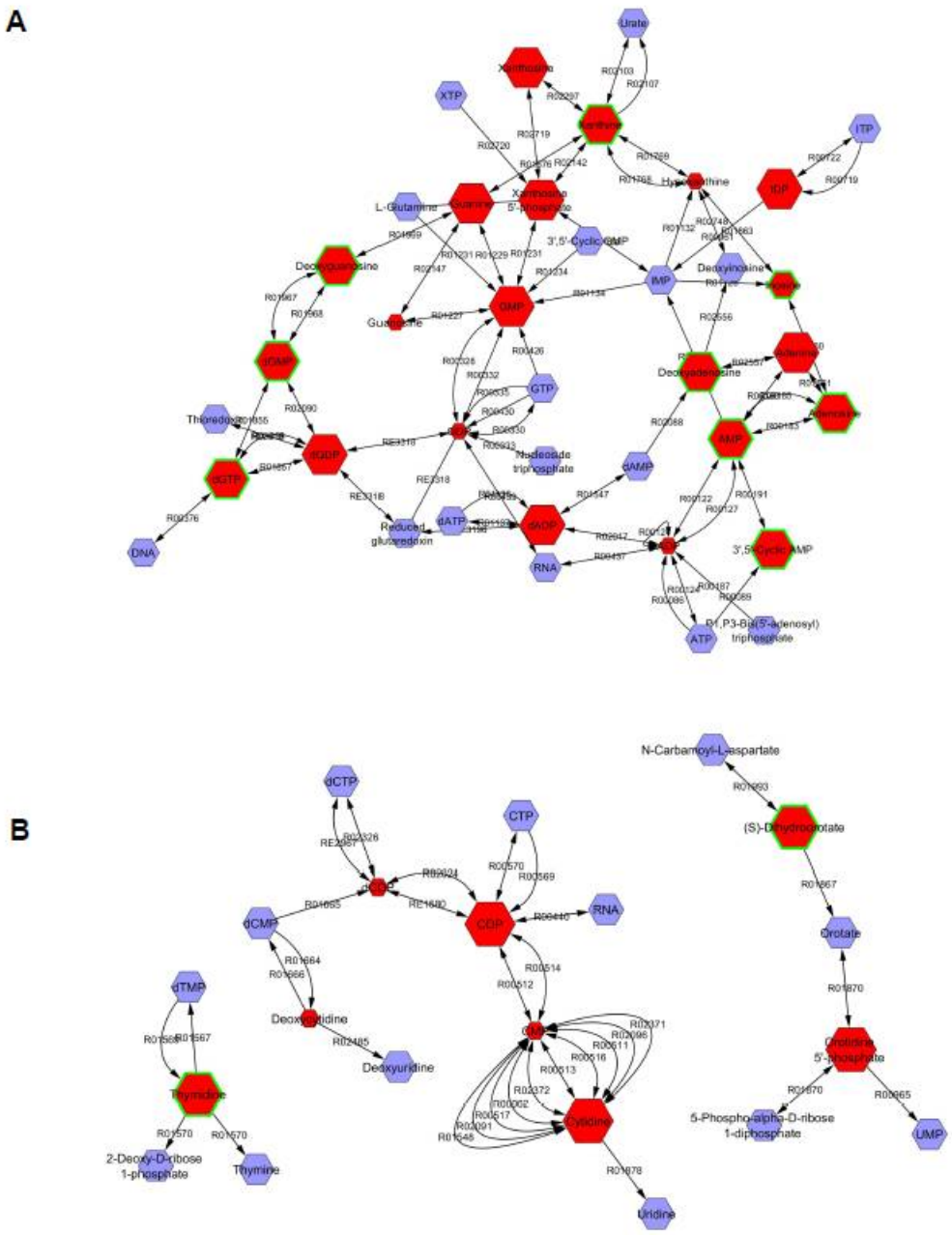

Figure IV.2: Nucleotide synthesis pathways are altered upon p38γ knockdown
A. Purine synthesis pathway B. Pyrimidine synthesis pathway

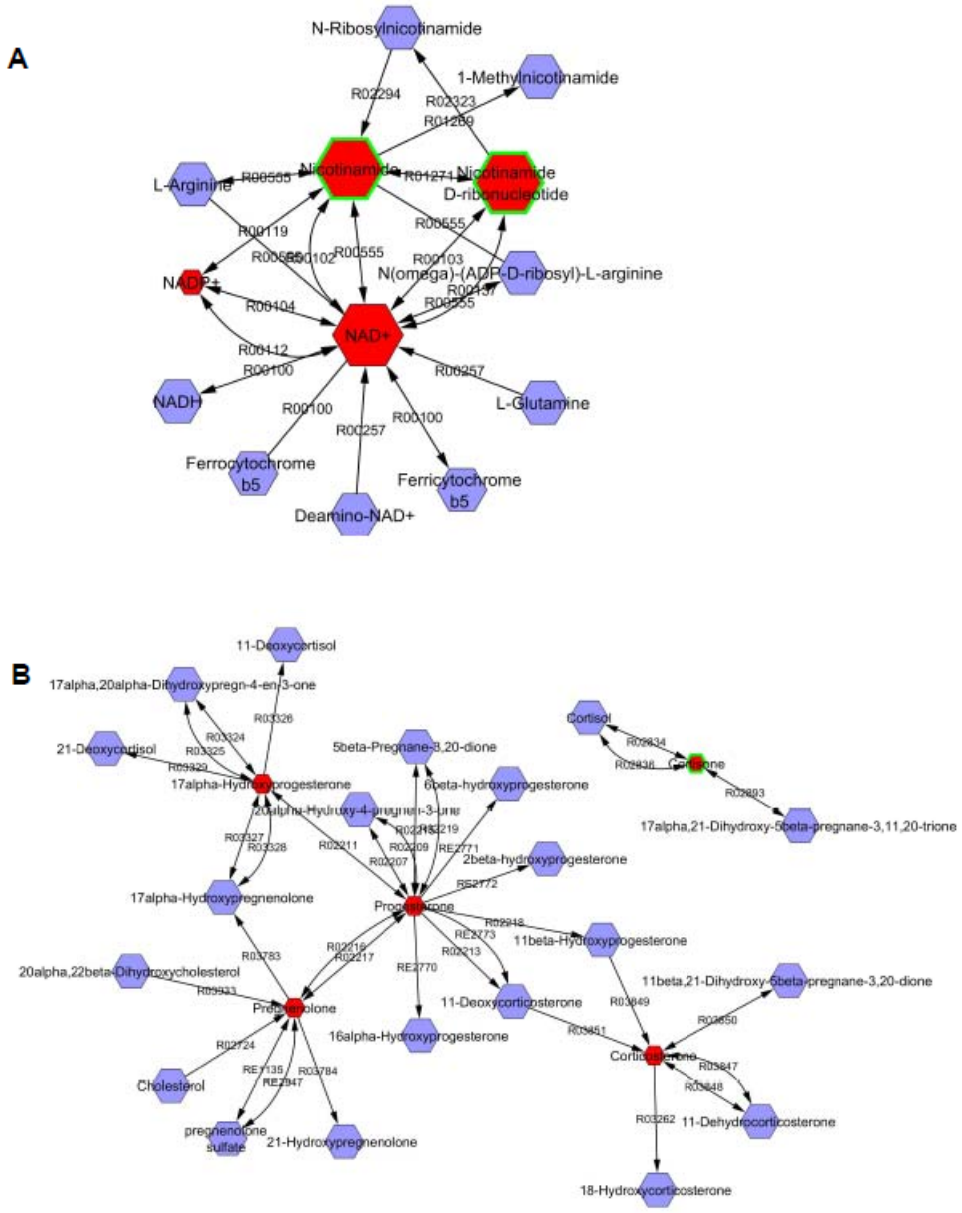

Figure IV.3: NADPH synthesis and C-21 steroid hormone biosynthesis pathways are altered upon p38γ knockdown
NADPH synthesis pathway B. C-21 steroid hormone biosynthesis pathway

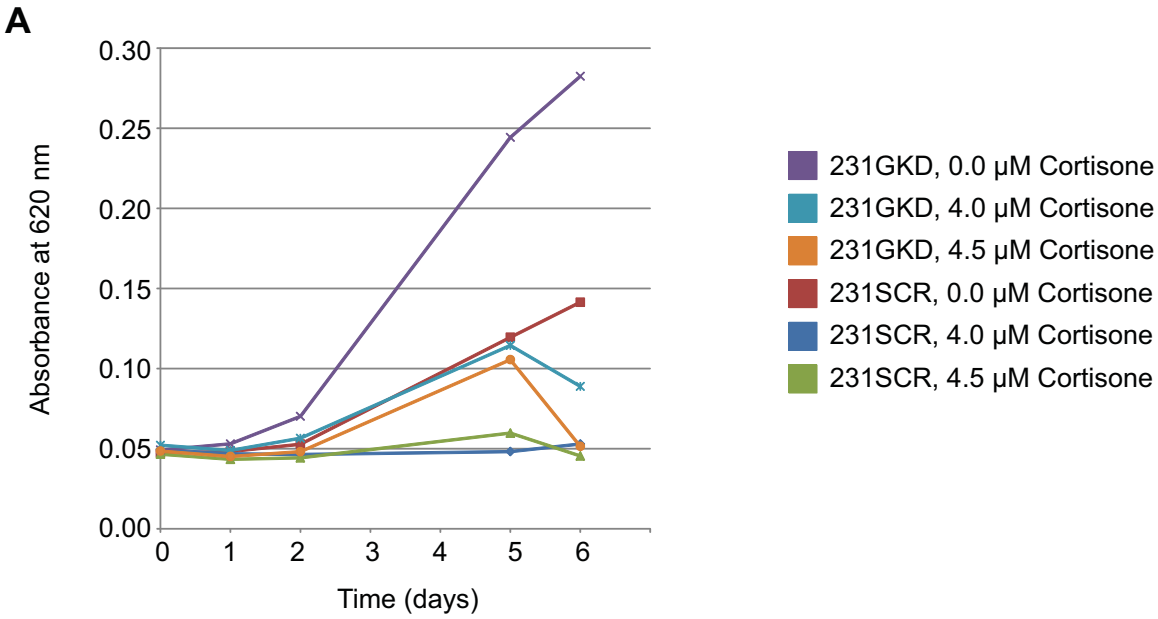

Figure IV.4: Addition of cortisone lowers proliferation back to normal levels
A. MTT Cellular Proliferation Assay

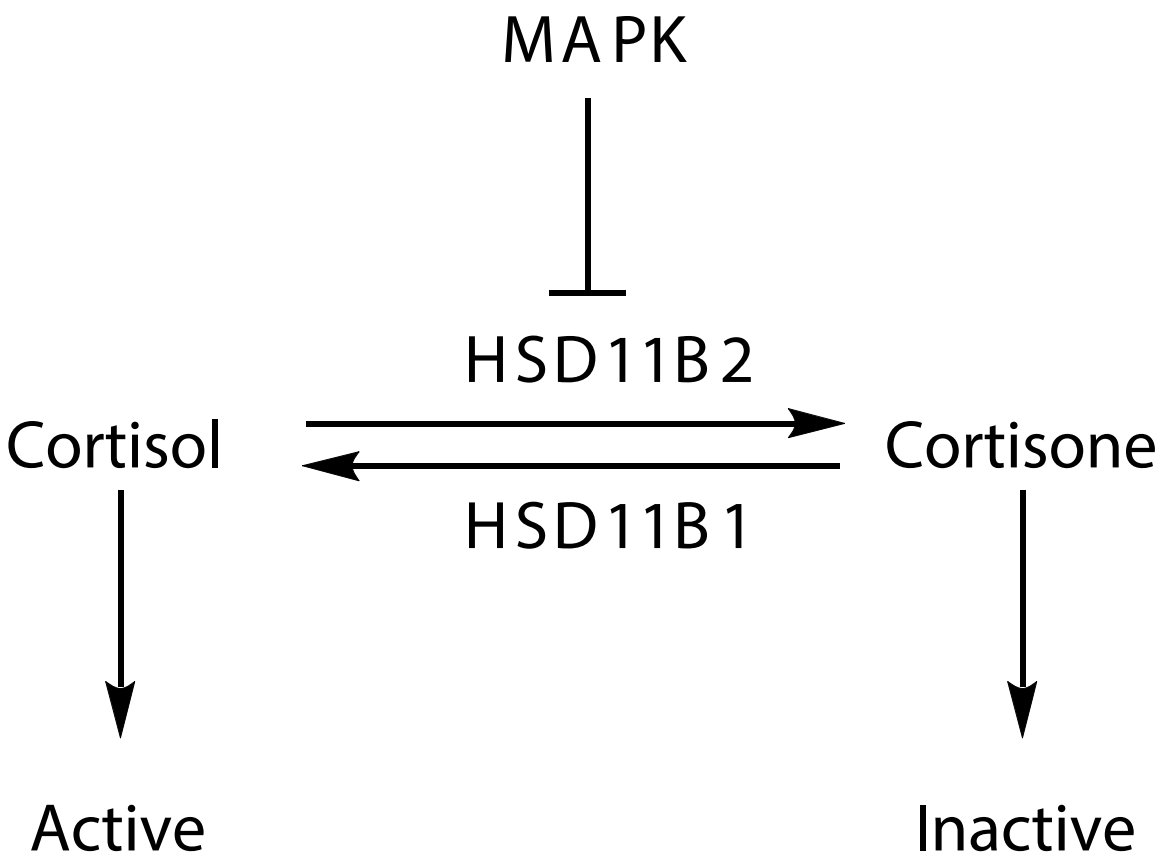

Figure IV.5: Model of Cortisone Regulation

This chapter represents a "manuscript in progress" and will be submitted for publication under the title "Unbiased metabolomic screening reveals key metabolic pathways responsible for energy switch from proliferation to motility in breast cancer cells" by Lauren D. Van Wassenhove, Michelle L. Wynn, ZhiFen Wu, LiWei Bao, Sepideh Ashrafzadeh, Christopher W. Beecher, Charles F. Burant, and Sofia D. Merajver.

Chapter V

Conclusions and Future Directions

Conclusions

Understanding the changes that occur in cancer cells that allow them to leave their area of origin and locally invade and metastasize is crucial in order to target this process and reduce mortality. In the literature, the process of metastasis has been studied in the context of identifying cancer stem cells that can generate metastatic cells, as well as the epithelial to mesenchymal transition (EMT) which enables some cell types to gain metastatic capabilities. Studying the process of metastasis from a metabolic viewpoint has provided new insights into the process by which aggressive cancer cells acquire this ability. In these studies, we utilized breast cell lines to examine the metastatic process. We used immortalized normal breast epithelial cells (MCF-10A), aggressive and metastatic breast cancer cells (MDA-MB-231) and inflammatory breast cell line (SUM149), which are also metastatic. Using these two very different metastatic cell lines enabled us to determine some of the different mechanisms that cells use to acquire metastatic properties. This work identified the mevalonate pathway, an alternative acetyl-CoA metabolic pathway, and the C-21 steroid hormone biosynthesis pathways as important regulators of motility and metastasis. In the following section, I will discuss the important conclusions of each chapter.

Chapter II: Zoledronic acid treatment prevents phosphorylation of CUB-domain containing protein 1 and leads to decreased motility and invasion in breast cancer

In this chapter, we found that the mevalonate pathway is important in the regulation of prenylation and activation of small GTPases including RhoC, Cdc42, and Rac. These small GTPases are critical in the regulation of cell movement through actin-myosin contractility and are part of the process necessary for invasion and metastasis. The mevalonate pathway synthesizes and attaches prenyl groups to these small GTPases, which targets them to their site of activity, the cell membrane. Recent work in our lab has shown RhoC to be required for metastasis, thus the role of the mevalonate pathway in targeting of Rho C to the cell membrane is vital [128]. Mevalonate pathway inhibitors atorvastatin (AT), zoledronic acid (ZA) and geranylgeranyl transferase inhibitor 298 (GGTI) were all able to reduce the ability of breast cancer cells to move and invade to differing extents. ZA was found to be not as effective as the other mevalonate pathway inhibitors in most of the *in vitro* assays conducted, usually only affecting MDA-MB-231 breast cancer, and not the SUM149 breast cancer cell line, perhaps due to its inability to affect the localization of the small GTPases (Figure II.5). Because we observed that ZA was effective in some of the assays, but did not affect GTPase localization as hypothesized, we conducted a microarray to look for alternative targets that ZA could be affecting. Among the many genes in the microarray that showed differential expression after ZA treatment, we selected CUB-domain containing protein 1 (CDCP1) for further study because it has been proposed in the literature to regulate invasion and motility in cancer and to interact with the AKT pathway [97, 98]. From this, we identified CUB-domain containing protein 1 (CDCP1) as an important target of ZA. We identified a

novel mechanism in which ZA inhibits the phosphorylation, and thus activation of CDCP1. CDCP1 plays a very important role in the regulation of motility and invasion, presumably through interaction with the AKT pathway [95, 98]. Other labs have studied the effect of the mevalonate pathway in breast cancer motility and invasion, and our results are consistent with the literature [86, 89-91]

Chapter III: Alternative pathway for acetyl CoA metabolism prevents inflammatory breast cancer cell line SUM149 from undergoing oxidative phosphorylation

In our work studying inflammatory breast cancer, we discovered that SUM149 cells do not undergo oxidative phosphorylation. While it has been extensively shown in the literature that cancer cells undergo the Warburg effect[2, 4, 10, 16, 17, 26, 115], such a severe phenotype in which cancer cells are unable to undergo oxidative phosphorylation and do not consume oxygen has not been seen, except in cells that lack mitochondria entirely (Human 143B osteosarcoma ρ° cells) [129]. In the Warburg effect, cancer cells preferentially use the process of glycolysis alone to metabolize glucose to lactic acid and 2 molecules of ATP, even in the presence of excess oxygen, instead of metabolizing glucose to enter the TCA cycle and then oxidative phosphorylation, breaking it down to CO_2 and 32-36 molecules of ATP [16, 130]. In this paper, we found that SUM149 cells had sufficient numbers of morphologically normal mitochondria (Figure III. 7). Additionally, while SUM149 cells expressed reduced protein levels of both citrate synthase and pyruvate dehydrogenase, which both had reduced catalytic activity *in vitro* (Figure III.3), this was not sufficient to explain the phenotype in the cells. After completing both directed and unbiased metabolomics studies, an alternate pathway for acetyl-CoA metabolism in the SUM149 cell line was identified. Normal cells will use

pyruvate derived-acetyl CoA to make citrate, beginning the tricarboxylic acid (TCA) cycle. This pathway eventually breaks down the six carbon citrate to four carbon oxaloacetate, releasing two molecules of carbon dioxide (CO_2) as well as producing two molecules of nicotinamide adenine dinucleotide (NADH) and one molecule of flavin adenine dinucleotide ($FADH_2$) (Figure I.3). NADH and $FADH_2$ act as reducing agents, carrying electrons that are used as an energy source for the electron transport chain. Besides these electrons, the oxidative phosphorylation also requires oxygen consumption. However, in SUM149 cells, we found that they did not use pyruvate-derived acetyl CoA for citrate synthesis, but instead use it to make N-acetyl-aspartate. It is unclear at this time where the synthesis of N-acetyl aspartate is the cause of these cells inability to undergo oxidative phosphorylation or an effect of this inability. We propose, however, that the production of N-acetyl aspartate leads to a deficiency in citrate. Because of the lack of citrate to run the TCA cycle, it may be that the cells cannot produce enough of the TCA cycle intermediates necessary for oxidative phosphorylation. This inability to perform oxidative phosphorylation may confer the ability to survive and thrive under hypoxic conditions to SUM149 cells, thereby facilitating metastases. In fact, recent work has shown that SUM149 cells are constitutively adapted to hypoxia via constitutive upregulation of hypoxia inducible factors (HIFs) [131]. Our work suggests a mechanism which allows SUM149 cells to prevent reliance on oxidative phosphorylation, reducing its need for oxygen consumption. We hypothesize that siRNA knockdown of acetyl transferase enzyme encoded by N-acetyl-aspartate transferase 8-like (NAT8L), which synthesizes N-acetyl aspartate from acetyl-CoA and oxaloacetate, will restore the ability of SUM149 cells to undergo oxidative phosphorylation. Additionally, overexpression of

aspartoacylase (ASPA) enzyme necessary to break down N-acetyl aspartate may also rescue this phenotype. These experiments will also allow us to determine if N-acetyl aspartate synthesis is the cause of the oxidative phosphorylation defect or if it is an effect.

Chapter IV: Unbiased metabolomic screening reveals key metabolic pathways responsible for energy switch from proliferation to motility in breast cancer cells

In this study, we examined the role of p38γ in the regulation of proliferation and motility in the aggressive, metastatic breast cell line MDA-MB-231. Previous work in our lab showed that shRNA knockdown of p38γ resulted in a reduction of cellular motility and an increase in proliferation in these cells [62]. Further work showed that p38γ regulates the stability of small GTPase motility protein RhoC, and that p38γ knockdown resulted in the formation of abnormal actin structures, thus inhibiting the ability of these cells to move in a productive manner [62]. The p38γ knockdown cells acted like a less aggressive cancer in every *in vitro* measure of metastatic potential, suggesting that p38γ is an important factor in breast cancer aggressiveness [62]. Further work in a murine xenograft model showed that p38γ knockdown cells formed larger tumors that grew more quickly than the scrambled control cell line [unpublished data], but they also metastasized significantly less frequently [62].

In total, these studies suggest that p38γ may regulate an important metabolic switch that selects whether energy should be used to proliferate or to move. This switch may be crucial in understanding what occurs in the process of metastasis in terms of factors involved in the cell when it begins to reactivate motility programs in order to metastasize. In this work, through the use of unbiased metabolic screening, we have identified C-21 steroid hormone biosynthesis as being essential for the metabolic switch

between proliferating and motile cellular behaviors. This pathway, through the generation of hormones such as estrogen and testosterone, plays a key role in the regulation of cancers of the reproductive system including breast, ovarian, and prostate cancers. In this chapter, we found that C-21 steroid hormone biosynthesis was decreased in MDA-MB-231 when p38γ was knocked down. We hypothesized that the addition of cortisone, an important member of this pathway and precursor to hormones such as estrogen, may rescue the effects of p38γ knockdown. We found that the addition of cortisone did slow the proliferation rate of p38γ knockdown cells back to the level of the scrambled control. Further experiments will need to be done to find out if cortisone addition can also rescue the motility defect in p38γ knockdown cells. The results of these experiments suggest the importance of the C-21 steroid hormone biosynthesis pathway in the regulation of the switch from proliferation to motility in the cancer cell.

The final portion of this chapter will discuss future directions for each of the research findings.

Future Directions

Chapter II: Zoledronic acid treatment prevents phosphorylation of CUB-domain containing protein 1 and leads to decreased motility and invasion in breast cancer

In this chapter, the effect of the mevalonate pathway in modulating motility and metastasis in breast cancer and normal breast cells was examined. The mevalonate pathway was found to play an important role in regulating cell shape, individual motility, collective cell motility, and invasion. In addition, an alternative mechanism of action for zoledronic acid (ZA) was identified. ZA prevents the tyrosine phosphorylation and thus activation of CUB-domain containing protein 1 (CDCP1). This protein plays important

roles in cancer, especially in regulating metastasis and invasion processes. Further work to fully characterize the role of ZA in the inhibition of CDCP1 activation will be necessary in order to uncover the details of this mechanism. The exact mechanism of the inhibition of CDCP1 by ZA has yet to be determined. Perhaps ZA prevents phosphorylation by directly binding to CDCP1, causing a conformational change so that the tyrosine residue is no longer accessible for phosphorylation. Alternatively, ZA could bind to the src-family kinase responsible for phosphorylation of CDCP1. Teasing out this mechanism could be accomplished by analyzing how ZA affects the expression or prevents binding of src-family kinases to CDCP1. To determine if ZA directly binds CDCP1, isothermal titration calorimetry could be conducted with varying amounts of ZA to measure the binding affinity and thermodynamic properties[132]. Also, CDCP1 is an important activator of the AKT/MAPK pathway [97, 98]. To see if the inhibition of CDCP1 via ZA affects the AKT pathway, measuring AKT activation via phosphorylation of AKT isoforms AKT1, AKT2, and AKT3 will be important. This can be accomplished using AKT1, 2, and 3 specific antibodies to pull down these proteins, and then Western blotting with a pan-Phospho-AKT antibody.

The present paper found that ZA did not change the localization of small GTPase proteins as hypothesized due to its proposed role in mevalonate pathway regulation via inhibition of farnesyl pyrophosphate synthase. Because of this, a microarray was conducted in order to identify possible targets of ZA. Further validation and study of this data may lead to more complete knowledge of the effect of ZA on breast cancer cells. Although we did not validate every hit, in Chapter II, we focused on CDCP1 because of its importance in cancer motility. One other target that we pursued is methionine

transferase 2A (MAT2A) because of our interest in metabolism. MAT2A is the gene for a subunit of the MAT II complex, which is responsible for the production of s-adenosyl methionine (SAM) from methionine and ATP [133]. SAM is a potent anti-proliferation signal that acts to regulate MATII, thereby preventing further SAM production. MAT2A protein expression is decreased in the two cancer cell lines compared to normal cells, which is the anticipated result, given its anti-proliferative role. ZA treatment further reduced the expression of MAT2A in the cancer cells (Figure V.1A). MAT2A has been shown to play an important role in breast cancer as the methyl donor for DNA methylation, which often occurs in breast cancer [134]. Inhibitors of SAM in breast cancer cells are very effective antitumor agents, possibly acting through activation of MAPK and STAT signaling [135]. In our proposed model, ZA acts on MAT2A, reducing the amount of SAM available for DNA methylation, and activates MAPK and STAT pathways, leading to reduced invasion and proliferation (Figure V.1B). It will be important to further identify the role of ZA in MAT2A regulation by measuring DNA methylation, as well as JAK/STAT pathway activation upon ZA treatment.

In addition to the target MAT2A, we identified 10 other targets that we were able to verify via qRT-PCR (Figure II.9). These targets, listed in Table V.1A, need to be examined further. Additionally, we found in this work that ZA often had opposite effects in the two breast cancer cell lines MDA-MB-231 and SUM 149 (See Chapter II). In agreement with that work, we identified several targets in the microarray that were differentially regulated upon ZA treatment between these two cell lines. These genes are listed in Table V.1B, and may help to uncover the differential mode of action of ZA in these two breast cancer cell lines.

Due to the number of targets identified in the microarray, this drug may have many non-specific, off-target effects. Further work characterizing commonalities among the drug targets to identify how ZA interacts with each target, perhaps through a specific binding motif, could lead to information that may help in the generation of more specific drugs. Additionally, work to improve the specificity of other mevalonate pathway inhibitors, such as GGTIs or FTIs (farnesyl transferase inhibitors) may lead to less toxic therapies that may prove very effective in the clinic.

Chapter III: Alternative pathway for acetyl CoA metabolism prevents inflammatory breast cancer cell line SUM149 from undergoing oxidative phosphorylation

This work identified an alternate pathway for acetyl-CoA metabolism in the inflammatory breast cancer cell line SUM 149. In this pathway, acetyl-CoA is redirected from the synthesis of TCA cycle intermediate citrate and is instead used to acetylate aspartate, making N-acetyl aspartate. This metabolite has no known function outside of the nervous system. If most of acetyl-CoA is directed into N-acetyl aspartate synthesis, then very little will be available for use in the TCA cycle to generate intermediates necessary for oxidative phosphorylation. This may explain a least part of the oxidative phosphorylation defect in SUM149 cells. We found that the acetyltransferase enzyme NAT8L, which forms N-acetyl aspartate from aspartate and acetyl-CoA, is highly upregulated at the mRNA level in SUM 149 cells (III.4D). In addition, the deacetylating enzyme ASPA, which converts N-acetyl aspartate back to acetic acid and aspartate, is absent at both the mRNA and the protein level in SUM 149 cells (III.4D, E). We hypothesize that either knockdown of NAT8L or overexpression of ASPA enzymes may be able to rescue at least part of the oxidative phosphorylation defect in SUM149 cells.

Additionally, overexpression of NAT8L in normal breast cells MCF-10A may induce a reduction in their oxidative capacity. Other work has shown that SUM 149 cells are constitutively adapted to hypoxia [131]. If the production of N-acetyl aspartate does prevent oxidative phosphorylation, the ability to make this metabolite may account for a large portion of this phenotype. This study highlights the importance of this enzyme and metabolite in the aggressiveness of SUM 149 cells.

Further work should be done to determine if accumulation of N-acetyl aspartate is specific to only SUM149 cells, or if it can be generalized to aggressive breast cancers or cancer as a whole. In our studies, we did find that aggressive breast cancer cell line MDA-MB-231 was also able to make N-acetyl aspartate, but only accumulated about half that of what SUM149 cells did (Figure III.4A, B). Also, the mRNA and protein expression of NAT8L was much lower in MDA-MB-231 cells (Figure III.4D). However, because MDA-MB-231 cells express ASPA protein, (Figure III.4 E), we hypothesize that they can efficiently break down N-acetyl aspartate, allowing these cells to retain the ability to perform oxidative phosphorylation (Figure III.1A). Recent work has also shown an accumulation of this metabolite in human ovarian cancer samples, with higher amounts in metastatic compared to epithelial ovarian tumors [136]. Staining tumor samples with NAT8L antibodies may show a correlation of higher expression of NAT8L with more aggressive tumors and may be associated with poor clinical outcomes.

Other work has shown the correlation of N-acetyl aspartate with inflammation [137]. Inflammation is an important component of the development and progression of cancer [138, 139], and the role of this metabolite in either inducing or sustaining inflammation may be an important area to investigate. There is a large body literature

regarding tumor associated macrophages (TAMs), and their role in the cancer microenvironment. TAMs have been found to play both tumor-promoting and tumor-inhibiting roles. TAMs have been found to play cancer promoting roles by secreting cytokines which provide cancer cells with growth and migration signals, as well as recruiting more immune cells to the area to produce even more cytokines[139]. Additionally, TAMs can secrete angiogenic factors like vascular endothelial growth factor (VEGF) that aid the cancer cells in making new blood vessels to provide a greater oxygen and nutrient supply[140, 141]. Also, TAMs can secrete matrix metalloproteases (MMPs) which can aid the cell in the invasion process, and they can secrete additional cytokines that activate the MMPs [141]. TAMs have also been shown to have an anticancer effect, as in gastric cancer and non-small cell lung cancer, infiltration of the tumor with TAMs correlates with improved prognosis [138, 142, 143]. These cells may play an important role in mediating the inflammatory effect of N-acetyl aspartate. Further study into how N-acetyl-aspartate may regulate inflammation in the context of breast cancer and how TAMs may mediate this effect should be pursued. Co-culturing SUM149 cells with TAMs may enable us to identify an effect of N-acetyl aspartate as well as uncover any role that TAMs may play in promoting an inflammatory microenvironment due to increased cytokine and pro-angiogenic factor secretion ([139-141])

Because of the lack of knowledge of the function of N-acetyl aspartate outside the brain, further work should be done to examine its presence in both tumor and normal tissue samples. If, indeed it is not found in normal non-brain tissue, this may make an ideal drug target. The blood-brain barrier is highly selective and prevents toxins and

chemicals from reaching the brain. A drug that was manufactured to target NAT8L or N-acetyl aspartate could be engineered so that it would not pass through the blood-brain barrier and affect normal brain function. Wiame et al. [114] developed a radiochemical *in vitro* assay that can measure NAT8L activity, and Tahay et al. [113] modified the assay to use DNTB [5,5-dithiobis-(2-nitrobenzoic acid)] as an indicator for a colorimetric *in vitro* assay to measure activity. This assay could be coupled with a small molecule screen to look for molecules that inhibit NAT8L activity.

When we first observed the inability of SUM 149 cells to undergo oxidative phosphorylation (Figure III.1B), we hypothesized that these cells were unable to transport pyruvate into the mitochondria. We first conducted ^{13}C-2,3-pyruvate stable isotope tracing experiments in order to determine if pyruvate was entering into the mitochondrial TCA cycle. These experiments showed low amounts of citrate being labeled by pyruvate in SUM149 cells, as well as low unlabeled citrate (Figure III.3C), which seemed to confirm this hypothesis. To observe the role of the mitochondrial transporter directly, we performed these same ^{13}C-2,3-pyruvate stable isotope tracing experiments with and without the phenyl succinate, which inhibits this transporter. We found that inhibition of the transporter had similar effects on all three cell lines, and led to decreased amounts of labeled substrate in TCA cycle intermediates, consistent with its role of inhibiting the mitochondrial pyruvate transporter (Figure V.2). This data was unable to explain the lack of oxidative phosphorylation in SUM149 cells, as we would have expected to see a much stronger effect of phenyl succinate in MCF-10A and MDA-MB-231 cells, and little to no effect on SUM 149 cells if their mitochondrial pyruvate transporter was not functional.

After additional examination of the ^{13}C-2,3-pyruvate stable isotope tracing experiments, we found that although there were low amounts of unlabeled and labeled citrate in SUM 149 cells, acetyl-CoA was being efficiently made in these cells (Figure III.3B), which suggests that there is no defect of the mitochondrial pyruvate transporter.

Because of the high rate of glutamine degradation in cell media [144] and the known importance of glutamine as a TCA cycle substrate in cancers through the process of glutaminolysis [26, 115], we decided to investigate whether there was sufficient glutamine in the media we were using to conduct both the bioenergetic profile experiments to measure oxidative phosphorylation as well as the ^{13}C-2,3-pyruvate stable isotope tracing experiments. The same media is used for both, and when we quantified the amount of glutamine in media samples saved and frozen from a ^{13}C-2,3-pyruvate stable isotope tracing experiment, we found that the levels of glutamine were much lower than that of the expected 2.5 mM, and were lower than the published k_m of 3 mM for glutaminase, the enzyme which converts glutamine to glutamate for preparation of its entry for use as a TCA cycle fuel (See Table V.2 and Figure I.3) [145]. If glutamine concentrations are low, glutaminolysis is probably not occurring in the cell lines. If there is a block in the TCA cycle early between acetyl-CoA and citrate, and this causes deficient oxidative phosphorylation due to the inability to produce TCA cycle intermediates necessary for this process, providing glutamine for glutaminolysis may rescue this phenotype. Because of this, I decided to measure oxidative phosphorylation in SUM149 cells with and without glutamine. In this experiment, I found that in both cases, SUM149 had very low rates of oxygen consumption and did not respond to any of

the mitochondrial inhibitors, showing that the inability of SUM149 cells to undergo oxidative phosphorylation is a glutamine-independent phenotype (Figure V.3).

It is important to note that due to the low amounts of glutamine that I observed in the media (Table V.2), all of my ^{13}C-2,3-pyruvate stable isotope tracing experiments may have had low glutamine concentrations. I would expect that if I prepared the media with fresh glutamine before the experiment, I may see an increase in the amount of unlabeled citrate being made in SUM149 cells; however, I would not expect to see an increase in labeled citrate, because the 15-minute incubation time with ^{13}C-2,3-pyruvate would not be enough time to label sufficient amounts of glutamine to then be used as a TCA cycle substrate. Completing a^{13}C-2,3-pyruvate stable isotope tracing experiment with and without glutamine may also inform us of the importance of glutaminolysis in SUM149 cells by allowing us to measure the fraction of TCA cycle intermediates that are produced with and without the presence of glutamine.

In order to directly quantify glutaminolysis in all three cell lines, we also performed glutamine tracer experiments with uniformly labeled 13C-glutamine. Because SUM 149 does not appear to use much pyruvate derived acetyl-CoA for the synthesis of citrate and other TCA cycle intermediates, we hypothesized that these cells may rely more on glutaminolysis in order to generate these intermediates. We hypothesized that cells without glucose will rely more on glutaminolysis for making both energy and bioenergetic material, and we would observe a higher percentage of labeling in intermediates when no glucose is given. We found that indeed the SUM 149 cells do perform more glutaminolysis than MDA-MB-231 and MCF-10A cells (Figure V.4). Additionally, when the cells are not given glucose, they appear to metabolize glutamine

more rapidly. However, the 15 minute timepoint we used may not be the ideal time point as it appears that very little glutamine label is getting into the cells. Further optimization is needed to find ideal the time points to detect adequate label incorporation.

Surprisingly, this work showed that breast cancer cells undergo gluconeogenesis (Figure III.3E, F). To our knowledge, only cells of liver, kidney, or intestinal origin have been found to perform gluconeogenesis [27]. This is a paradigm-altering finding. It may be that other cancers also undergo gluconeogenesis, making this process a possible target for cancer therapy or a useful biomarker for cancer diagnosis in normally non-gluconeogenic tissues. However, due to the prevalence of this process in normal human tissues of liver, kidney, or intestinal origin, it may not make an ideal target for therapy. Further study will need to be undertaken to understand how and why these cells use this mechanism to make glucose from lactate and pyruvate. Utilizing this process may be more efficient than oxidative phosphorylation in terms of energy cost and time to complete. Additionally, in our ^{13}C-2,3-pyruvate stable isotope tracing experiments that identified gluconeogenesis in our cell lines, we were unable to quantify glucose production, just labeled glycolysis intermediates upstream of pyruvate including fructose-1,6-bisphosphate, 2-phosphoglycerate, and 3-phosphoglycerate (Figure III.3, I.4). It may be that these cell lines are instead using gluconeogenesis only to produce metabolites upstream of pyruvate in order to generate intermediates necessary for nucleotide and serine synthesis and are not using gluconeogenesis to make more glucose. Measuring the protein expression of gluconeogenesis enzymes (listed in red in Figure I.4) in our cancer cell lines to look for which ones are upregulated might give us an idea of whether the cells are taking lactate and pyruvate all the way back to glucose or not. For example if

glucose-6-phosphatase expression is low, it would suggest that the cells are not taking lactate and pyruvate all the way back to glucose, as this enzyme catalyzes the last step in gluconeogenesis, the conversion of glucose-6-phosphate to glucose. To examine if using gluconeogenesis is widespread in cancer, examining the mRNA expression of gluconeogenesis enzymes may be informative.

In order to further understand the differences between the SUM149, MCF-10A, and MDA-MB-231 cell lines we conducted quantitative-RT-PCR arrays of mitochondrial energy metabolism (Figure V.5, Table V.3). This led to some interesting observations, such as very high expression of lysosomal ATPase pumps in SUM149 cells. Due to the high amount of lactic acid production in this cell line, it may be that these pumps need to be utilized in order to pump lactic acid out of the cell. Further study into the importance of these pumps may result in the identification of new targets for this aggressive breast cancer. Additionally, changes in mRNA expression were found in subunits of succinate dehydrogenase and NADH dehydrogenase complexes. These complexes are required for oxidative phosphorylation, and further exploration of how their expression might be regulated differently in SUM149 cells may lead a more robust description of how these cells are unable to perform oxidative phosphorylation.

Chapter IV: Unbiased metabolomic screening reveals key metabolic pathways responsible for energy switch from proliferation to motility in breast cancer cells

In this chapter we used unbiased metabolomics screening to determine the effect of p38γ knockdown on breast cancer cell line MDA-MB-231. We found previously that p38γ knockdown increased proliferation and decreased motility, causing these cells to revert to a less aggressive state. We hypothesized that this single molecular change

resulted in the alterations of metabolic pathways leading from the phenotypic switch from motile to proliferative cells. Our screen identified several key pathways that seemed to be altered upon p38γ knockdown. In this chapter we studied the C-21 steroid hormone biosynthesis pathway in further detail because of the known importance of steroid hormones in breast cancer. We found that the addition of pathway intermediate cortisone rescued the effects of p38γ knockdown by reducing proliferation. Further work should be done to examine the effect of cortisone addition on motility and invasion. We hypothesize that cortisone addition will allow the cells to overcome the motility defect and increase invasion. This work highlights the importance of this pathway in regulating the phenotypic switch between proliferation and motility. Further work will need to be done to characterize the mechanism by which p38γ regulates this metabolic pathway.

In addition, this work identified alterations in the bile-acid synthesis pathway and the NADH synthesis pathway. Further investigations into both of these pathways may help to characterize this phenotypic switch. In p38γ knockdown cells, the bile-acid synthesis pathway seemed to be downregulated overall. The molecule taurine was significantly downregulated in p38γ knockdown compared to scrambled control cells. Taurine derivatives have been shown to play a role in the regulation of cancer cell proliferation [146]. Experiments stimulating the p38γ knockdown cells with taurine may rescue the knockdown phenotype as well. Additionally, NADH synthesis seemed to be upregulated in p38γ knockdown cells. Inhibiting this process with a small molecule inhibitor may rescue the knockdown phenotype. Additionally, understanding the role of p38γ knockdown in the direct or indirect regulation of these pathways should be pursued.

When we first began to tease out the metabolic differences between the p38γ knockdown and the scrambled control cells, we conducted a bioenergetic profile to measure oxidative phosphorylation. In the literature, cancer cell lines display reduced oxidative capacity (due to a preference for lactate production). More aggressive cancer cells usually display less oxidative capacity than less aggressive cells [147]. We found that p38γ knockdown cells displayed a higher oxidative capacity (Figure V.6), which is consistent with their less aggressive phenotype.

Methods

Cell Culture and drug treatment

MCF-10A cells were cultured in 1:1 Ham's F-12 and Dulbecco's modified Eagle's medium (DMEM) with 2 mM L-glutamine supplemented with 5% horse serum, extracellular growth factor, cholera toxin, insulin, hydrocortisone, gentamycin, fungizone, and penicillin/streptomycin at 37ºC under 5% CO_2. MDA-MB-231 cells were cultured in RPMI 1640 supplemented with 10% fetal bovine serum, gentamycin, fungizone and penicillin/streptomycin at 37ºC under 5% CO_2. SUM149 cells were cultured in Ham's F-12 with L-glutamine supplemented with 5% fetal bovine serum, insulin, hydrocortisone, gentamycin, fungizone and penicillin/streptomycin under 10% CO_2. For drug treatment, all cells were grown to 30-50% confluence, serum starved for 16-20 hours, then treated with 10μM ZA (dissolved in PBS) for 72 hours total in serum-containing medium. Medium containing ZA was replaced after 48 hours. Drug concentration and treatment times were determined based on what has been previously reported in literature [83, 102-105] and results from cell proliferation assays (MTT

assays, data not shown). The concentrations used were effective at inhibiting growth of MDA-MB-231 and SUM149, but not MCF10A cells.

Protein Extraction and Western Blot

Cells were washed with cold phosphate-buffered saline (PBS) and lysed in radioimmunoprecipitation assay (RIPA) buffer plus Complete protein inhibitor cocktail (Roche). Cells were sheared with a 23 gauge syringe and protein was collected after centrifugation to remove cellular debris. 30-60μg of protein was electrophoresed onto a SDS-PAGE gel. The protein was transferred to a nitrocellulose membrane using a semidry apparatus (BioRad). The membrane was blocked using 5% milk in TBST and incubated in either 5% milk in TBST or 5% bovine serum albumin (BSA) in TBST. Membranes were incubated with the appropriate secondary antibodies conjugated to horseradish peroxidase (HRP) at concentrations of 1:5000 in 5% milk in TBST. Protein bands were detected by electrochemiluminescence.

Microarray Methods

RNA was isolated from MCF10A, MD-MBA-231, and SUM-149 cell lines grown with or without ZA treatment using Trizol according to the instructions. RNA was cleaned using the RNAeasy MinElute Cleanup Kit (Qiagen) according to instructions, and submitted to the University of Michigan Microarray Core. One experiment was done in duplicate. Expression values for each gene were calculated using the robust multi-array average method [108] . Only probesets with a 2 fold or higher change (when ZA treated cells were compared to untreated cells) were selected for comparison across the three cells lines, provided that one of the two samples had an expression value of at least 2^6.

Quantitative RT-PCR methods

RNA was isolated from cell lines grown with or without ZA treatment using Trizol. The Promega Reverse Transcription System was used according to package instructions to make cDNA from isolated RNA. SYBR Green Mastermix was used according to directions for Quantitative PCR. Three experiments were done in triplicate.

Preparation of Extracts for Targeted Metabolomics and ^{13}C mass isotopomer analysis

Cell extracts were prepared and analyzed according to a modified protocol from Lorenz et al, [118]. Cells were grown to 80% confluence on 6 cm culture plates. Cells were then changed to XF Assay Medium Modified DMEM (Seahorse Biosciences) supplemented with 11 mM glucose and 10 mM pyruvate or Dulbecco's Modified Eagle's Medium (DME) Base without L-Glutamine, Glucose, Phenol Red, Sodium Pyruvate, or Sodium Bicarbonate supplemented with 11mM glucose and 10 mM sodium pyruvate, 2.5 mM glutamine and .015g/L phenol red and incubated at 37°C for 1 hour in a non-CO_2 incubator. Cells were then changed to the same media with uniformly labeled 13C-glutamine or ^{13}C-2,3 pyruvate and incubated for the indicated 15 minutes. Cells were then rinsed by rapid addition and removal of 3 mL of distilled water, after which metabolism was immediately quenched by pouring liquid nitrogen into the plate. Plates were stored at -80°C until extraction. Cells were extracted by adding 500 µL of ice-cold 8:1:1 methanol:water:chloroform to the frozen cell surface and scraping with a cell scraper. The extract and residual cell debris were transferred to polypropylene microcentrifuge tubes and centrifuged for 5 min at 15,000 x g at 4°C. The supernatant was transferred to autosampler vials and analyzed by LC-MS.

LC-MS Methods and Data Analysis

For targeted metabolomics and ^{13}C mass isotopomer analysis, samples were analyzed on an Agilent 1200 LC / 6520 qTOF MS system. To obtain good retention of the polar, predominantly anionic metabolites of glycolysis and the TCA cycle, chromatographic separation was performed by mixed mode hydrophilic interaction – anion exchange using a Luna NH2 3µ column, 150 mm x 1 mm ID (Phenomenex, Torrance, CA). Mobile phase A was acetonitrile and mobile phase B was 5 mM ammonium acetate in water, adjusted to pH 9.9 using ammonium hydroxide. The gradient was a 15 minute linear ramp from 20 to 100%B, followed by a 5 minute hold at 100%B and a 17-minute requilibration period at 20%B. The column temperature was 25°C and the flow rate was 0.07 mL/min, which was ramped to 0.09 mL/min between 20 to 32 minutes. The injection volume was 10 µL. Electrospray ionization was carried out in negative ion mode using a source gas temperature of 350° C, a drying gas temperature of 10 L/min, a nebulizer pressure of 20 psig, and a capillary voltage of 3500 V. Data were collected in TOF full-scan mode over m/z 50-1200 at an acquisition rate of 1 spectra/s with reference mass correction enabled. Data were analyzed using Masshunter Quantitative Analysis software. Metabolites and their ^{13}C isotopes were identified by retention time and m/z values determined from authentic standards. Quantification was performed by peak area after manual inspection of integration accuracy.

Protein Normalization of Mass Spectrometry Data

Three additional plates were grown up in each experiment per cell line. Cells were rinsed twice with cold PBS, and then treated with RIPA buffer with complete protease inhibitor cocktail (Roche) added at recommended concentrations for 5 minutes

with gentle agitation at 4°C. Protein was scraped off the plate and sheared with a 23-gauge syringe 3-4 times. Protein was collected in microcentrifuge tubes and spun for 15 minutes at 13,000 rpm at 4°C to pellet cellular debris. A Bradford was performed to quantify the amount of protein in each sample. This data was averaged and used to normalize the mass spectrometry data to account for differences in the growth rate of cells.

Bioenergetic Profiles (BEP) and Extracellular Acidification Rate (ECAR) Measurements

Cells were trypsinized and seeded with 100 μL fresh growth media into 24 well plates. After 1 hour of incubation, an additional 150 μL of media was added. The day of the experiment, media was replaced with XF Assay Medium Modified DMEM (Seahorse Biosciences) supplemented with 11 mM glucose and 10 mM pyruvate or Dulbecco's Modified Eagle's Medium (DME) Base without L-Glutamine, Glucose, Phenol Red, Sodium Pyruvate, or Sodium Bicarbonate supplemented with 11mM glucose and 10 mM sodium pyruvate, 2.5 mM glutamine and .015g/L phenol red. Cells were incubated in a 37°C non-CO_2 for 1 hour before being used for experiments. Oligomycin, FCCP, and rotenone were used to achieve final concentrations of 1uM, 300 nM, and 100 nM respectively in the cell. Galactose, when present, was at 11 mM final concentration. All experiments were done in XF-24 Machine (Seahorse Biosciences)

Quantitative-RT-PCR arrays

Quantitative-RT-PCR arrays were purchased from Qiagen. RNA was isolated using RNeasy Mini Kit (Qiagen) and cDNA was made using RT^2 First Strand Kit (Qiagen) Arrays were used according to instructions and analyzed using the supplied technical tools.

Figures

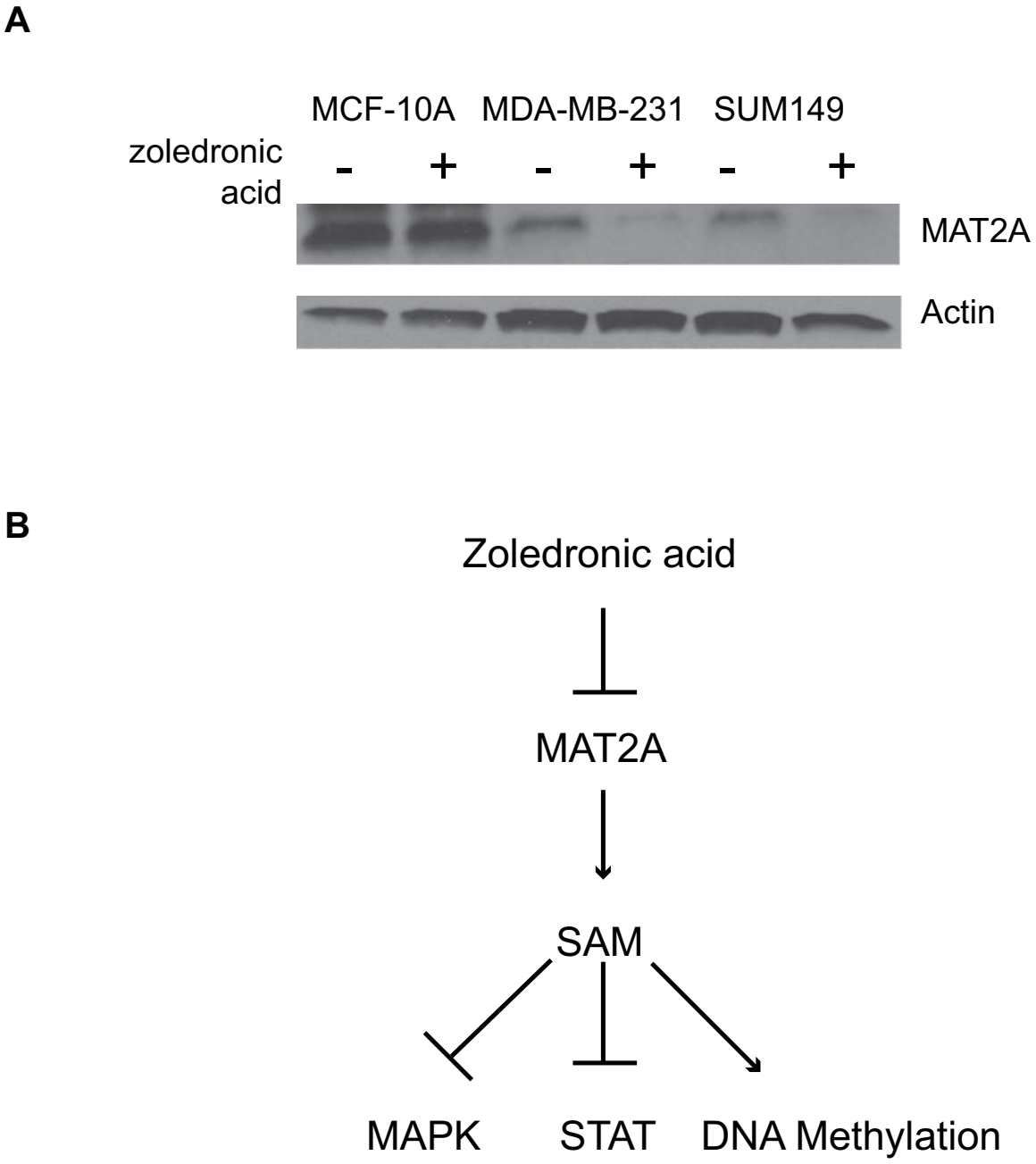

Figure V.1: MAT2A is a target of ZA
MAT2A Western Blot B. MAT2A Model

Table 1

A

List of Validated ZA Targets

Symbol	Name
IL24	interleukin 24
TMEM45A	transmembrane protein 45A
EREG	epiregulin
AHNAK2	AHNAK nucleoprotein 2
NAV3	neuron navigator 3
ROBO4	roundabout, axon guidance receptor, homolog 4

B

List of ZA targets regulated in opposing directions

Symbol	Name	MDA-MB-231	SUM 149
THBS1	thrombospondin 1	DOWN	UP
ENY2	enhancer of yellow 2 homolog	DOWN	UP
PDLIM2	PDZ and LIM domain 2	DOWN	UP
CDK6	cyclin-dependent kinase 6	DOWN	UP
RIMKLB	ribosomal modification protein rimK-like family member B	DOWN	UP
PDLIM7	PDZ and LIM domain 7	DOWN	UP
NFYA	nuclear transcription factor Y, alpha	DOWN	UP
GFPT1	glutamine--fructose-6-phosphate transaminase 1	UP	DOWN
TRIB3	tribbles homolog 3	UP	DOWN
C5orf41	chromosome 5 open reading frame 41	UP	DOWN
VEGFA	vascular endothelial growth factor A	UP	DOWN
JDP2	Jun dimerization protein 2	UP	DOWN
N4BP2L2	NEDD4 binding protein 2-like 2	UP	DOWN
ATP6V0D2	ATPase, H+ transporting, lysosomal 38kDa, V0 subunit d2	UP	DOWN
MALAT1	metastasis associated lung adenocarcinoma transcript 1	UP	DOWN
NEAT1	nuclear paraspeckle assembly transcript 1	UP	DOWN
CTH	cystathionase (cystathionine gamma-lyase)	UP	DOWN
TXNIP	thioredoxin interacting protein	UP	DOWN
KLHL24	kelch-like 24	UP	DOWN
GART	phosphoribosylglycinamide formyltransferase	UP	DOWN
BHLHE40	basic helix-loop-helix family, member e40	UP	DOWN

Table V.1: List of other targets identified in ZA microarray
A. List of Validated ZA targets B. List of ZA targets that are in opposite directions in MDA-MB-231 and SUM 149

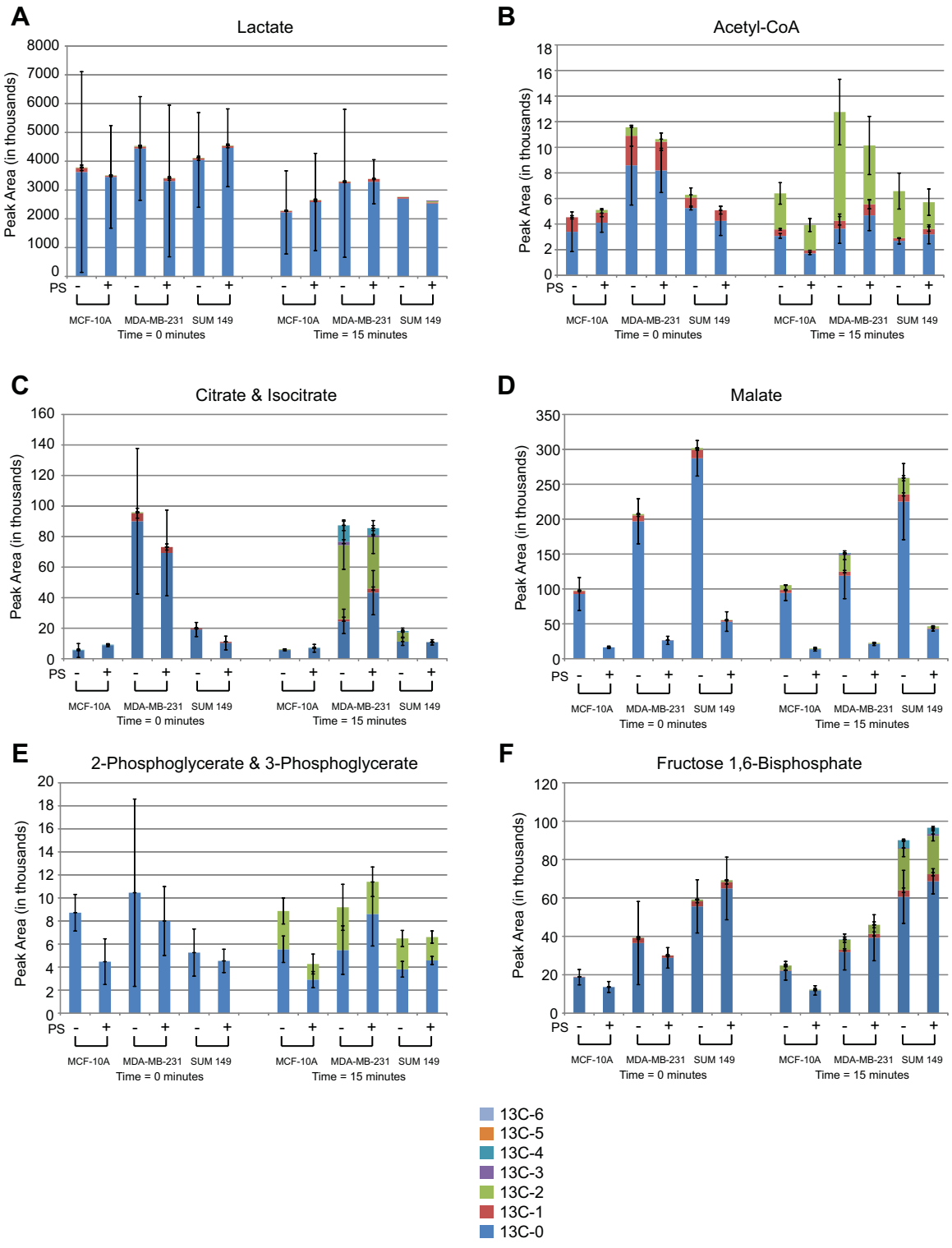

Figure V.2: SUM 149 cells do not have a defect in mitochondrial pyruvate transport
Stable isotope tracer experiments with 13C-2,3-pyruvate measuring peak intensity area under the curve of the following metabolites A. Lactate B. Citrate/Isocitrate C. Acetyl-CoA D. Malate E. 2 Phosphoglycerate/3-Phosphoglycerate F. Fructose-1,6-Bisphosphate

Expected and Measured Glutamine Concentration in Media used for 13C-2,3-Pyruvate Stable Isotope Tracer Experiments

Cell Line	Actual Glutamine Concentration	Expected Glutamine Concentration
MCF-10A	0.013 ± 0.012 mM	2.50 mM
MDA-MB-231	0.017 ± 0.006 mM	2.50 mM
SUM149	0.017 ± 0.012 mM	2.50 mM

Table V.2: Media used in isotope tracer experiments and oxidative phosphorylation measurements may have had low glutamine
Actual concentration of glutamine in media was much lower than expected 2.5 mM

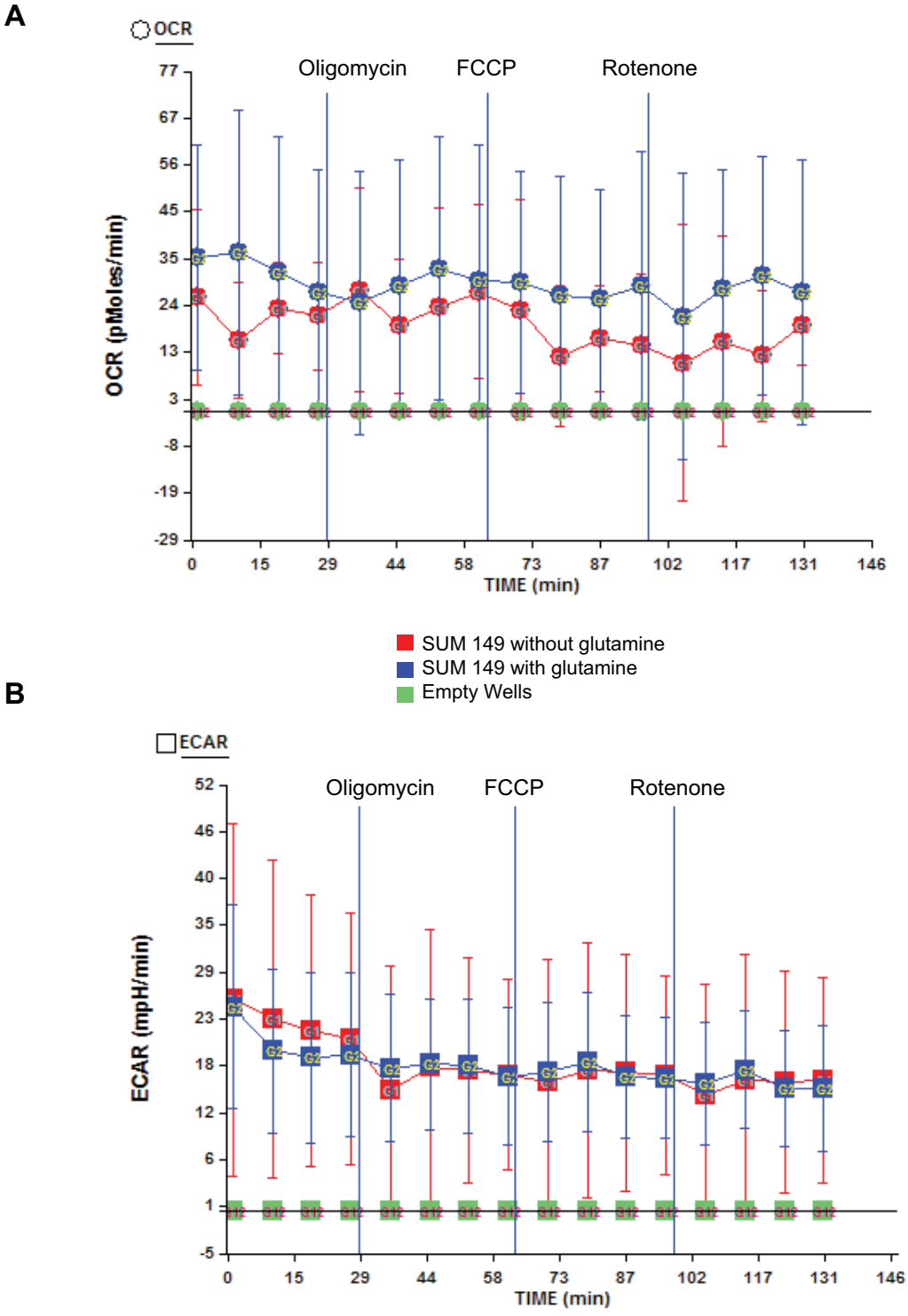

Figure V.3: Oxidative phosphorylation defect in SUM149 cells is glutamine independent
The addition of glutamine to the media does not induce SUM149 cells to undergo oxidative phosphorylation. A. Bioenergetic profiles measuring oxidative consumption rate (OCR) B. Extracellular acidification rate (ECAR).

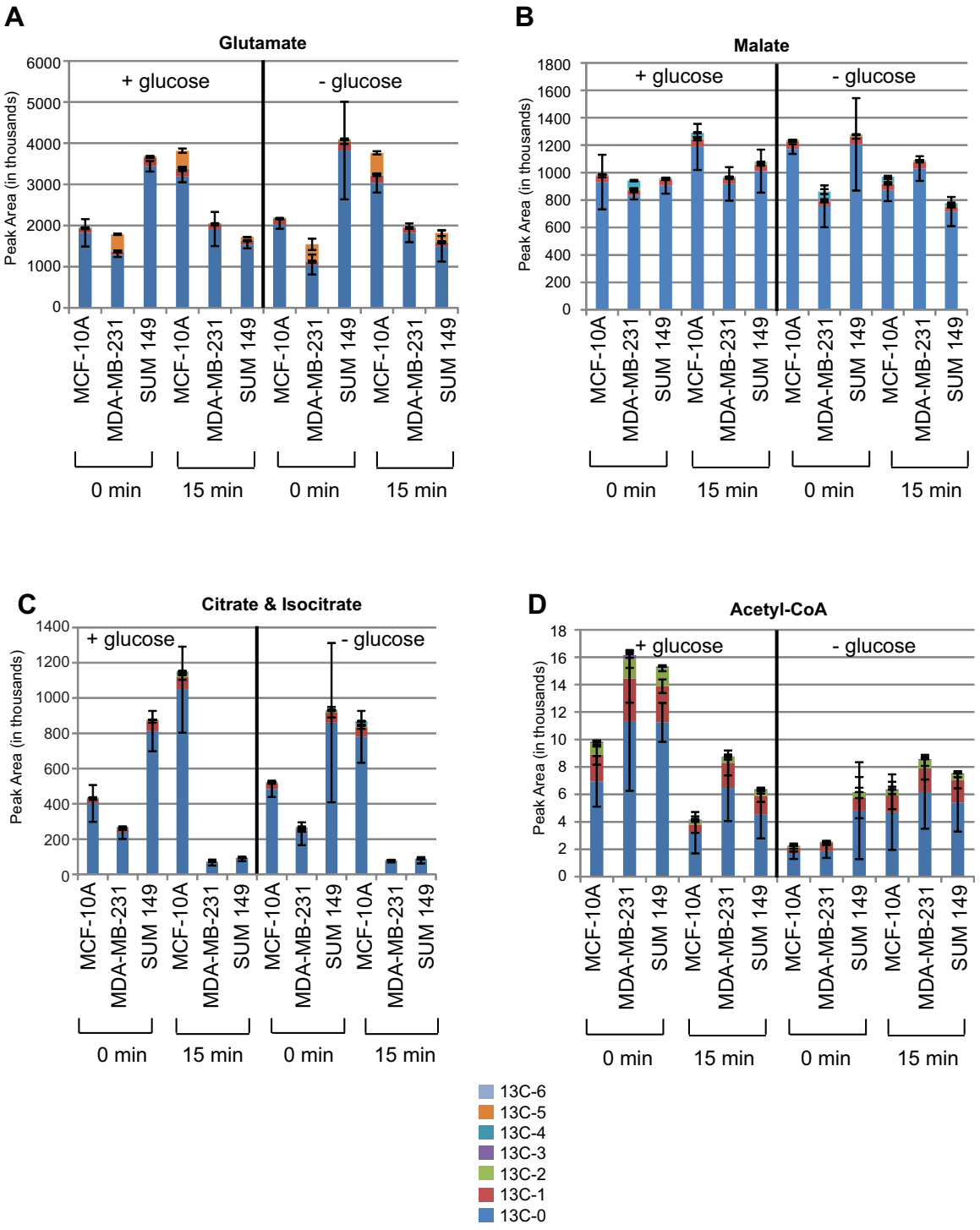

Figure V.4: Stable isotope tracer experiments using uniformly-labeled 13C-Glutamine
Glutamate B. Malate C. Citrate/ Isocitrate D. Acetyl-CoA

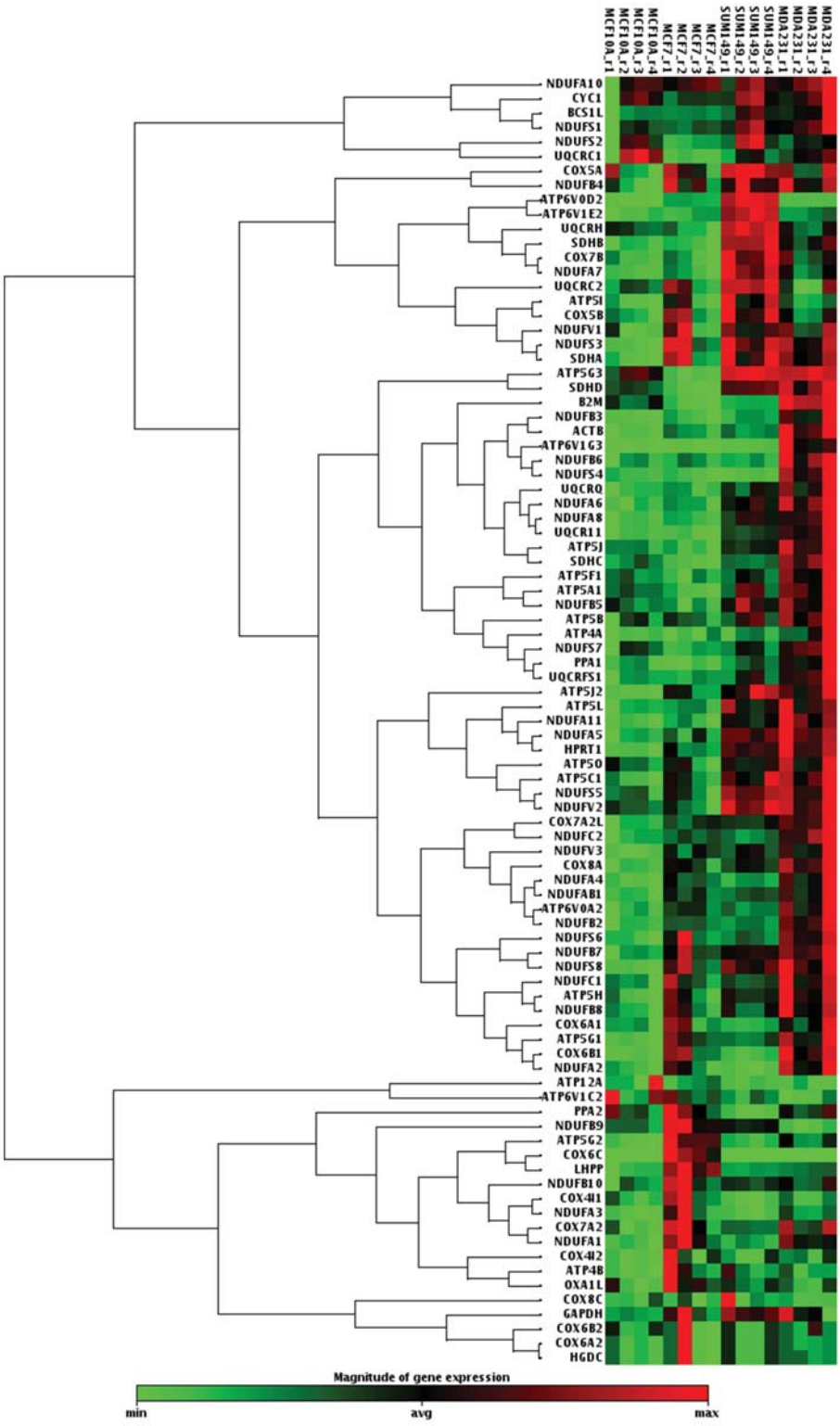

Figure V.5: QPCR Array Heatmap showing expression changes in mitochondrial genes

A

Fold change of significant genes in SUM 149 cells compared to MCF-10A cells

Symbol	Name	Fold Change
ATP6V0D2	ATPase, H+ transporting, lysosomal 38kDa, V0 subunit d2	260.43
ATP6V1E2	ATPase, H+ transporting, lysosomal 31kDa, V1 subunit E2	7.83
COX6C	cytochrome c oxidase subunit Vic	6.02
ATP5J2	ATP synthase, H+ transporting, mitochondrial Fo complex, subunit F2	5.22
HPRT1	hypoxanthine phosphoribosyltransferase 1	5.11
NDUFS8	NADH dehydrogenase (ubiquinone) Fe-S protein 8, 23kDa (NADH-coenzyme Q reductase)	4.73
SDHA	succinate dehydrogenase complex, subunit A, flavoprotein (Fp)	4.24
NDUFS3	NADH dehydrogenase (ubiquinone) Fe-S protein 3, 30kDa (NADH-coenzyme Q reductase)	4.08
NDUFA7	NADH dehydrogenase (ubiquinone) 1 alpha subcomplex, 7, 14.5kDa	3.74
ACTB	actin, beta	3.59
ATP5I	ATP synthase, H+ transporting, mitochondrial Fo complex, subunit E	3.50
ATP6V1G3	ATPase, H+ transporting, lysosomal 13kDa, V1 subunit G3	3.53
NDUFA11	NADH dehydrogenase (ubiquinone) 1 alpha subcomplex, 11, 14.7kDa	3.42
COX7B	cytochrome c oxidase subunit VIIb	3.35
ATP5L	ATP synthase, H+ transporting, mitochondrial Fo complex, subunit G	3.30
SDHB	succinate dehydrogenase complex, subunit B, iron sulfur (Ip)	3.29
NDUFA8	NADH dehydrogenase (ubiquinone) 1 alpha subcomplex, 8, 19kDa	3.12
UQCR11	ubiquinol-cytochrome c reductase, complex III subunit XI	3.01

B

Fold change of significant genes in SUM 149 cells compared to MDA-MB-231 cells

Symbol	Name	Fold Change
ATP6V0D2	ATPase, H+ transporting, lysosomal 38kDa, V0 subunit d2	17.70
ATP6V1E2	ATPase, H+ transporting, lysosomal 31kDa, V1 subunit E2	3.11
COX6B1	cytochrome c oxidase subunit VIb polypeptide 1 (ubiquitous)	-3.20
NDUFS4	NADH dehydrogenase (ubiquinone) Fe-S protein 4, 18kDa (NADH-coenzyme Q reductase)	-3.42
NDUFB6	NADH dehydrogenase (ubiquinone) 1 beta subcomplex, 6, 17kDa	-3.79
B2M	beta-2-microglobulin	-4.06
ATP6V1G3	ATPase, H+ transporting, lysosomal 13kDa, V1 subunit G3	-17.90

Table V.3: Mitochondrial Genes found to be significantly different in SUM149 cells
A. SUM149 cells compared to MCF-10A cells. B. SUM149 cells compared to MDA-MB-231 cells.

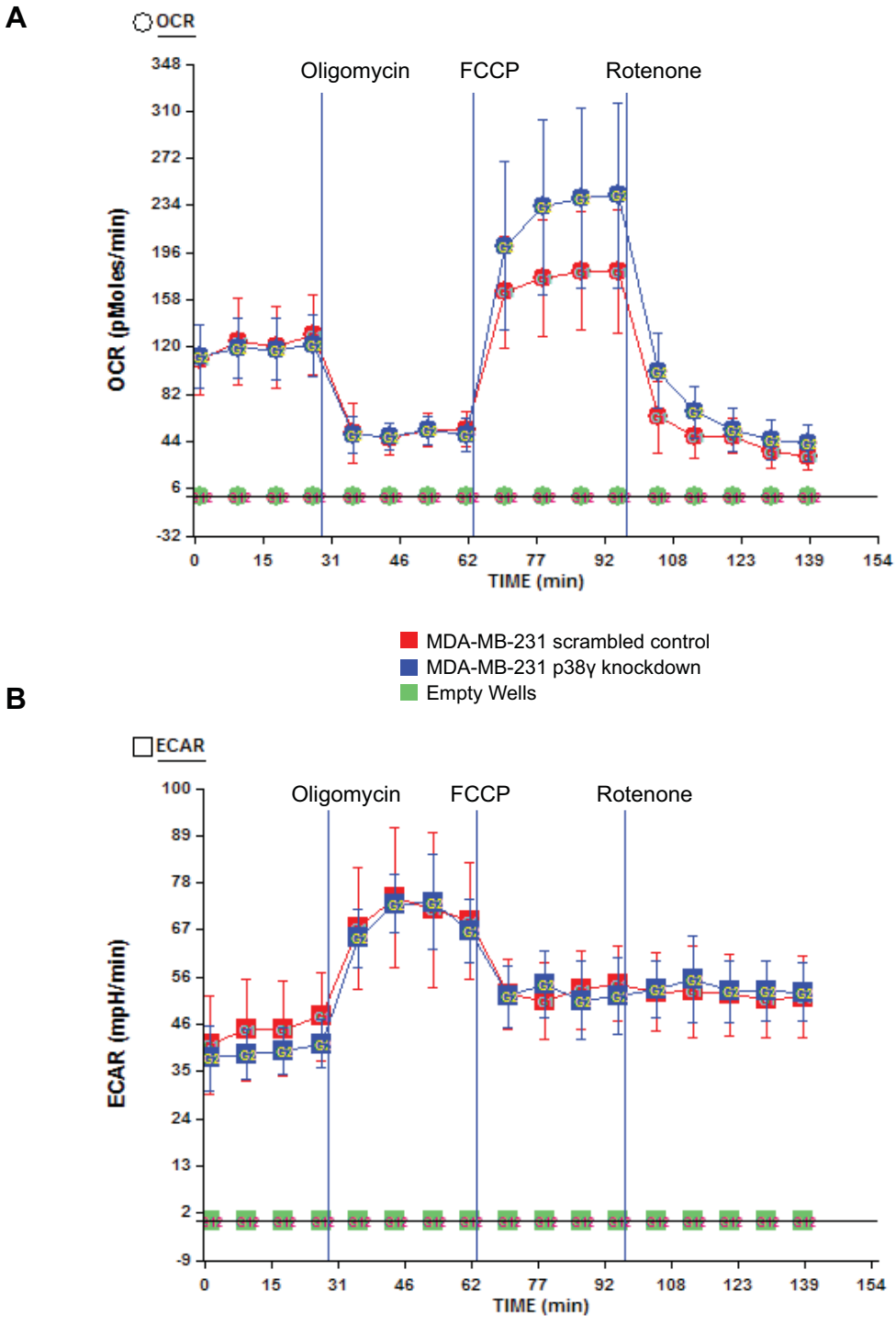

Figure V.6: MDA-MB-231 p38γ knockdown cells display increased oxidative capacity
Difference in oxidative capacity between MDA-MB-231 scrambled control cells and MDa-MB-231 p38γ knockdown cells was found to be statistically significant (p-value < 0.05) A. Bioenergetic profiles measuring oxidative consumption rate (OCR) B. Extracellular acidification rate (ECAR)

Bibliography

1. Siegel R, Naishadham D, Jemal A: **Cancer statistics, 2012.** *CA: a cancer journal for clinicians* 2012, **62:**10-29.
2. Warburg O, Wind F, Negelein E: **The Metabolism of Tumors in the Body.** *J Gen Physiol* 1927, **8:**519-530.
3. Weiss RA, Vogt PK: **100 years of Rous sarcoma virus.** *J Exp Med* 2011, **208:**2351-2355.
4. Zhu A, Marcus DM, Shu HK, Shim H: **Application of metabolic PET imaging in radiation oncology.** *Radiat Res* 2012, **177:**436-448.
5. Bombardieri E, Crippa F: **PET imaging in breast cancer.** *Q J Nucl Med* 2001, **45:**245-256.
6. Macheda ML, Rogers S, Best JD: **Molecular and cellular regulation of glucose transporter (GLUT) proteins in cancer.** *J Cell Physiol* 2005, **202:**654-662.
7. Hanahan D, Weinberg RA: **The hallmarks of cancer.** *Cell* 2000, **100:**57-70.
8. Gatenby RA: **The potential role of transformation-induced metabolic changes in tumor-host interaction.** *Cancer Res* 1995, **55:**4151-4156.
9. Wang Y, Zhang C, Liu J, Huang G: **Is 18F-FDG PET accurate to predict neoadjuvant therapy response in breast cancer? A meta-analysis.** *Breast Cancer Res Treat* 2012, **131:**357-369.
10. Luo W, Semenza GL: **Emerging roles of PKM2 in cell metabolism and cancer progression.** *Trends Endocrinol Metab* 2012.
11. Hitosugi T, Kang S, Vander Heiden MG, Chung TW, Elf S, Lythgoe K, Dong S, Lonial S, Wang X, Chen GZ, et al: **Tyrosine phosphorylation inhibits PKM2 to promote the Warburg effect and tumor growth.** *Sci Signal* 2009, **2:**ra73.
12. Ye J, Mancuso A, Tong X, Ward PS, Fan J, Rabinowitz JD, Thompson CB: **Pyruvate kinase M2 promotes de novo serine synthesis to sustain mTORC1 activity and cell proliferation.** *Proc Natl Acad Sci U S A* 2012, **109:**6904-6909.
13. Eigenbrodt E, Leib S, Kramer W, Friis RR, Schoner W: **Structural and kinetic differences between the M2 type pyruvate kinases from lung and various tumors.** *Biomed Biochim Acta* 1983, **42:**S278-282.
14. Mazurek S: **Pyruvate kinase type M2: a key regulator of the metabolic budget system in tumor cells.** *Int J Biochem Cell Biol* 2011, **43:**969-980.
15. Yalcin A, Telang S, Clem B, Chesney J: **Regulation of glucose metabolism by 6-phosphofructo-2-kinase/fructose-2,6-bisphosphatases in cancer.** *Exp Mol Pathol* 2009, **86:**174-179.
16. Gatenby RA, Gillies RJ: **Why do cancers have high aerobic glycolysis?** *Nat Rev Cancer* 2004, **4:**891-899.
17. Brand KA, Hermfisse U: **Aerobic glycolysis by proliferating cells: a protective strategy against reactive oxygen species.** *FASEB J* 1997, **11:**388-395.

18. Yan H, Parsons DW, Jin G, McLendon R, Rasheed BA, Yuan W, Kos I, Batinic-Haberle I, Jones S, Riggins GJ, et al: **IDH1 and IDH2 mutations in gliomas.** *N Engl J Med* 2009, **360:**765-773.
19. Dang L, White DW, Gross S, Bennett BD, Bittinger MA, Driggers EM, Fantin VR, Jang HG, Jin S, Keenan MC, et al: **Cancer-associated IDH1 mutations produce 2-hydroxyglutarate.** *Nature* 2009, **462:**739-744.
20. Xu W, Yang H, Liu Y, Yang Y, Wang P, Kim SH, Ito S, Yang C, Xiao MT, Liu LX, et al: **Oncometabolite 2-hydroxyglutarate is a competitive inhibitor of alpha-ketoglutarate-dependent dioxygenases.** *Cancer Cell* 2011, **19:**17-30.
21. Frezza C, Pollard PJ, Gottlieb E: **Inborn and acquired metabolic defects in cancer.** *J Mol Med (Berl)* 2011, **89:**213-220.
22. King A, Selak MA, Gottlieb E: **Succinate dehydrogenase and fumarate hydratase: linking mitochondrial dysfunction and cancer.** *Oncogene* 2006, **25:**4675-4682.
23. He W, Miao FJ, Lin DC, Schwandner RT, Wang Z, Gao J, Chen JL, Tian H, Ling L: **Citric acid cycle intermediates as ligands for orphan G-protein-coupled receptors.** *Nature* 2004, **429:**188-193.
24. Joyal JS, Omri S, Sitaras N, Rivera JC, Sapieha P, Chemtob S: **Neovascularization in retinopathy of prematurity: opposing actions of neuronal factors GPR91 and semaphorins 3A.** *Acta Paediatr* 2012, **101:**819-826.
25. Swinnen JV, Brusselmans K, Verhoeven G: **Increased lipogenesis in cancer cells: new players, novel targets.** *Curr Opin Clin Nutr Metab Care* 2006, **9:**358-365.
26. DeBerardinis RJ, Mancuso A, Daikhin E, Nissim I, Yudkoff M, Wehrli S, Thompson CB: **Beyond aerobic glycolysis: transformed cells can engage in glutamine metabolism that exceeds the requirement for protein and nucleotide synthesis.** *Proc Natl Acad Sci U S A* 2007, **104:**19345-19350.
27. Schutz Y: **Protein turnover, ureagenesis and gluconeogenesis.** *Int J Vitam Nutr Res* 2011, **81:**101-107.
28. Mithieux G, Rajas F, Gautier-Stein A: **A novel role for glucose 6-phosphatase in the small intestine in the control of glucose homeostasis.** *J Biol Chem* 2004, **279:**44231-44234.
29. Hirschhaeuser F, Sattler UG, Mueller-Klieser W: **Lactate: a metabolic key player in cancer.** *Cancer Res* 2011, **71:**6921-6925.
30. Ridley AJ, Schwartz MA, Burridge K, Firtel RA, Ginsberg MH, Borisy G, Parsons JT, Horwitz AR: **Cell migration: integrating signals from front to back.** *Science* 2003, **302:**1704-1709.
31. Sahai E, Marshall CJ: **RHO-GTPases and cancer.** *Nat Rev Cancer* 2002, **2:**133-142.
32. Turner SJ, Zhuang S, Zhang T, Boss GR, Pilz RB: **Effects of lovastatin on Rho isoform expression, activity, and association with guanine nucleotide dissociation inhibitors.** *Biochem Pharmacol* 2008, **75:**405-413.
33. Zalcman G, Closson V, Camonis J, Honore N, Rousseau-Merck MF, Tavitian A, Olofsson B: **RhoGDI-3 is a new GDP dissociation inhibitor (GDI).**

Identification of a non-cytosolic GDI protein interacting with the small GTP-binding proteins RhoB and RhoG. *J Biol Chem* 1996, **271:**30366-30374.
34. Valastyan S, Weinberg RA: **Tumor metastasis: molecular insights and evolving paradigms.** *Cell* 2011, **147:**275-292.
35. Tang SS, Twelves DJ, Isacke CM, Gui GP: **Mammary ductoscopy in the current management of breast disease.** *Surg Endosc* 2011, **25:**1712-1722.
36. Jiang L, Greenwood TR, Artemov D, Raman V, Winnard PT, Jr., Heeren RM, Bhujwalla ZM, Glunde K: **Localized hypoxia results in spatially heterogeneous metabolic signatures in breast tumor models.** *Neoplasia* 2012, **14:**732-741.
37. Jain RK: **Normalization of tumor vasculature: an emerging concept in antiangiogenic therapy.** *Science* 2005, **307:**58-62.
38. Ilina O, Friedl P: **Mechanisms of collective cell migration at a glance.** *J Cell Sci* 2009, **122:**3203-3208.
39. Farooqui R, Fenteany G: **Multiple rows of cells behind an epithelial wound edge extend cryptic lamellipodia to collectively drive cell-sheet movement.** *J Cell Sci* 2005, **118:**51-63.
40. Kinjo M: **Lodgement and extravasation of tumour cells in blood-borne metastasis: an electron microscope study.** *Br J Cancer* 1978, **38:**293-301.
41. Warren BA: **Some aspects of blood borne tumour emboli associated with thrombosis.** *Z Krebsforsch Klin Onkol Cancer Res Clin Oncol* 1976, **87:**1-15.
42. Joyce JA, Pollard JW: **Microenvironmental regulation of metastasis.** *Nat Rev Cancer* 2009, **9:**239-252.
43. Gupta GP, Nguyen DX, Chiang AC, Bos PD, Kim JY, Nadal C, Gomis RR, Manova-Todorova K, Massague J: **Mediators of vascular remodelling co-opted for sequential steps in lung metastasis.** *Nature* 2007, **446:**765-770.
44. Mathot L, Stenninger J: **Behavior of seeds and soil in the mechanism of metastasis: a deeper understanding.** *Cancer Sci* 2012, **103:**626-631.
45. Kang Y, Siegel PM, Shu W, Drobnjak M, Kakonen SM, Cordon-Cardo C, Guise TA, Massague J: **A multigenic program mediating breast cancer metastasis to bone.** *Cancer Cell* 2003, **3:**537-549.
46. Muller A, Homey B, Soto H, Ge N, Catron D, Buchanan ME, McClanahan T, Murphy E, Yuan W, Wagner SN, et al: **Involvement of chemokine receptors in breast cancer metastasis.** *Nature* 2001, **410:**50-56.
47. Hamaguchi T, Wakabayashi H, Matsumine A, Sudo A, Uchida A: **TNF inhibitor suppresses bone metastasis in a breast cancer cell line.** *Biochem Biophys Res Commun* 2011, **407:**525-530.
48. Lopez-Lazaro M: **Why do tumors metastasize?** *Cancer biology & therapy* 2007, **6:**141-144.
49. Colen CB, Shen Y, Ghoddoussi F, Yu P, Francis TB, Koch BJ, Monterey MD, Galloway MP, Sloan AE, Mathupala SP: **Metabolic targeting of lactate efflux by malignant glioma inhibits invasiveness and induces necrosis: an in vivo study.** *Neoplasia* 2011, **13:**620-632.
50. Burdon RH: **Superoxide and hydrogen peroxide in relation to mammalian cell proliferation.** *Free Radic Biol Med* 1995, **18:**775-794.
51. Szatrowski TP, Nathan CF: **Production of large amounts of hydrogen peroxide by human tumor cells.** *Cancer Res* 1991, **51:**794-798.

52. Krishnamachary B, Berg-Dixon S, Kelly B, Agani F, Feldser D, Ferreira G, Iyer N, LaRusch J, Pak B, Taghavi P, Semenza GL: **Regulation of colon carcinoma cell invasion by hypoxia-inducible factor 1.** *Cancer Res* 2003, **63:**1138-1143.
53. Esteban MA, Tran MG, Harten SK, Hill P, Castellanos MC, Chandra A, Raval R, O'Brien T S, Maxwell PH: **Regulation of E-cadherin expression by VHL and hypoxia-inducible factor.** *Cancer Res* 2006, **66:**3567-3575.
54. Goldstein JL, Brown MS: **Regulation of the mevalonate pathway.** *Nature* 1990, **343:**425-430.
55. Nurenberg G, Volmer DA: **The analytical determination of isoprenoid intermediates from the mevalonate pathway.** *Anal Bioanal Chem* 2012, **402:**671-685.
56. Fritz G: **Targeting the mevalonate pathway for improved anticancer therapy.** *Curr Cancer Drug Targets* 2009, **9:**626-638.
57. Gnant M, Dubsky P, Hadji P: **Bisphosphonates: prevention of bone metastases in breast cancer.** *Recent Results Cancer Res* 2012, **192:**65-91.
58. Paterson AH, Kanis JA, Powles TJ, McCloskey E, Hanson J, Ashley S: **Role of bisphosphonates in prevention and treatment of bone metastases from breast cancer.** *Can J Oncol* 1995, **5 Suppl 1:**54-57.
59. Chlebowski RT, Col N: **Bisphosphonates and breast cancer incidence and recurrence.** *Breast Dis* 2011, **33:**93-101.
60. Lochhead P, Chan AT: **Statins and Colorectal Cancer.** *Clin Gastroenterol Hepatol* 2012.
61. Chlebowski RT, Col N: **Bisphosphonates and breast cancer prevention.** *Anticancer Agents Med Chem* 2012, **12:**144-150.
62. Rosenthal DT, Iyer H, Escudero S, Bao L, Wu Z, Ventura AC, Kleer CG, Arruda EM, Garikipati K, Merajver SD: **p38gamma promotes breast cancer cell motility and metastasis through regulation of RhoC GTPase, cytoskeletal architecture, and a novel leading edge behavior.** *Cancer Res* 2011, **71:**6338-6349.
63. Katz M, Amit I, Yarden Y: **Regulation of MAPKs by growth factors and receptor tyrosine kinases.** *Biochim Biophys Acta* 2007, **1773:**1161-1176.
64. English JM, Cobb MH: **Pharmacological inhibitors of MAPK pathways.** *Trends Pharmacol Sci* 2002, **23:**40-45.
65. De Luca A, Maiello MR, D'Alessio A, Pergameno M, Normanno N: **The RAS/RAF/MEK/ERK and the PI3K/AKT signalling pathways: role in cancer pathogenesis and implications for therapeutic approaches.** *Expert Opin Ther Targets* 2012, **16 Suppl 2:**S17-27.
66. Hernandez-Aya LF, Gonzalez-Angulo AM: **Targeting the phosphatidylinositol 3-kinase signaling pathway in breast cancer.** *Oncologist* 2011, **16:**404-414.
67. Leber MF, Efferth T: **Molecular principles of cancer invasion and metastasis (review).** *Int J Oncol* 2009, **34:**881-895.
68. Morales J, Alpaugh ML: **Gain in cellular organization of inflammatory breast cancer: A 3D in vitro model that mimics the in vivo metastasis.** *BMC Cancer* 2009, **9:**462.
69. Schmalhofer O, Brabletz S, Brabletz T: **E-cadherin, beta-catenin, and ZEB1 in malignant progression of cancer.** *Cancer Metastasis Rev* 2009, **28:**151-166.

70. Vignjevic D, Montagnac G: **Reorganisation of the dendritic actin network during cancer cell migration and invasion.** *Semin Cancer Biol* 2008, **18:**12-22.
71. Zohrabian VM, Forzani B, Chau Z, Murali R, Jhanwar-Uniyal M: **Rho/ROCK and MAPK signaling pathways are involved in glioblastoma cell migration and proliferation.** *Anticancer Res* 2009, **29:**119-123.
72. Wu M, Wu ZF, Rosenthal DT, Rhee EM, Merajver SD: **Characterization of the roles of RHOC and RHOA GTPases in invasion, motility, and matrix adhesion in inflammatory and aggressive breast cancers.** *Cancer* 2010, **116:**2768-2782.
73. Parri M, Chiarugi P: **Rac and Rho GTPases in cancer cell motility control.** *Cell Commun Signal* 2010, **8:**23.
74. Olson MF, Sahai E: **The actin cytoskeleton in cancer cell motility.** *Clin Exp Metastasis* 2009, **26:**273-287.
75. Pille JY, Denoyelle C, Varet J, Bertrand JR, Soria J, Opolon P, Lu H, Pritchard LL, Vannier JP, Malvy C, et al: **Anti-RhoA and anti-RhoC siRNAs inhibit the proliferation and invasiveness of MDA-MB-231 breast cancer cells in vitro and in vivo.** *Mol Ther* 2005, **11:**267-274.
76. Woodward WA, Cristofanilli M: **Inflammatory breast cancer.** *Semin Radiat Oncol* 2009, **19:**256-265.
77. Dirix LY, Van Dam P, Prove A, Vermeulen PB: **Inflammatory breast cancer: current understanding.** *Curr Opin Oncol* 2006, **18:**563-571.
78. Ventura AC, Merajver SD: **Genetic determinants of aggressive breast cancer.** *Annu Rev Med* 2008, **59:**199-212.
79. Wu M, Wu ZF, Kumar-Sinha C, Chinnaiyan A, Merajver SD: **RhoC induces differential expression of genes involved in invasion and metastasis in MCF10A breast cells.** *Breast Cancer Res Treat* 2004, **84:**3-12.
80. Rorth P: **Collective cell migration.** *Annu Rev Cell Dev Biol* 2009, **25:**407-429.
81. Collisson EA, Kleer C, Wu M, De A, Gambhir SS, Merajver SD, Kolodney MS: **Atorvastatin prevents RhoC isoprenylation, invasion, and metastasis in human melanoma cells.** *Mol Cancer Ther* 2003, **2:**941-948.
82. Konstantinopoulos PA, Karamouzis MV, Papavassiliou AG: **Post-translational modifications and regulation of the RAS superfamily of GTPases as anticancer targets.** *Nat Rev Drug Discov* 2007, **6:**541-555.
83. Kusama T, Mukai M, Tatsuta M, Nakamura H, Inoue M: **Inhibition of transendothelial migration and invasion of human breast cancer cells by preventing geranylgeranylation of Rho.** *Int J Oncol* 2006, **29:**217-223.
84. Raikkonen J, Monkkonen H, Auriola S, Monkkonen J: **Mevalonate pathway intermediates downregulate zoledronic acid-induced isopentenyl pyrophosphate and ATP analog formation in human breast cancer cells.** *Biochem Pharmacol* 2010, **79:**777-783.
85. Stresing V, Fournier PG, Bellahcene A, Benzaid I, Monkkonen H, Colombel M, Ebetino FH, Castronovo V, Clezardin P: **Nitrogen-containing bisphosphonates can inhibit angiogenesis in vivo without the involvement of farnesyl pyrophosphate synthase.** *Bone* 2011, **48:**259-266.
86. Denoyelle C, Vasse M, Korner M, Mishal Z, Ganne F, Vannier JP, Soria J, Soria C: **Cerivastatin, an inhibitor of HMG-CoA reductase, inhibits the signaling**

pathways involved in the invasiveness and metastatic properties of highly invasive breast cancer cell lines: an in vitro study. *Carcinogenesis* 2001, **22:**1139-1148.

87. Farina HG, Bublik DR, Alonso DF, Gomez DE: **Lovastatin alters cytoskeleton organization and inhibits experimental metastasis of mammary carcinoma cells.** *Clin Exp Metastasis* 2002, **19:**551-559.
88. Graaf MR, Richel DJ, van Noorden CJ, Guchelaar HJ: **Effects of statins and farnesyltransferase inhibitors on the development and progression of cancer.** *Cancer Treat Rev* 2004, **30:**609-641.
89. Kang S, Kim ES, Moon A: **Simvastatin and lovastatin inhibit breast cell invasion induced by H-Ras.** *Oncol Rep* 2009, **21:**1317-1322.
90. Kusama T, Mukai M, Tatsuta M, Matsumoto Y, Nakamura H, Inoue M: **Selective inhibition of cancer cell invasion by a geranylgeranyltransferase-I inhibitor.** *Clin Exp Metastasis* 2003, **20:**561-567.
91. Dudakovic A, Tong H, Hohl RJ: **Geranylgeranyl diphosphate depletion inhibits breast cancer cell migration.** *Invest New Drugs* 2010.
92. Gnant M, Mlineritsch B, Schippinger W, Luschin-Ebengreuth G, Postlberger S, Menzel C, Jakesz R, Seifert M, Hubalek M, Bjelic-Radisic V, et al: **Endocrine therapy plus zoledronic acid in premenopausal breast cancer.** *N Engl J Med* 2009, **360:**679-691.
93. Coleman R, Cook R, Hirsh V, Major P, Lipton A: **Zoledronic acid use in cancer patients: more than just supportive care?** *Cancer* 2011, **117:**11-23.
94. Denoyelle C, Hong L, Vannier JP, Soria J, Soria C: **New insights into the actions of bisphosphonate zoledronic acid in breast cancer cells by dual RhoA-dependent and -independent effects.** *Br J Cancer* 2003, **88:**1631-1640.
95. Uekita T, Sakai R: **Roles of CUB domain-containing protein 1 signaling in cancer invasion and metastasis.** *Cancer Sci* 2011, **102:**1943-1948.
96. Rosenthal DT, Iyer H, Escudero S, Ventura AC, Arruda EM, Garikipati K, Merajver SD: **From in vitro to in silico and back again: using biological and mathematical synergy to decipher breast cancer cell motility.** *Conf Proc IEEE Eng Med Biol Soc* 2010, **2010:**3261-3264.
97. Benes CH, Poulogiannis G, Cantley LC, Soltoff SP: **The SRC-associated protein CUB Domain-Containing Protein-1 regulates adhesion and motility.** *Oncogene* 2012, **31:**653-663.
98. Casar B, He Y, Iconomou M, Hooper JD, Quigley JP, Deryugina EI: **Blocking of CDCP1 cleavage in vivo prevents Akt-dependent survival and inhibits metastatic colonization through PARP1-mediated apoptosis of cancer cells.** *Oncogene* 2012, **31:**3924-3938.
99. Palm D, Lang K, Brandt B, Zaenker KS, Entschladen F: **In vitro and in vivo imaging of cell migration: two interdepending methods to unravel metastasis formation.** *Semin Cancer Biol* 2005, **15:**396-404.
100. Casar B, He Y, Iconomou M, Hooper JD, Quigley JP, Deryugina EI: **Blocking of CDCP1 cleavage in vivo prevents Akt-dependent survival and inhibits metastatic colonization through PARP1-mediated apoptosis of cancer cells.** *Oncogene* 2011.

101. Lobell RB, Omer CA, Abrams MT, Bhimnathwala HG, Brucker MJ, Buser CA, Davide JP, deSolms SJ, Dinsmore CJ, Ellis-Hutchings MS, et al: **Evaluation of farnesyl:protein transferase and geranylgeranyl:protein transferase inhibitor combinations in preclinical models.** *Cancer Res* 2001, **61:**8758-8768.
102. Sun J, Ohkanda J, Coppola D, Yin H, Kothare M, Busciglio B, Hamilton AD, Sebti SM: **Geranylgeranyltransferase I inhibitor GGTI-2154 induces breast carcinoma apoptosis and tumor regression in H-Ras transgenic mice.** *Cancer Res* 2003, **63:**8922-8929.
103. Huang EH, Johnson LA, Eaton K, Hynes MJ, Carpentino JE, Higgins PD: **Atorvastatin induces apoptosis in vitro and slows growth of tumor xenografts but not polyp formation in MIN mice.** *Dig Dis Sci* 2010, **55:**3086-3094.
104. Sanchez CA, Rodriguez E, Varela E, Zapata E, Paez A, Masso FA, Montano LF, Loopez-Marure R: **Statin-induced inhibition of MCF-7 breast cancer cell proliferation is related to cell cycle arrest and apoptotic and necrotic cell death mediated by an enhanced oxidative stress.** *Cancer Invest* 2008, **26:**698-707.
105. Seeger H, Wallwiener D, Mueck AO: **Statins can inhibit proliferation of human breast cancer cells in vitro.** *Exp Clin Endocrinol Diabetes* 2003, **111:**47-48.
106. Del Pozo MA, Kiosses WB, Alderson NB, Meller N, Hahn KM, Schwartz MA: **Integrins regulate GTP-Rac localized effector interactions through dissociation of Rho-GDI.** *Nat Cell Biol* 2002, **4:**232-239.
107. Lee GY, Kenny PA, Lee EH, Bissell MJ: **Three-dimensional culture models of normal and malignant breast epithelial cells.** *Nat Methods* 2007, **4:**359-365.
108. Irizarry RA, Hobbs B, Collin F, Beazer-Barclay YD, Antonellis KJ, Scherf U, Speed TP: **Exploration, normalization, and summaries of high density oligonucleotide array probe level data.** *Biostatistics* 2003, **4:**249-264.
109. Kleer CG, van Golen KL, Merajver SD: **Molecular biology of breast cancer metastasis. Inflammatory breast cancer: clinical syndrome and molecular determinants.** *Breast Cancer Res* 2000, **2:**423-429.
110. Doria ML, Cotrim Z, Macedo B, Simoes C, Domingues P, Helguero L, Domingues MR: **Lipidomic approach to identify patterns in phospholipid profiles and define class differences in mammary epithelial and breast cancer cells.** *Breast Cancer Res Treat* 2012, **133:**635-648.
111. Osawa T, Muramatsu M, Watanabe M, Shibuya M: **Hypoxia and low-nutrition double stress induces aggressiveness in a murine model of melanoma.** *Cancer Sci* 2009, **100:**844-851.
112. Brown RM, Head RA, Morris AA, Raiman JA, Walter JH, Whitehouse WP, Brown GK: **Pyruvate dehydrogenase E3 binding protein (protein X) deficiency.** *Dev Med Child Neurol* 2006, **48:**756-760.
113. Tahay G, Wiame E, Tyteca D, Courtoy PJ, Van Schaftingen E: **Determinants of the enzymatic activity and the subcellular localization of aspartate N-acetyltransferase.** *Biochem J* 2012, **441:**105-112.
114. Wiame E, Tyteca D, Pierrot N, Collard F, Amyere M, Noel G, Desmedt J, Nassogne MC, Vikkula M, Octave JN, et al: **Molecular identification of**

aspartate N-acetyltransferase and its mutation in hypoacetylaspartia. *Biochem J* 2010, **425:**127-136.
115. Chen JQ, Russo J: **Dysregulation of glucose transport, glycolysis, TCA cycle and glutaminolysis by oncogenes and tumor suppressors in cancer cells.** *Biochim Biophys Acta* 2012, **1826:**370-384.
116. Frezza C, Cipolat S, Scorrano L: **Organelle isolation: functional mitochondria from mouse liver, muscle and cultured fibroblasts.** *Nat Protoc* 2007, **2:**287-295.
117. Schwab MA, Kolker S, van den Heuvel LP, Sauer S, Wolf NI, Rating D, Hoffmann GF, Smeitink JA, Okun JG: **Optimized spectrophotometric assay for the completely activated pyruvate dehydrogenase complex in fibroblasts.** *Clin Chem* 2005, **51:**151-160.
118. Lorenz MA, Burant CF, Kennedy RT: **Reducing time and increasing sensitivity in sample preparation for adherent mammalian cell metabolomics.** *Anal Chem* 2011, **83:**3406-3414.
119. Wagner EF, Nebreda AR: **Signal integration by JNK and p38 MAPK pathways in cancer development.** *Nat Rev Cancer* 2009, **9:**537-549.
120. Hu J, Zhang Z, Shen WJ, Azhar S: **Cellular cholesterol delivery, intracellular processing and utilization for biosynthesis of steroid hormones.** *Nutr Metab (Lond)* 2010, **7:**47.
121. Arpino G, Wiechmann L, Osborne CK, Schiff R: **Crosstalk between the estrogen receptor and the HER tyrosine kinase receptor family: molecular mechanism and clinical implications for endocrine therapy resistance.** *Endocr Rev* 2008, **29:**217-233.
122. Brandenberger AW, Tee MK, Jaffe RB: **Estrogen receptor alpha (ER-alpha) and beta (ER-beta) mRNAs in normal ovary, ovarian serous cystadenocarcinoma and ovarian cancer cell lines: down-regulation of ER-beta in neoplastic tissues.** *J Clin Endocrinol Metab* 1998, **83:**1025-1028.
123. Jordan VC: **Selective estrogen receptor modulation: concept and consequences in cancer.** *Cancer Cell* 2004, **5:**207-213.
124. Justenhoven C, Obazee O, Brauch H: **The pharmacogenomics of sex hormone metabolism: breast cancer risk in menopausal hormone therapy.** *Pharmacogenomics* 2012, **13:**659-675.
125. Osborne CK, Schiff R: **Mechanisms of endocrine resistance in breast cancer.** *Annu Rev Med* 2011, **62:**233-247.
126. Teicher BA, Linehan WM, Helman LJ: **Targeting cancer metabolism.** *Clin Cancer Res* 2012, **18:**5537-5545.
127. Hall JM, Couse JF, Korach KS: **The multifaceted mechanisms of estradiol and estrogen receptor signaling.** *J Biol Chem* 2001, **276:**36869-36872.
128. Rosenthal DT, Zhang J, Bao L, Zhu L, Wu Z, Toy K, Kleer CG, Merajver SD: **RhoC Impacts the Metastatic Potential and Abundance of Breast Cancer Stem Cells.** *PLoS ONE* 2012, **7:**e40979.
129. King MP, Attardi G: **Human cells lacking mtDNA: repopulation with exogenous mitochondria by complementation.** *Science* 1989, **246:**500-503.
130. Young CD, Anderson SM: **Sugar and fat - that's where it's at: metabolic changes in tumors.** *Breast Cancer Res* 2008, **10:**202.

131. Silvera D, Schneider RJ: **Inflammatory breast cancer cells are constitutively adapted to hypoxia.** *Cell Cycle* 2009, **8:**3091-3096.
132. Kemp MM, Weiwer M, Koehler AN: **Unbiased binding assays for discovering small-molecule probes and drugs.** *Bioorg Med Chem* 2012, **20:**1979-1989.
133. Lu SC, Mato JM: **S-Adenosylmethionine in cell growth, apoptosis and liver cancer.** *Journal of gastroenterology and hepatology* 2008, **23 Suppl 1:**S73-77.
134. Garcia-Faroldi G, Sanchez-Jimenez F, Fajardo I: **The polyamine and histamine metabolic interplay in cancer and chronic inflammation.** *Curr Opin Clin Nutr Metab Care* 2009, **12:**59-65.
135. Hu X, Washington S, Verderame MF, Demers LM, Mauger D, Manni A: **Biological activity of the S-adenosylmethionine decarboxylase inhibitor SAM486A in human breast cancer cells in vitro and in vivo.** *Int J Oncol* 2004, **25:**1831-1838.
136. Fong MY, McDunn J, Kakar SS: **Identification of metabolites in the normal ovary and their transformation in primary and metastatic ovarian cancer.** *PLoS ONE* 2011, **6:**e19963.
137. Surendran S: **Upregulation of N-acetylaspartic acid alters inflammation, transcription and contractile associated protein levels in the stomach and smooth muscle contractility.** *Mol Biol Rep* 2009, **36:**201-206.
138. Demaria S, Pikarsky E, Karin M, Coussens LM, Chen YC, El-Omar EM, Trinchieri G, Dubinett SM, Mao JT, Szabo E, et al: **Cancer and inflammation: promise for biologic therapy.** *J Immunother* 2010, **33:**335-351.
139. Grivennikov SI, Greten FR, Karin M: **Immunity, inflammation, and cancer.** *Cell* 2010, **140:**883-899.
140. DeNardo DG, Barreto JB, Andreu P, Vasquez L, Tawfik D, Kolhatkar N, Coussens LM: **CD4(+) T cells regulate pulmonary metastasis of mammary carcinomas by enhancing protumor properties of macrophages.** *Cancer Cell* 2009, **16:**91-102.
141. Mantovani A: **Molecular pathways linking inflammation and cancer.** *Curr Mol Med* 2010, **10:**369-373.
142. Ohno S, Inagawa H, Dhar DK, Fujii T, Ueda S, Tachibana M, Suzuki N, Inoue M, Soma G, Nagasue N: **The degree of macrophage infiltration into the cancer cell nest is a significant predictor of survival in gastric cancer patients.** *Anticancer Res* 2003, **23:**5015-5022.
143. Welsh TJ, Green RH, Richardson D, Waller DA, O'Byrne KJ, Bradding P: **Macrophage and mast-cell invasion of tumor cell islets confers a marked survival advantage in non-small-cell lung cancer.** *J Clin Oncol* 2005, **23:**8959-8967.
144. Khan K, Elia M: **Factors affecting the stability of L-glutamine in solution.** *Clin Nutr* 1991, **10:**186-192.
145. Roberg BA, Torgner IA, Kvamme E: **Kinetics of a novel isoform of phosphate activated glutaminase (PAG) in SH-SY5Y neuroblastoma cells.** *Neurochem Res* 2010, **35:**875-880.
146. Chatzakos V, Slatis K, Djureinovic T, Helleday T, Hunt MC: **N-acyl taurines are anti-proliferative in prostate cancer cells.** *Lipids* 2012, **47:**355-361.

147. Formentini L, Martinez-Reyes I, Cuezva JM: **The mitochondrial bioenergetic capacity of carcinomas.** *IUBMB Life* 2010, **62:**554-560.